THE IMPACT OF MOLECULAR COMPLEXATION ON INTESTINAL MEMBRANE PERMEATION

by

Jonathan Mark Miller

A dissertation submitted in partial fulfillment
of the requirements for the degree of
Doctor of Philosophy
(Pharmaceutical Sciences)
In The University of Michigan
2009

Doctoral Committee:

       Professor Gordon L. Amidon, Chair
       Professor Steven P. Schwendeman
       Professor Henry Yee-Neen Wang
       Associate Professor Gus Rosania
       Research Professor Gregory E. Amidon

TABLE OF CONTENTS

LIST OF FIGURES

LIST OF TABLES

ABSTRACT

**THE IMPACT OF MOLECULAR COMPLEXATION ON INTESTINAL
MEMBRANE PERMEATION**

by

Jonathan Mark Miller

Chair: Gordon L. Amidon

This dissertation focuses on the impact of molecular complexation on intestinal membrane permeation. Two cases in which molecular complexation in solution affects intestinal membrane transport are considered: 1) enhancement of membrane transport of low-permeability drugs through ion-pairing with lipophilic counterions and 2) reduction of apparent permeability of low-solubility drugs as a consequence of complexation with cyclodextrins. Quasi-equilibrium mass transport analyses were developed to describe: 1) the ion-pair mediated octanol-buffer partitioning and membrane permeation of the low-permeability drugs phenformin, GS 4109, and zanamivir heptyl ester and 2) the effect of cyclodextrins on the membrane transport of the low-solubility drug progesterone.

The counterion 1-hydroxy-2-naphthoic acid (HNAP) enhanced the lipophilicity of the low-permeability drugs by up to 3.7 log units. As predicted from a quasi-equilibrium analysis of ion-pair mediated membrane transport, a log increase in permeability was observed per log increase in HNAP concentration in the parallel artificial membrane permeation (PAMPA) and Caco-2 monolayer assays. Only the rat jejunal permeability of zanamivir heptyl ester was enhanced by HNAP and this was explained by its stronger binding constant (388 M^{-1}) as compared to the phenformin-HNAP and GS 4109-HNAP ion-pairs (3 M^{-1}). Key attributes for successful ion-pair mediated membrane transport were proposed: 1) ion-pair log P_{AB} value in the range of 2-5 to provide sufficient lipophilicity and 2) strong aqueous binding constant on the order of 100-1000 M^{-1} to prevent ion-pair dissociation during membrane permeation.

The transport analysis quantitatively predicted the apparent permeability decrease of progesterone with increasing cyclodextrin concentration (C_{cd}) in the PAMPA, Caco-2 monolayer, and rat jejunal perfusion assays. The model considers the effect of C_{cd} on both the apparent membrane permeability (P_m) and aqueous boundary layer permeability (P_{aq}). The model revealed that: 1) P_{aq} increases with increasing C_{cd}, as the boundary layer thickness quickly decreases as the progesterone bound fraction increases and 2) P_m decreases with increasing C_{cd}, due to the decrease in progesterone free fraction.

In summary, this work provides an increased understanding of the underlying mechanisms that govern the effects of molecular complexation on intestinal membrane transport, and enables the more efficient and intelligent use of molecular complexation strategies to facilitate oral absorption.

CHAPTER ONE

INTRODUCTION

Ion-Pair Mediated Membrane Transport of Low-Permeability Drugs

Background and Significance

Poor intestinal membrane permeability continues to be a major obstacle to the oral

delivery of many molecules with potential therapeutic utility. The majority of viable drug

molecules are able to permeate intestinal membranes via the process of passive diffusion,

which includes both paracellular and transcellular routes. However, the tremendous

selectivity of biological membranes limits the pool of potential drug candidates that can

be passively transported to those with a narrow range of molecular weight, lipophilicity,

and charge state (Martinez and Amidon, 2002). Active uptake via molecular transporters

enables some molecules to circumvent cell membranes (Lipka *et. al.*, 1996; Walter *et. al.*,

1996; Amidon *et. al.*, 1998; Shin *et. al.*, 2003). However, many potential drug candidates

are not substrates for these active transport processes. Due to these limitations in cell

membrane transport, many promising drug candidates that are highly potent *in-vitro* do

not possess adequate cell membrane permeability to be orally active *in-vivo*.

The prodrug approach has proven to be successful in overcoming the intestinal

membrane permeability problem for many drugs (Ettmayer *et. al.*, 2004). Classical

prodrug designs using the non-specific approach of covalently attaching lipophilic

moieties to the molecule of interest to increase passive permeability have had some success (Ettmayer *et. al.*, 2004). Over the last 20 years, more sophisticated prodrug strategies have emerged in which promoieties are covalently attached to the molecule of interest to selectively target certain membrane transporters and enzymes (Fleisher *et. al.*, 1985; Amidon and Johnson, 1987; Amidon and Lee, 1994; Han and Amidon, 2000; Amidon, 2006). These covalent prodrug strategies offer tremendous potential for improving drug bioavailability and selectivity. However, a prodrug is indeed a new molecular entity, thus the impact on other important parameters must be considered when applying this approach, e.g. efficacy, distribution, metabolism, excretion and toxicity.

An analogous strategy to a covalent prodrug approach is an ion-pairing approach, wherein a highly charged, polar molecule with poor membrane permeability is coupled with a lipophilic counterion of equal and opposite charge to form an ion-pair in solution that is able to passively permeate cell membranes (Schanker, 1960). The concept of ion-pair partitioning is illustrated in Figure 1.1, in which the association constant for complex formation, K_{11}, is given by (Connors, 1987):

$$K_{11} = \frac{[BH^+A^-]}{[BH^+][A^-]}$$
(Equation 1.1)

Where $[BH^+A^-]$, $[BH^+]$, and $[A^-]$ are the concentrations of the complex, organic cation, and organic anion, respectively.

$$[BH^+]_{aq} + [A^-]_{aq} \leftrightarrow [BH^+A^-]_{aq} \leftrightarrow [BH^+A^-]_{membrane}$$

Aqueous   Lipophilic
Phase   Phase

Membrane
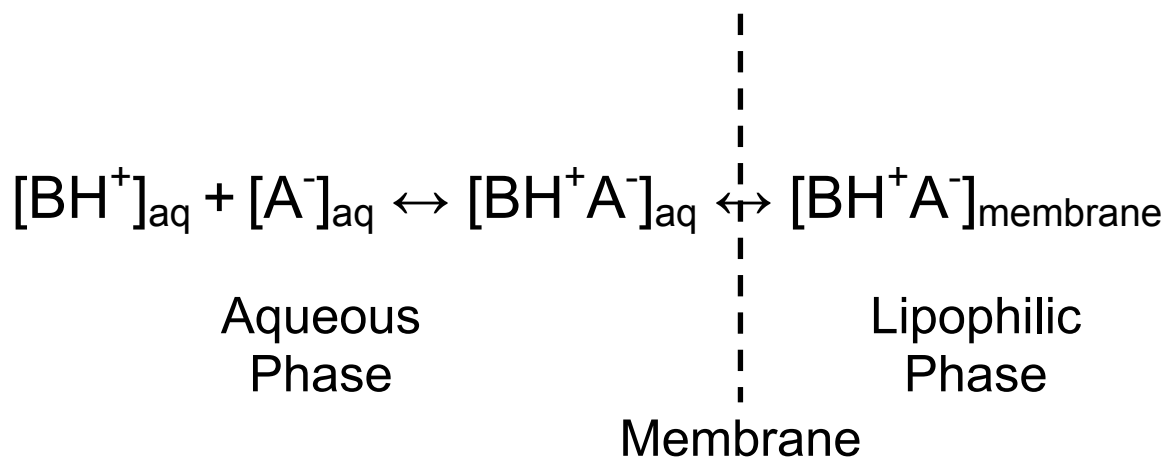
Figure 1.1: Ion-pair partitioning concept. Adapted from Grant and Higuchi, (1990)

As summarized in Table 1.1, an ion-pairing approach for increasing oral absorption has several advantages. The approach is simple in principle and eliminates the need for prodrug uptake by transports and activation by specific enzymes. The ion-pair in solution may be absorbed and then readily dissociate after absorption via dilution in the bloodstream. Moreover, the approach does not rely on disrupting membrane integrity to facilitate absorption. A potential disadvantage of the ion-pairing approach is that the ionic bonding and other non-covalent interactions (i.e hydrogen bonding) may be too weak in solution to facilitate membrane permeation.

Table 1.1: Advantages and disadvantages of an ion-pairing approach to increase membrane permeation

Advantages	Disadvantages
No need for enzymes and transporters for pro-drug activation and uptake	Non-covalent interactions may be too weak to facilitate membrane permeation
Equilibrium may be manipulated to enable complex absorption followed by facile dissociation of available drug	
No need for additives which may compromise membrane integrity and lead to toxicity	

Absorption enhancement using ion-pairs has been the topic of much discussion and debate in the literature (Tomlinson, 1980; Jonkman and Hart 1983; Neubert, 1989; Quintanar-Guerrero *et. al*., 1997; Meyer and Manning, 1998; Lengsfeld, 2002). There are a few reports of significant increases in absorption using ion-pairs (Irwin *et. al*., 1969. Gibaldi and Grundhofer, 1973, Walkling *et. al.*, 1978, Dal Pozzo *et. al.*, 1989, Ross *et. al*., 2004, Mrestani *et. al.*, 2006). Mrestani *et. al.*, (2006) recently used an ion-pair approach to improve the oral absorption of cefpirom, a peptido-mimetic cephalosporin β-lactam antibiotic. The highly polar, zwitterionic structure of cefpirom leads to very poor absorption via the oral route, hence it is only delivered intravenously or intramuscularly. The oral absorption of cefpirom was dramatically improved when dosed intraduodenally with the cationic ion-pairing agent hexadecyldimethylbenzylammonium chloride (BAC) and the anionic ion-pairing agent hexylsalicylic acid (HSA) in rabbits. The fraction absorbed of cefpirom increased 21 fold when dosed at 100 mg/kg in solution with 243 mg/kg BAC and 15 fold with 100 mg/kg HSA.

The cefpirom case discussed above is one of the few examples in which an ion-pairing approach has proved successful in increasing the oral bioavailability of a poorly absorbed drug. Table 1.2 contains an extensive list of examples from the literature in which various investigators have attempted to use ion-pairs to increase oral absorption. Few of the studies have been successful in significantly increasing oral exposure. This is largely because the mechanism by which ion-pairs may increase oral absorption, including the important parameters and key attributes that determine success or failure of a given ion-pair, are not well understood. Moreover, mathematical models describing ion-pair mediated membrane transport remain under utilized.

Table 1.2: Summary of previous *in-vivo* studies using ion-pairs

Drug	Counter-ion	clogP	Species	Route	Absorption Enhancement	Reference
LMW-Heparin	Bis-N,N-dibutylamino-ethylene carbonate	6.83	Rat	Intraduodenal	≥ 31X (Emax)	Dal Pozzo *et. al.*, 1989
Cefpirom	Hexadecyldimethylbenzyl ammonium chloride	~10	Rabbit	Intraduodenal	22X (Cmax)	Mrestani *et. al.*, 2006
Cefpirom	Hexylsalicylic acid	5.18	Rabbit	Intraduodenal	20X (Cmax)	Mrestani *et. al.*, 2006
Heparin	Bis-N,N-dibutylamino-ethylene carbonate	6.83	Rat	Intraduodenal	≥ 17X (Emax)	Dal Pozzo *et. al.*, 1989
NBPCMDA	Trichloroacetate	1.67	Rat	Intraduodenal	7.1X (C60min)	Gibaldi *et. al.*, 1973
NBPCMDA	Salicylate	2.06	Rat	Intraduodenal	5.7X (C60min)	Gibaldi *et. al.*, 1973
Gentamicin	*N*-[1-D,L,Carboxytridecyl] α,β-glucopyranuronamide	4.56	Rat	Oral	5.5X (Cmax)	Ross *et. al.*, 2004
Mixidine	2-Napthalenesulfonic acid	1.70	Rat	Intraduodenal	4.0X (Cmax)	Walkling *et. al.*, 1978
Isopropamide	Trichloroacetate	1.67	Mouse	Oral	3.5X (Emax)	Irwin *et. al.*, 1969
AMD3000	Taurocholate	0.05	Rabbit	Oral	2.5X (Cmax)	Van Gelder *et. al.*, 1999
Pholedrine	Hexylsalicylate	5.18	Rabbit	Oral	1.6X (Cmax)	Neubert *et. al.*, 1988
Thiazinamium	Salicylate	2.06	Human	Oral	1.5X (FEU)	Jonkman *et. al.*, 1979
Propranolol	Taurodeoxycholate	2.10	Rabbit	Oral	1.4X (Cmax)	Gasco *et. al.*, 1984
Emepronium	Lauryl sulfate	5.40	Mouse	Oral	1.0X (FEU)	Hallén *et. al.*, 1985
Isopropamide	Glycocholate	1.49	Rat	Intraduodenal	0.7X (C60min)	Gaginella *et. al.*, 1973

Analysis of the data in Table 1.2 reveals the following potential reasons for why the ion-pair approach has been marginally successful thus far:

- The most successful studies are those in which the ion-pair is dosed directly to the intestine. This decreases the likelihood that ion-exchange will occur in the stomach upon oral dosing.

- While the use of excess counter-ion may shift the equilibrium towards forming the ion-pair in solution, too much counter-ion may lead to the formation of micelles that are less likely to be transported by passive diffusion. For example, exposure of isopropamide decreased when dosed with 100 fold excess glycholate due to the formation of micelles (Gaginella *et. al.*, 1973).

- Most of the counter ions used are not pharmaceutically acceptable, which may lead to membrane irritation and toxicity, especially when dosed in excess.

- **The mechanism for success or failure in enhancing oral absorption is not well understood.**

Thus, the following ideas are proposed to increase the intestinal membrane permeability of an ion-pair:

- The cell membrane permeability of the complex should be maximized. The log P of the complex in solution should be in the range of 2-5 so that the passive membrane permeability of the complex is optimal.

- The binding constant of the complex should be maximized. The difference in pK_a between the acidic drug and organic base should be large. Complimentary hydrogen bonding, hydrophobic interactions, van der Waal interactions, and pi-pi

interactions should also be present as to maximize the binding constant of the complex.

Research Objectives

- To **investigate** the utility of an ion-pairing approach for increasing the intestinal membrane permeation of low-permeability drugs

- To **understand** the mechanism by which ion-pairs in solution increase intestinal membrane permeation

- To develop and apply **mass transport analyses** that describe the mechanism by which ion-pairs increase intestinal membrane permeation

Hypotheses

- The apparent **intestinal membrane permeation** of a low-permeability drug may be **enhanced** by forming ion-pairs with hydrophobic counter-ions

- The ion-pair must provide sufficient **lipophilicity (Log P_{AB})** to effectively enhance intestinal membrane permeation

- The ion-pair must exhibit a strong **binding constant (K_{11})** between acidic and basic components to effectively enhance intestinal membrane permeation

Model Compounds
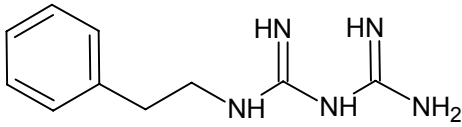
BCS class III drugs will be used as model compounds to investigate the utility of an ion-pairing approach for increasing intestinal membrane permeation. BCS class III drugs are typically polar, highly charged molecules which exhibit high solubility but low

cell membrane permeability which limits their oral absorption (Amidon *et. al.*, 1995). An estimated 25-35% of immediate release drugs on the WHO and top 200 drug lists are classified as BCS class III (Kasim *et. al.*, 2004; Takagi *et. al.*, 2006), which illustrates the pervasive problem posed by molecules with poor membrane permeability. BCS class III drugs are ideal candidates for increasing membrane permeation via an ion-pairing approach.

<u>Phenformin</u>

Phenformin is a hepatic gluconeogenesis inhibitor from the biguanide class of anti-diabetic compounds. The compound is a potent hypoglycemic agent, however, it was removed from the United States market in the late 1970s due to lactic acidosis induced toxicity (Luft *et. al.*, 1978). As shown in Table 1.3, phenformin possesses a strongly basic biguanidine functionality, which imparts high polarity and hence low lipophilicity (clogP = -0.60) and transcellular permeability to the molecule. Protonation of the first guanidinium, which leads to the mono-cation, has a cpK_a of 12.7 (Table 1.3). Protonation of the second gaunidinium, which leads to the di-cation, has a much weaker pK_a of 2.9, as determined experimentally by Goizman *et. al.*, 1985. Thus, phenformin exists as a mono-cation at pH 6.5. These attributes make phenformin an ideal candidate for permeability enhancement via an ion-pairing approach.
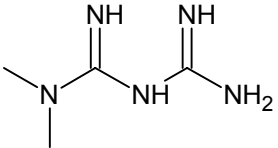
Table 1.3: Properties of phenformin (Luft *et. al.*, 1985; Goizman *et. al.*, 1985)

Structure	
Indication	Diabetes mellitus type 2
Mechanism of Action	Glucose absorption inhibitor, hepatic gluconeogenesis inhibitor
cLogP	-0.60
pK_as	12.7(B), 2.9 (B)
cLogD pH 7	-2.60
F_{abs}	0.56

Metformin

Like phenformin, metformin is also a hepatic gluconeogenesis inhibitor from the biguanide class of anti-diabetic compounds. Metformin is much less toxic than phenformin and has therefore emerged as a primary therapeutic agent for the treatment of Type II diabetes. The physical-chemical properties of metformin are summarized in Table 1.4. Metformin also possesses the highly basic biguanidinium functionality ($cpK_a =$ 13.86) and is even less lipophilic than phenformin with a very low clog P of -2.31. Like phenformin, metformin exists as a mono-cation at pH 6.5 making it an ideal candidate for permeability enhancement via an ion-pairing approach with lipophilic counter acids.

Table 1.4: Properties of metformin (Chiou *et. al.*, 2000)

Structure	
Indication	Diabetes mellitus type 2
Mechanism of Action	Glucose absorption inhibitor, hepatic gluconeogenesis inhibitor
cLogP	-2.31
pK_as	13.86(B), 2.9 (B)
cLogD pH 7	-4.31
F_{abs}	0.55
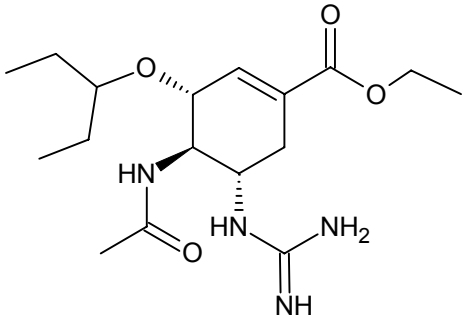
GS 4109

GS 4109 is an influenza virus neuraminidase inhibitor with potential therapeutic utility in the treatment of influenza virus types A and B and also avian influenza (Li *et. al.*, 1998). GS 4109 is the guanidinium analog of the anti-influenza agent oseltamivir, which has a primary amine functionality off the 5 position of the primary ring instead of guanidinium (Table 1.5). Oseltamivir exhibits high oral absorption of 60-80% in humans, whereas GS 4109 is very poorly absorbed (F = 0.02). Both oseltamivir and GS 4109 are ethyl ester prodrugs of the active carboxylate.

The physical chemical, pharmacological, and pharmacokinetic properties of GS 4109 are summarized in Table 1.5. The active carboxylate is a very potent influenza virus neuraminidase inhibitor with IC_{50} of 0.9 nM. The clog P of 0.83 of GS 4109 indicates the unionized form of the molecule is fairly lipophillic. However, GS 4109 possesses a highly basic guanidinium functionality (cpK_a = 12.8) which makes the compound positively charged over the entire physiologically relevant pH range. This highly charged nature of GS 4109 gives rise to a low clog D of -1.17 at pH 7, which leads

to very poor permeability and fraction absorbed. The highly basic guanidinium functionality of GS 4109 makes it an ideal candidate for ion-pair formation with lipophillic acids.

Table 1.5: Properties of GS 4109 (Li *et. al.*, 1998)

Structure	
Indication	Influenza virus A and B, Avian Influenza
Mechanism of Action	Influenza virus neuraminidase inhibitor
Neuraminidase IC_{50}	0.9 nM (carboxylate)
cLogP	0.83
cpK_a	12.8(B)
cLogD pH 7	-1.17
F_{abs}	0.02
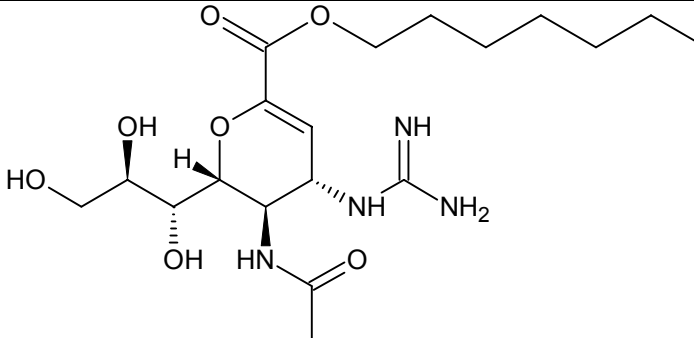
Zanamivir Heptyl Ester

Zanamivir is an influenza virus neuraminidase inhibitor currently on the market for the treatment of influenza virus types A and B and has also been shown to have potential therapeutic utility against avian influenza (Li *et. al.*, 1998). Zanamivir carboxylate is highly polar and extraordinarily hydrophilic (clogP = -3.63) and therefore lacks sufficient intestinal permeability to allow delivery via the oral route (F = 0.04). Thus, zanamivir is currently delivered by inhalation, which creates complications and increased risk of bronchospasms in asthma and COPD patients. Given the extremely low

lipophilicity of zanamivir carboxylate, formation of lipophilic esters do not provide enough increase in lipophilicity to improve intestinal membrane permeation. However, the formation of esters of zanamivir imparts high positive charge to the molecule by eliminating the negatively charged carboxylate, thus making zanamivir esters amenable to ion-pairing with lipophilic counter acids. Therefore, the combination of a lipophilic (e.g. heptyl) ester with a lipophilic anion could enable increased intestinal membrane permeation for zanamivir.

The physical chemical, pharmacological, and pharmacokinetic properties of zanamivir and its heptyl ester are summarized in Table 1.6. Zanamivir is a very potent influenza virus neuraminidase inhibitor with IC_{50} of 1-7.4 nM. Zanamivir carboxylate is highly polar (clogP = -3.63), however, the heptyl ester provides significantly improved lipophilicity (clogP = 0.69). Zanamivir heptyl ester also possesses a highly basic guanidinium functionality (cpK_a = 11.26) and elimination of the carboxylate through formation of the ester makes the compound positively charged over the entire physiologically relevant pH range. This makes zanamivir heptyl ester an ideal candidate for permeability enhancement via an ion-pairing approach with lipophilic counter acids.

Table 1.6: Properties of zanamivir esters (Li *et. al.*, 1998; Buxton *et. al.,* 2000)

Structure	
Indication	Influenza virus A and B, Avian Influenza
Mechanism of Action	Influenza virus neuraminidase inhibitor
Neuraminidase IC_{50}	1.0-7.5 nM (Zanamivir carboxylate)
cLogP	0.69
cpK_a	11.26(B)
cLogD pH 7	-1.17
F_{abs}	0.04 (Zanamivir carboxylate)
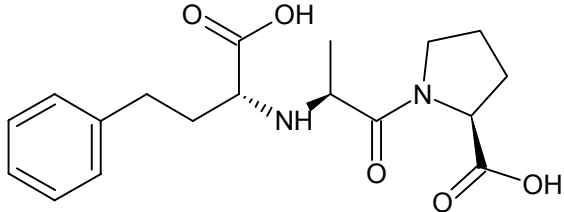
Enalaprilat

Enalaprilat is an angiotensin converting enzyme (ACE) inhibitor used for the treatment of high blood pressure. Enalaprilat exhibits poor oral absorption due to its highly polar structure (Table 1.7). Thus, enalaprilat is delivered as the ethyl ester pro-drug, enalapril, which exhibits increased oral absorption of about 60% in humans (Todd and Goa, 1992). Enalapril is readily hydrolyzed by esterases in the liver to form the active metabolite, enalaprilat.

The physical-chemical, pharmacological, and pharmacokinetic properties of enalaprilat are summarized in Table 1.7. The compound is a very potent ACE inhibitor with IC_{50} of 2.8 nM. The log P of 1.17 of the compound indicates the unionized form of the molecule is fairly lipophillic, however, the structure contains three ionizable centers which leads to a very low log D of <-3 at pH 7. The highly charged nature of enalaprilat at pH 7 leads to very poor permeability and fraction absorbed (<0.10). Enalaprilat has

two acidic pK_as, making it an ideal candidate for permeability enhancement via ion-pairing with lipophillic bases.

Table 1.7: Properties of enalaprilat (Kubo and Cody, 1985; Ranadive *et. al.*, 1992; Lennernäs *et. al.*, 1994; Yee and Amidon, 1995; Kim *et. al.*, 2006)

Structure	
Indication	Hypertension
Mechanism of Action	Angiotension converting enzyme (ACE) inhibitor
ACE IC_{50}	2.8 nM
logP	1.17
pK_as	2.83(A) 3.46(A) 7.57(B)
logD pH 7	< -3
Permeability	0.2×10^4 cm/s
F_{abs}	< 0.10
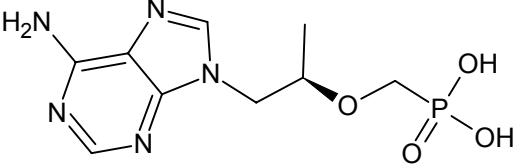
Tenofovir

Tenofovir is a reverse transcriptase inhibitor used in the treatment of human immunodeficiency virus-1 (HIV-1). The compound exhibits extremely poor absorption (F = 0.02) via the oral route due to its highly polar structure (Table 1.8). A more lipophilic disoproxil ester pro-drug of tenofovir with improved oral absorption (F = 0.20) has been developed to enable the oral delivery of tenofovir (Naesens *et. al.*, 1998).

The physical chemical, pharmacological, and pharmacokinetic properties of tenofovir are summarized in Table 1.8. The compound is a potent HIV-1 reverse transcriptase inhibitor with IC_{50} of 100 nM. The extremely high polarity of tenofovir results in a very low clog P of -1.71. The structure of tenofovir contains three ionizable

centers which gives rise to an extraordinarily low clog D of -5.44 at pH 7. The highly

charged nature of tenofovir at pH 7 leads to very poor permeability and fraction

absorbed. Tenofovir has two acidic pK_as, making it an ideal candidate for ion-pairing

with lipophillic bases to enhance membrane permeation.
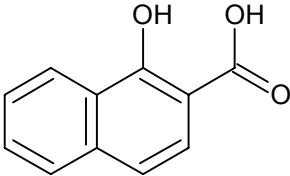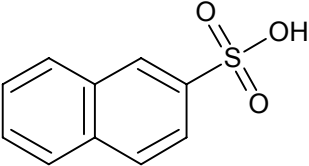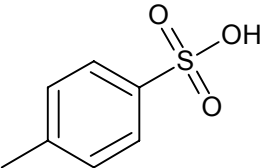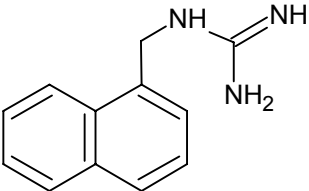
Table 1.8: Properties of tenofovir (Naesens *et. al.*, 1998)

Structure	
Indication	Human immunodeficiency virus-1 (HIV-1)
Mechanism of Action	HIV-1 reverse transcriptase inhibitor
HIV-1 RT EC_{50}	100 nM
cLogP	-1.71
cpK_as	1.61(A) 4.11(B) 7.02(A)
clogD pH 7	-5.44
F_{abs}	0.02 (Tenofovir) 0.20 (Tenofovir Disoproxil)

Lipophilic Counterions

The acidic counterions employed for ion-pairing are 1-hydroxy-2-naphthoic acid

(HNAP), 2-naphthalenesulfonic acid (NAPSA), and *p*-toluenesulfonic acid (*p*-TSA). The

physical chemical properties and structures of the acidic counterions are summarized in

Table 1.9. These counterions were chosen based on the following criteria: high

lipophicility, strong acidity, and precedented use in humans (Stahl and Wermuth, 2002).

All the counterions have previously been used in pharmaceutical product(s); HNAP in

salmeterol, NAPSA in propoxyphene, and *p*-TSA in sultamicillin. The basic counterion

1-naphthylmethyl guanidine (NMG) was chosen for ion-pairing with acidic drugs (Table

1.9). This counterion is currently not used in any pharmaceutical products.

Table 1.9: Physical properties of lipophilic counterions used for ion-pairing (Stahl and Wermuth, 2002)

Counterion	Structure	pK_a	clogP	Pharmaceutical Use
1-Hydroxy-2-Naphthoic Acid (HNAP)		2.70	3.29	Salmeterol
2-Naphthalene Sulfonic Acid (NAPSA)		0.17	1.70	Propoxyphene
p-Toluene Sulfonic Acid (p-TSA)		-1.34	0.93	Sultamicillin
1-Napthylmethyl Guanidine (NMG)		12.3	1.52	Not Used

Effect of Cyclodextrins on Membrane Transport of Low-Solubility Drugs

Background and Significance

Modern drug discovery techniques (e.g., advances in high throughput screening methods, the introduction of combinatorial chemistry) have resulted in an increase in the number of drug candidates being selected that exhibit low solubility in water. By some estimates, more than 40% of new drug candidates are lipophilic and have poor aqueous solubility (Lipinski, 2001; Van de Waterbeemd *et. al.*, 2001; Dahan and Amidon, 2008). With very minor exceptions, dissolution of the drug substances in the aqueous gastrointestinal (GI) milieu is a prerequisite for absorption following oral administration. Hence, compounds with inadequate aqueous solubility often suffer from limited oral bioavailability. A great challenge facing the pharmaceutical scientist is to formulate these molecules into orally administered dosage forms with sufficient bioavailability (Dahan and Hoffman, 2007).

Among the various approaches to improve the aqueous solubility of lipophilic drugs, the utilization of cyclodextrins has become widespread in recent years (Davis and Brewster, 2004; Brewster and Loftsson, 2007). Cyclodextrins are crystalline, non-hygroscopic, cyclic oligosaccharides, with a hydrophilic outer surface and a less hydrophilic central cavity which is able to host hydrophobic solutes. From a drug delivery standpoint, cyclodextrins have gained extensive attention and use, due to their ability to increase the apparent solubility of hydrophobic drugs via the formation of more water soluble inclusion complexes (Loftsson and Brewster, 1996; Rajewski and Stella 1996).

According to the Biopharmaceutics Classification System (BCS), the extent of oral absorption of a drug is governed by two primary factors: 1) the effective permeability across the intestinal mucosa and 2) the solubility and dissolution characteristics in the GI milieu (Amidon *et. al.*, 1995; Lobenberg and Amidon, 2000; Martinez and Amidon, 2002; Yu *et. al.*, 2002). While increased apparent solubility of a lipophilic drug can be achieved by a cyclodextrin based delivery system, the effect of such a formulation on the apparent permeability is not completely understood. Several studies have shown that the use of cyclodextrins can reduce the apparent permeability of the drug (Loftsson *et. al.*, 2004; Carrier *et. al.*, 2007; Loftsson *et. al.*, 2007), an effect that is often qualitatively attributed to a decrease in the free fraction of the drug available for membrane permeation. These opposing effects of cyclodextrins on solubility and permeability can lead to paradoxical effects on the overall fraction of drug absorbed. A critical review of the literature revealed that the use of cyclodextrins can result in enhanced, unchanged, or even decreased oral bioavailability (Loftsson *et. al.*, 2004; Carrier *et. al.*, 2007; Loftsson *et. al.*, 2007). As a result of these observations, qualitative guidelines for the proper use of cyclodextrins have been proposed (Rao *et. al.*, 2003; Carrier *et. al.*, 2007; Miller *et. al.*, 2007), however no quantitative analysis that enables simulation of the overall effect of cyclodextrins on solubility and permeability is currently available.

Research Objectives

- To **investigate** the effect of cyclodextrins on intestinal membrane transport when using cyclodextrins to increase the apparent solubility of low-solubility drugs

- To develop and apply **mass transport analyses** that describe the mechanism by which cyclodextrins affect membrane permeation

- To **understand** the interplay between opposing effects of cyclodextrins on apparent solubility and apparent permeability

Hypotheses

- The apparent **intestinal membrane permeability** of a low-solubility drug may be **decreased** through molecular complexation with cyclodextrins

- When using cyclodextrins as a solubilizer, there exists an **interplay** between apparent **solubility increase** and apparent **permeability decrease**

- The **solubility gains** resulting from the use of cyclodextrins are effectively paid for by **loss of intestinal membrane permeability**
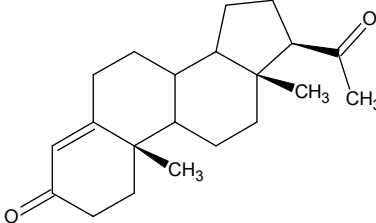
Model Compound

Progesterone

Progesterone is a naturally occurring steroid hormone used in the treatment of endometrial hyperplasia and secondary amenorrhea in postmenopausal women. The physical chemical and pharmacokinetic properties of progesterone are summarized in Table 1.8. The compound suffers from poor aqueous solubility (8 μg/mL) due to its highly lipophilic structure (cLog P 4.0). The low solubility and high cLog P make

progesterone a BCS class II drug. Progesterone for oral administration is delivered in a micronized form, in order to improve the dissolution rate and oral absorption. As summarized in Table 1.10, micronized progesterone enables an oral absorption of about 50-60% (Lignieres, 1999). The poor aqueous solubility and dissolution rate make progesterone an ideal candidate for solubility enhancement by complexation with cyclodextrin.

Table 1.10: Properties of progesterone (Lignieres, 1999)

Structure	
Indication	Endometrial hyperplasia, secondary amenorrhea
Mechanism of Action	Natural hormone replacement therapy
cLogP	4.0
Aqueous Solubility	8 µg/mL*
F_{abs}	50-60%

*Determined as part of the work in Chapter IV of this thesis.

CHAPTER TWO

ION-PAIR FACILITATED ORAL ABSORPTION: QUASI-EQUILIBRIUM ANALYSIS OF THE ION-PAIR MEDIATED OCTANOL-BUFFER PARTITIONING OF LOW-PERMEABILITY DRUGS

Theory

Quasi-Equilibrium Analysis of Ion-pair Mediated Octanol-Buffer (pH 6.5) Partitioning

Consider the ion-pair formation between a basic drug and an organic acid in a mixture of octanol and water. Assuming quasi-equilibrium conditions, that is, formation and destruction of ion-pairs as well as octanol-water partitioning processes are near thermodynamic equilibrium, the association constant for ion-pair formation in the aqueous phase, K_{11aq}, is given by (Connors, 1987; Grant and Higuchi, 1990):

$$K_{11aq} = \frac{[AB]_{aq}}{[A]_{aq}[B]_{aq}}$$
(Equation 2.1)

Where $[A]_{aq}$, $[B]_{aq}$, and $[AB]_{aq}$ are the aqueous phase concentrations of the organic acid, basic drug, and ion-pair, respectively.

Assuming the total amount of basic drug in the octanol phase, $[B_t]_{oct}$ exists only as ion-pair (i.e $[B_t]_{oct} \approx [AB]_{oct}$), the apparent octanol/aqueous distribution coefficient $D_B = [B_t]_{oct} / [B_t]_{aq}$, of the basic drug can be expressed as:

$$D_B = \frac{[AB]_{oct}}{[B]_{aq} + [AB]_{aq}}$$
(Equation 2.2)

Where the total amount of basic drug in the aqueous phase $[B_t]_{aq} = [B]_{aq} + [AB]_{aq}$ and

$[B]_{aq}$ represents the concentration of free drug in the aqueous phase.

The intrinsic octanol/water partition coefficient for the ion-pair, P_{AB}, can be defined as:

$$P_{AB} = \frac{[AB]_{oct}}{[AB]_{aq}}$$ (Equation 2.3)

Combining Equations 2.1, 2.2, and 2.3 gives the following relationship:

$$\frac{1}{D_B} = \frac{1}{K_{11_{aq}} P_{AB}[A]_{aq}} + \frac{1}{P_{AB}}$$ (Equation 2.4)

Where $[A]_{aq} \approx \frac{[A_i]_{aq}}{1+D_A}$ and $[A_i]$ is the initial concentration of organic acid in the aqueous

phase before equilibration with octanol, and D_A is the apparent octanol/aqueous

distribution coefficient of the organic acid.

Thus, a plot of $\frac{1}{D_B}$ versus $\frac{1}{[A]_{aq}}$ will yield a straight line with y-intercept $= \frac{1}{P_{AB}}$ and

slope $= \frac{1}{K_{11aq} P_{AB}}$ from which K_{11aq} and P_{AB}, may be ascertained.

The association constant for ion-pair formation in the octanol phase, K_{11oct}, can be

expressed as:

$$K_{11_{oct}} = \frac{[AB]_{oct}}{[A]_{oct}[B]_{oct}}$$ (Equation 2.5)

Where $[A]_{oct}$, $[B]_{oct}$, and $[AB]_{oct}$ are the octanol phase concentration of the organic acid,

organic base, and ion-pair, respectively.

Equations 2.1 and 2.5 can be combined to give:

$$K_{11oct} = \frac{P_{AB} K_{11_{aq}}}{D_A D_B}$$ (Equation 2.6)

Thus, K_{11oct} can be estimated from the experimentally determined values of P_{AB}, K_{11aq}, D_A, and D_B.

Materials and Methods

Materials

Phenformin hydrochloride and tenofovir were obtained from Waterstone Technologies (Carmel, IN). Enalaprilat was obtained from USP (Rockville, MD). Sodium 2-naphthalenesulfonate was obtained from Fluka (Buchs, Switzerland). 1-naphthylmethyl guanidine was obtained from Tyger Scientific (Ewing, NJ). Metformin hydrochloride was obtained from MP Biomedicals (Solon, OH). 1-hydroxy-2-naphthoic acid, *p*-toluenesulfonic acid monohydrate, trifluoroacetic acid, anhydrous dimethyl formamide (DMF), triethylamine and 1-octanol were obtained from Sigma-Aldrich (St. Louis, MO). Oseltamivir phosphate was obtained from Sequoia Research Products Ltd (Pangbourne, UK). Acetylneuraminic acid (sialic acid) for zanamivir synthesis was purchased from TCI America Ltd (Portland, OR). All compounds were of the highest available quality and were used as received.

GS 4109 Synthesis:

Scheme 1. Chemical Synthesis of GS 4109

Oseltamivir **1** → (with (BocNH)$_2$C=S, HgCl$_2$, TEA, DMF) → **2** → (with TFA, CH$_2$Cl$_2$) → Gaunidino Oseltamivir (GS 4109) **3**
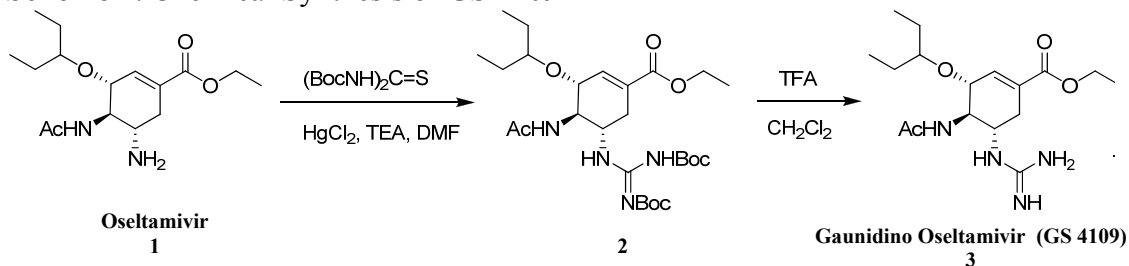
Guanidino oseltamivir was synthesized as shown in Scheme **1** (Shitara *et. al.*, 2000). Briefly, oseltamivir was first converted to its guanidine analogue which was later deprotected to give guanidine oseltamivir as trifloroacetate salt. The synthetic procedure is given as follows:

(3R,4R,5S)-ethyl-4-acetamido-5-(2,3-bis(tert-butoxycarbonyl)guanidino)-3-(pentan-3-yloxy)cyclohex-1-enecarboxylate (2). To a stirring solution of oseltamivir phosphate, **1**, (1g, 2.4 mmol), bis-boc thiourea (1.06g, 3.6 mmol) and triethyl amine (TEA, 1.1ml, 8 mmol) in 20ml DMF, was added Mercury (II) chloride (0.728g, 2.6 mmol) while stirring at 0 °C. The reaction was followed by thin layer chromatography (TLC) using ethylacetate:hexane (1:3). After approximately 1h, when all starting material was reacted, the reaction mixture was diluted with ethyl acetate and filtered. It was then washed with water and brine and dried over anhydrous magnesium sulfate. Column chromatography using hexane:ethyl acetate (10:1) gave pure intermediate, **2**, which is the precursor to guanidine oseltamivir, as white powder, in 89% overall yield. [^{1}H] NMR (CdCl$_3$, 500MHz) δ (ppm) 0.84-0.92 (m, 6H),1.23-1.30 (m, 3H), 1.49-1.55 (m, 22H), 1.91 (s, 3H), 2.37 (dd, 1H, *J* = 2.55, 2.55 Hz), 5.35 (dd, 1H, *J* = 5.35, 5.35 Hz), 3.34 (t, 1H, *J* = 5.65 Hz), 4.01-4.09 (m, 1H), 4.12-4.14 (m, 1H), 4.16-4.23 (m, 2H), 4.35-4.37 (m, 1H),

6.21 (d, 1H, J = 8.95 Hz) 8.64 (d, 1H, NH, J = 8.05), 11.39 (s, 1H, NH) ; ESI$^+$-MS, m/z: 555.3 (M+H)$^+$

(3R,4R,5S)-ethyl-4-acetamido-5-guanidino-3-(pentan-3-yloxy)cyclohex-1-enecarboxylate (3). Compound **2** was boc deprotected using trifloroacetic acid. It was then stirred with 40% trifloroacetic acid in dichloromethane for about two hours (Masuda *et. al.*, 2003). Following the completion of the reaction (TLC, ESI-MS), compound **3 (GS 4109)** was lyophilized for approximately 48 hours to give a white powder as amorphous 2-TFA salt. Yield was almost 100%. Purity was greater than 95% by HPLC. [^{1}H] NMR (Cd$_3$OD, 500MHz) δ (ppm) 0.90-0.96 (m, 6H), 1.32 (t, J = 7.1 Hz, 3H), 1.50-1.58 (m, 4H), 2.01 (s, 3H), 2.38 (dd, 1H, J = 9.1, 17.65Hz), 2.85 (dd, 1H, J = 5.05, 17.45 Hz), 3.42-3.45 (m, 1H), 3.85-3.88 (m, 1H), 3.93 (t, 1H, J = 9.65), 4.20-4.27 (m, 3H), 6.86 (s, 1H), 8.25 (d, 1H, NH, J = 8.3 Hz); ESI$^+$-MS, m/z: 355.2 (M+H)$^+$

Zanamivir Heptyl Ester Synthesis:

Scheme 2
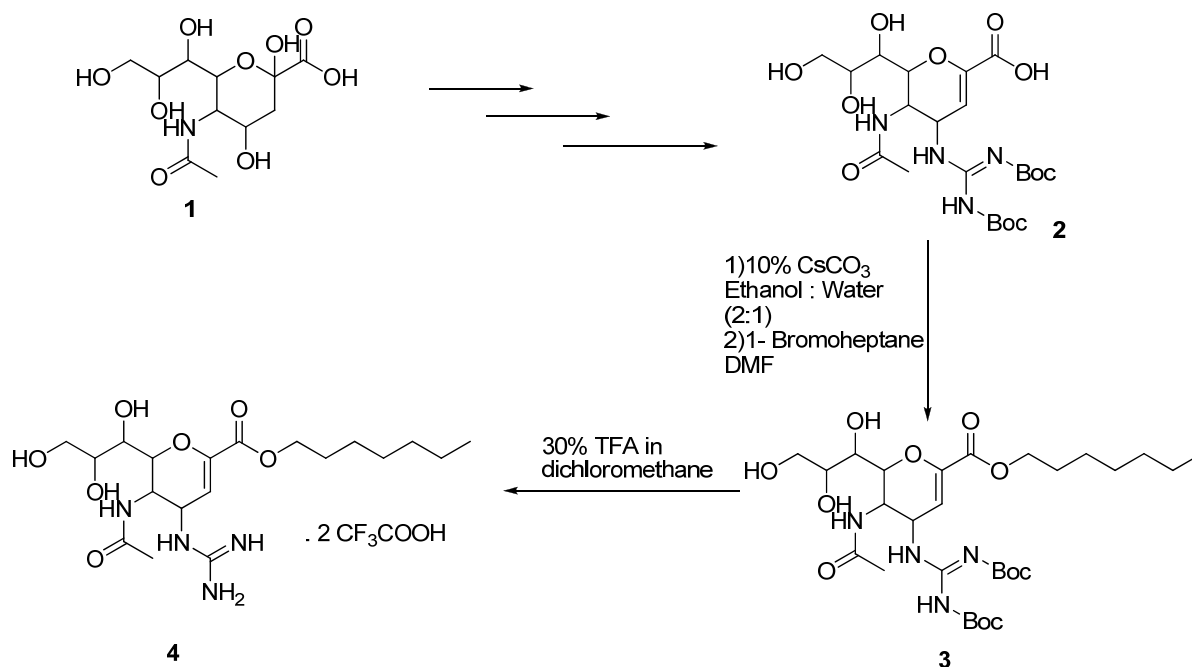
Zanamivir heptyl ester was synthesized as shown in Scheme **2**. Boc-protected zanamivir **2** was synthesized from sialic acid **1** using synthetic methods previously reported (Chandler *et. al.*, 1995; Martin *et. al.*, 1998; Masuda *et. al.*, 2003). The heptyl ester of Boc- zanamivir **3** was synthesized from Boc-zanamivir by first forming cesium salt followed by reaction with 1-bromoheptane in N,N-dimethyl formamide (Ogura *et. al.*, 1998). The final compound **4** was obtained by deprotection of Boc in presence of 30% trifluroacetic acid in dichloromethane.

5-Acetamido-2,6-anhydro-4-(2,3-bis(tert-butoxycarbonyl)guanidino)-3,4,5-trideoxy-D-glycero-D-galcto-non-2-enonic acid (Boc-Zan) 2. ^{1}H NMR (CD$_3$OD) δ (ppm) 5.6 (d, *J* = 2.0 Hz, 1H), 5.01 (dd, *J* = 9.6, 2.1 Hz, 1H), 4.25 (dd, *J* = 10.8, 1.1 Hz, 1H), 4.18 (dd, *J* = 10.6, 9.6 Hz, 1H), 3.89 (ddd, *J* = 9.4, 6.2, 2.7 Hz, 1H), 3.84 (dd, *J* = 11.3, 2.8 Hz,

1H), 3.67 (dd, J = 11.3, 5.8 Hz, 1H), 3.57(d, J = 9.3 Hz, 1H), 1.9 (s, 3H), 1.55 (s, 9H), 1.50 (s, 9H); ESI-MS: 533 (M+H)[+].

5-Acetamido-2,6-anhydro-4-(2,3-bis(tert-butoxycarbonyl)guanidino)-3,4,5-trideoxy-D-glycero-D-galcto-non-2-enonic acid heptyl ester 3 A solution of **2** (50 mg) in 2 mL ethanol:water (3:1) was made neutral with 10% cesium carbonate. The reaction mixture was concentrated under reduced pressure and was re-dissolved in water which was lyophilized for 48 hours to yield cesium salt of **2**. 25 mg of **2** was dissolved in N, N-dimethylformamide (2 mL) and to it 1-bromoheptane (17mg, 94.9 mmol) was added and the reaction was allowed to stir at room temperature for 20 hours. The reaction mixture was concentrated under reduced pressure. The crude reaction mixture was purified by flash column chromatography using chloroform: methanol (25:1) as eluent to obtain **3** as a colorless oil (21 mg, 72%).

^{1}H NMR (CDCl$_3$) δ (ppm) 5.8(d, J = 2.0 Hz, 1H), 5.1(m, 1H), 4.2(m, 2H), 4.15 (m, 2H), 3.9(m, 1H), 3.8(m, 1H) 3.45(m, 2H), 2.01(s, 3H), 1.88(m, 2H), 1.52 (s, 9H), 1.50 (s, 9H), 1.3-1.5(m, 8H), 0.9(m, 3H); ESI-MS: 631 (M+ H)[+].

5-Acetamido-2,6-anhydro-4-(guanidino)-3,4,5-trideoxy-D-glycero-D-galcto-non-2-enonic acid heptyl ester 4 To 20 mg **4** 30% trifluroacetic acid in dichloromethane (2mL) was added and the reaction was stirred at room temperature for one hour. The progression of the reaction was monitored by TLC. The reaction mixture was concentrated in vacuo. The concentrate was dissolved in water and lyophilized for 48 hours to yield the final compound as a white fluffy solid (18 mg, 82%) ^{1}H NMR (CD$_3$OD) δ (ppm) 5.9 (d, J = 2.0 Hz, 1H), 5.5(m, 1H) 4.22 (m, 2H) 4.07(m, 2H), 3.85 (m,

1H), 3.70(m, 1H), 3.5 (m, 2H), 2.03(s, 3H), 1.7(m, 2H), 1.38-1.56 (m, 8H), 0.9(m, 3H) ;

ESI-MS: 431.3 (M+H)$^{+}$.

High Performance Liquid Chromatography (HPLC)

HPLC experiments were performed on an Agilent Technologies (Palo Alto, CA) HPLC 1100 equipped with photodiode array detector and ChemStation for LC 3D software. Table 2.1 contains a summary of the HPLC method conditions used for each compound analyzed in this study. Injection volumes for all HPLC analyses ranged from 5 to 100 μL.

^{1}H Nuclear Magnetic Resonance (NMR) Spectroscopy

^{1}H NMR spectra of GS 4109, zanamivir heptyl ester, and related synthetic intermediates were recorded in CD$_3$OD (Cambridge Isotopes, Inc., Andover, MA) using a Varian (Palo Alto, CA) 500MHz NMR spectrometer.

Table 2.1: Summary of method conditions for HPLC analyses

Compound	Column	Column Temp (^{o}C)	Flow Rate (mL/min)	λ (nm)	Mobile Phase A	Mobile Phase B	Method
Enalaprilat	Zorbax (Aston, PA) SB-C$_8$ 150mm × 4.6mm 5 μm particle size	60	1.0	215	0.1% H$_3$PO$_4$	Acetonitrile	Isocratic 85:15 (v:v) A:B
GS 4109	Zorbax (Aston, PA) SB-C$_{18}$ 150mm × 4.6mm 5 μm particle size	Ambient	1.0	210	0.1% HFBA	Acetonitrile	Isocratic 65:35 (v:v) A:B
Metformin	Agilent (Palo Alto, CA) XDB-C$_{18}$ 150mm × 4.6mm 3.5 μm particle size	Ambient	0.5	233	50 mM NH$_4$ H$_2$PO$_4$	Methanol	Isocratic 100:0 (v:v) A:B for 10 minutes 50:50 (v:v) A:B for 10 minutes
Phenformin	Waters (Milford, MA) Symmetry C$_{18}$ 150mm × 4.6mm 3.5 μm particle size	Ambient	1.0	235	50 mM NH$_4$ H$_2$PO$_4$	Acetonitrile	Isocratic 85:15 (v:v) A:B for 10 minutes 50:50 (v:v) A:B for 10 minutes
Tenofovir	ES Industries (West Berlin, NJ) Hyperselect ODS-C$_{18}$ 100mm × 4.6mm 3.5 μm particle size	Ambient	1.0	260	1.5 mM TBAP 3.5 mM Na H$_2$PO$_4$	Methanol	Isocratic 85:15 (v:v) A:B for 10 minutes 30:70 (v:v) A:B for 10 minutes
Zanamivir esters (methyl, heptyl)	Agilent (Palo Alto, CA) XDB-C$_{18}$ 150mm × 4.6mm 5 μm particle size	Ambient	1.0	242	0.1% TFA	Acetonitrile	Isocratic 65:35 (v:v) A:B

TBAP = Tetrabutyl ammonium phosphate monobasic, HFBA = Heptafluorobutyric acid

Octanol-Buffer (pH 6.5) Partitioning Experiments

Solutions of each drug (50 μg/mL) were prepared in octanol saturated sodium phosphate buffer (50 mM, pH 6.5) with a molar excess of organic counterions (25 - 100X). These aqueous solutions were then equilibrated at 37 ^{o}C with an equivalent volume (0.5 mL) of buffer saturated octanol using magnetic stirring at 700 rpm for 24-36 hours. Three replicates of each determination were carried out to assess reproducibility. The octanol and aqueous phases were then separated by centrifugation. The total drug concentration in the aqueous phase, *[B$_t$]$_{aq}$*, was then determined by HPLC and the total drug concentration in the octanol phase, *[B$_t$]$_{oct}$*, was obtained by mass balance (i.e. *[B$_t$]$_{oct}$* = total drug put into system - [B$_t$]$_{aq}$). From these data, the apparent octanol/buffer (pH 6.5) distribution coefficient, *D$_B$* = *[B$_t$]$_{oct}$* / *[B$_t$]$_{aq}$*, is determined. Octanol-buffer (pH 6.5) distribution coefficients of the individual counterions without phenformin were also determined in triplicate using the above method.

Statistical Analysis

Values are expressed as the mean of at least 3 measurements, +/- the standard deviation (SD). Linear regression of the data using Equation 2.4 was carried out using SigmaPlot 2004 for Windows Version 9.01.

Results and Discussion

Octanol-Buffer (pH 6.5) Partitioning of the Ion-Pairs

The double reciprocal plots of the apparent octanol-buffer (pH 6.5) distribution coefficient of the drug as a function of counterion concentration are shown in Figures 2.1-2.12 for all of the ion-pairs studied in this work. The double reciprocal plots for all of the ion-pair systems gave highly linear results ($R^2 > 0.99$), indicating excellent agreement with the quasi-equilibrium transport model (Equation 2.4).
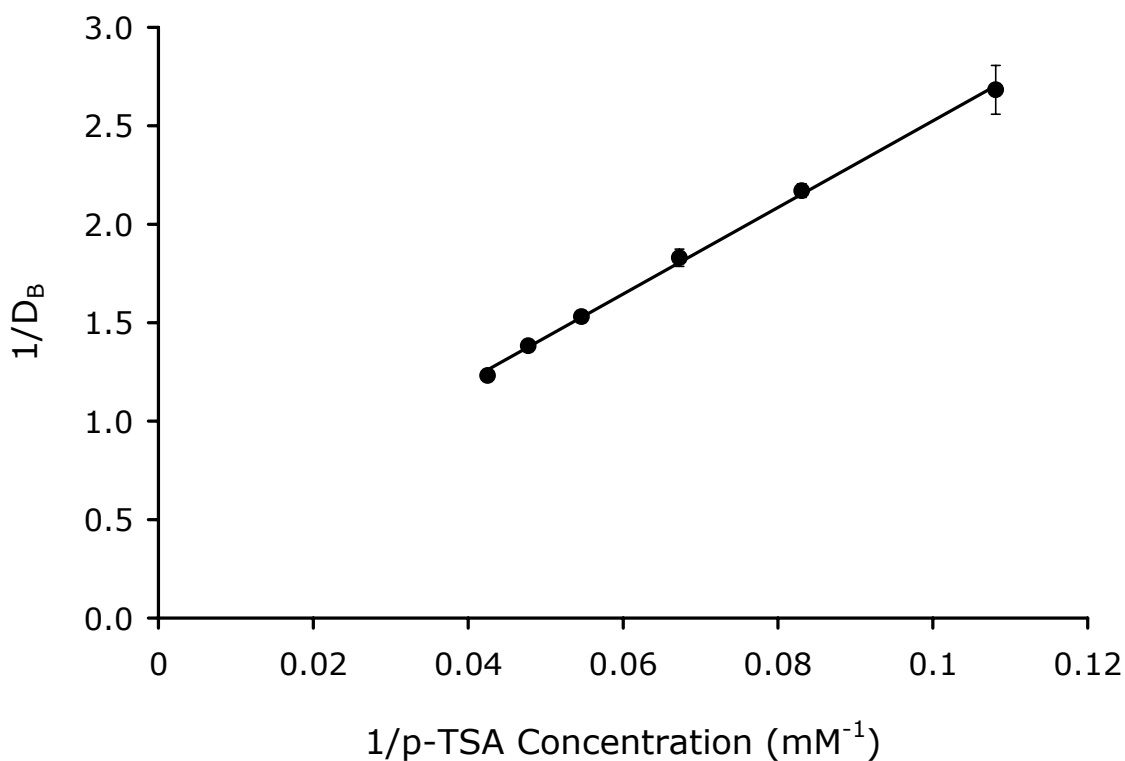
Figure 2.1: Double reciprocal plot of the apparent octanol-buffer (pH 6.5) distribution coefficient of phenformin as a function of *p*-toluene sulfonic acid concentration.
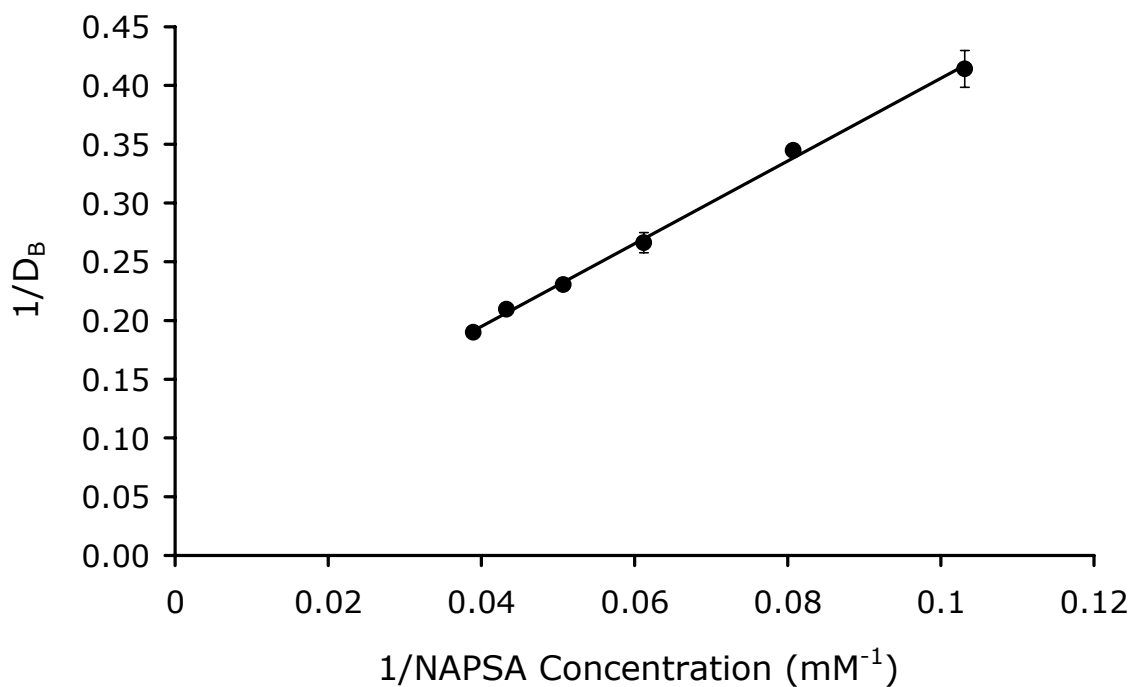
Figure 2.2: Double reciprocal plot of the apparent octanol-buffer (pH 6.5) distribution coefficient of phenformin as a function of 2-naphthalene sulfonic acid concentration.
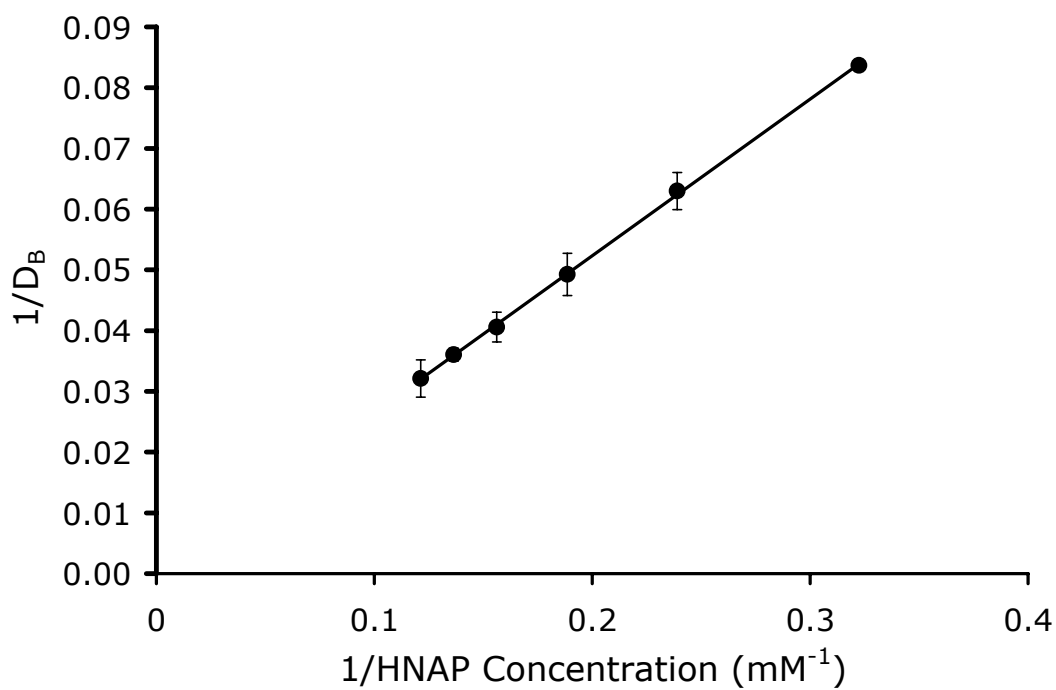
Figure 2.3: Double reciprocal plot of the apparent octanol-buffer (pH 6.5) distribution coefficient of phenformin as a function of 1-hydroxy-2-naphthoic acid concentration.
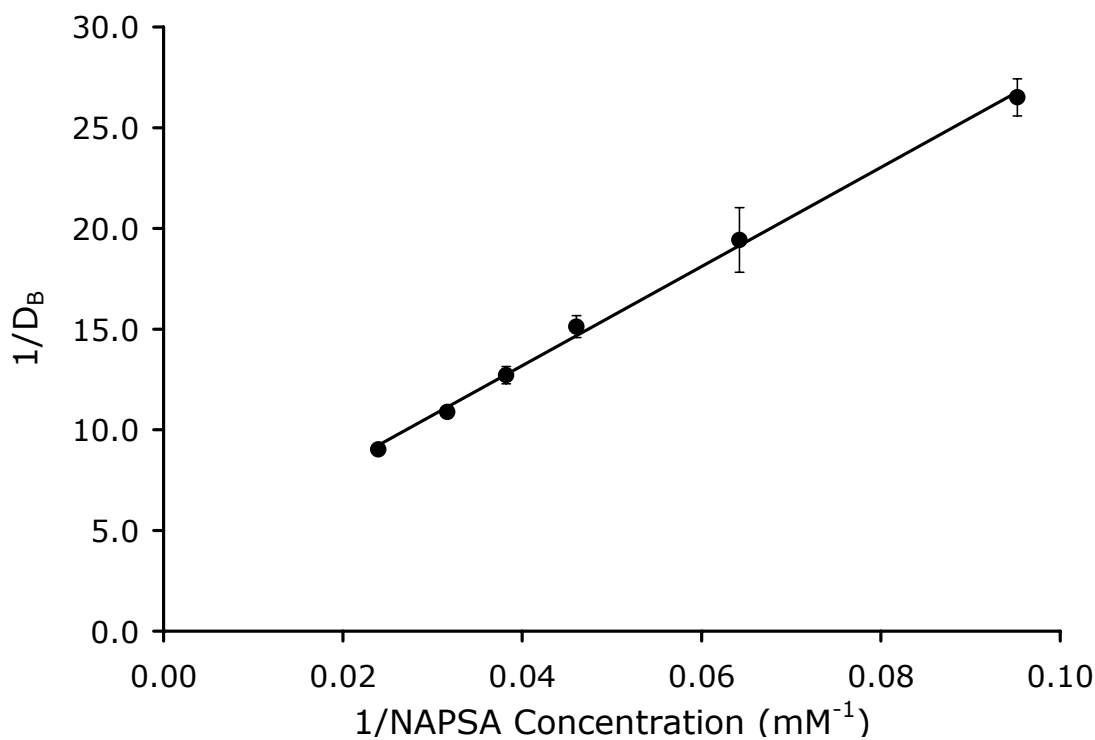
Figure 2.4: Double reciprocal plot of the apparent octanol-buffer (pH 6.5) distribution coefficient of metformin as a function of 2-naphthalene sulfonic acid concentration.
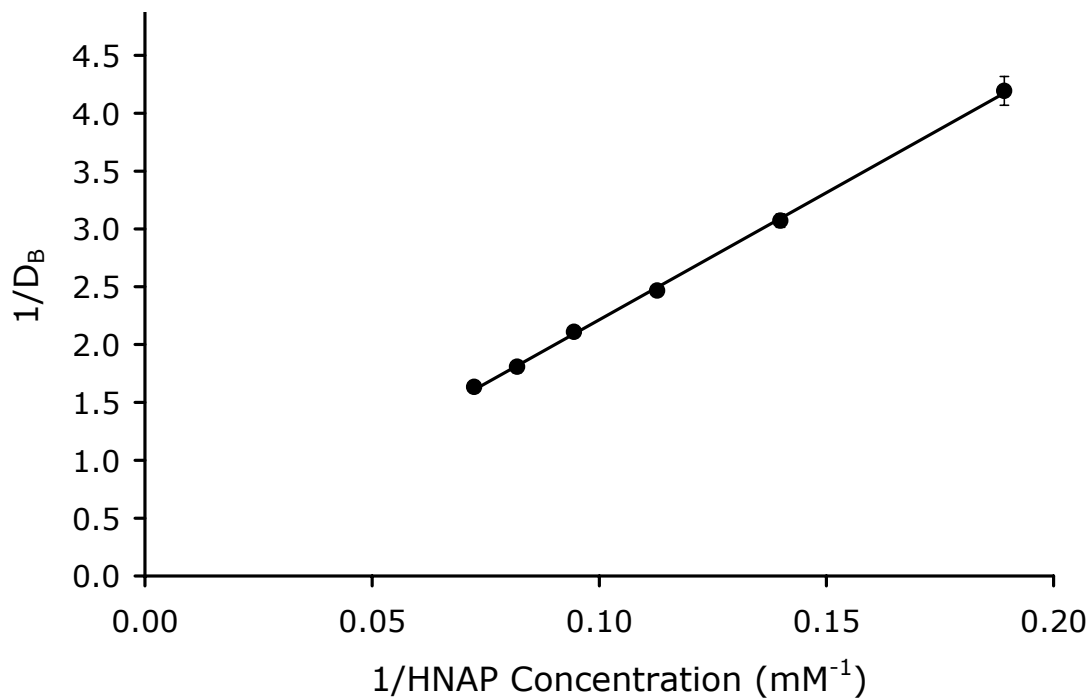
Figure 2.5: Double reciprocal plot of the apparent octanol-buffer (pH 6.5) distribution coefficient of metformin as a function of 1-hydroxy-2-naphthoic acid concentration.
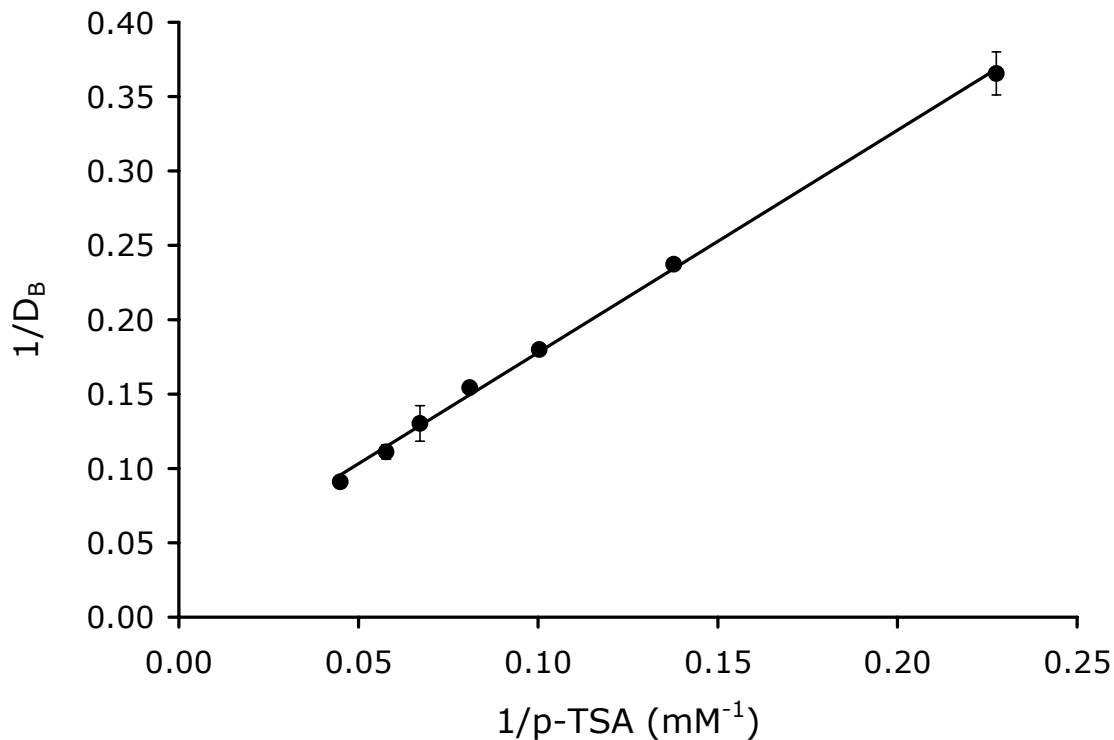
Figure 2.6: Double reciprocal plot of the apparent octanol-buffer (pH 6.5) distribution coefficient of GS 4109 as a function of *p*-toluene sulfonic acid concentration.
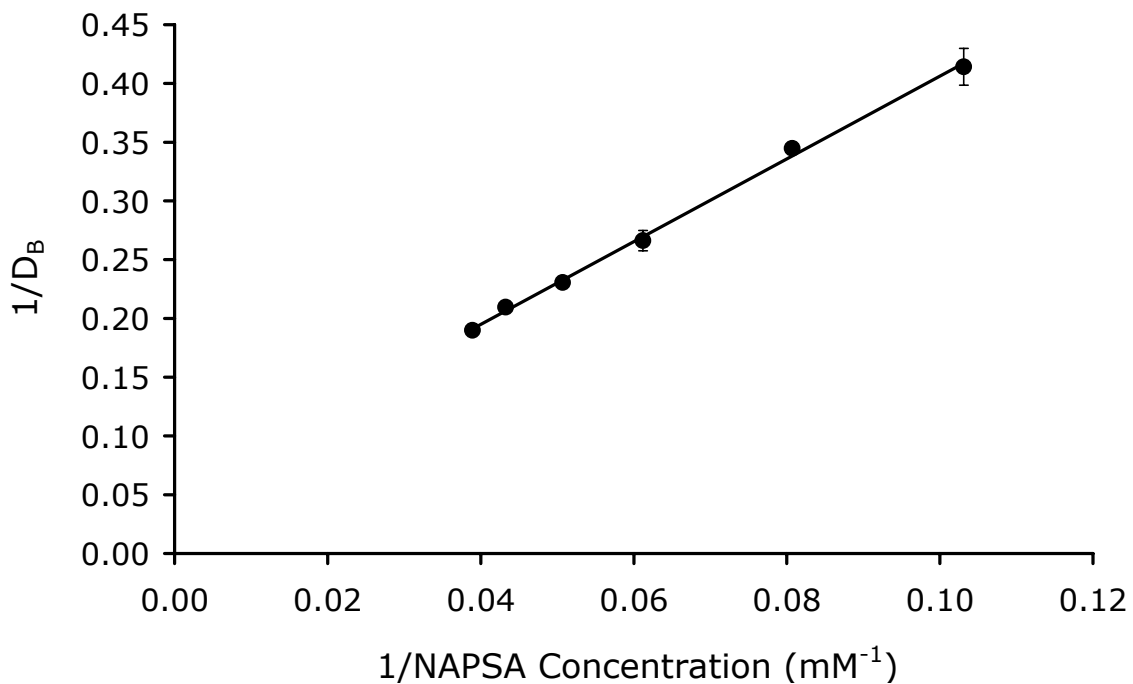
Figure 2.7: Double reciprocal plot of the apparent octanol-buffer (pH 6.5) distribution coefficient of GS 4109 as a function of 2-naphthalene sulfonic acid concentration.
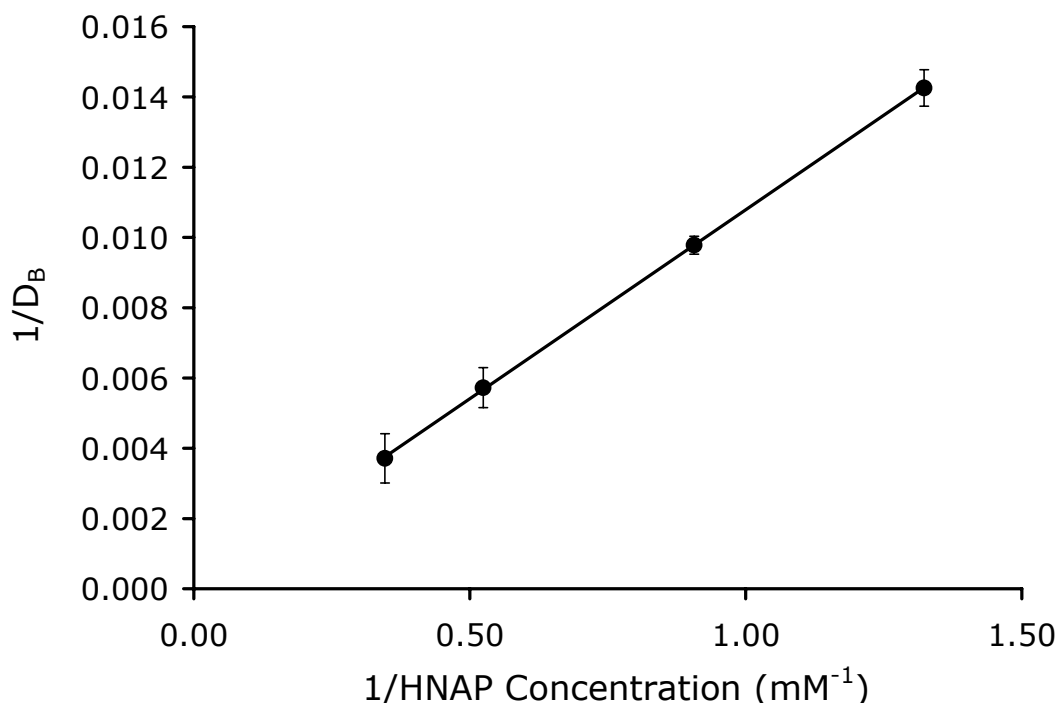
Figure 2.8: Double reciprocal plot of the apparent octanol-buffer (pH 6.5) distribution coefficient of GS 4109 as a function of 1-hydroxy-2-naphthoic acid concentration.
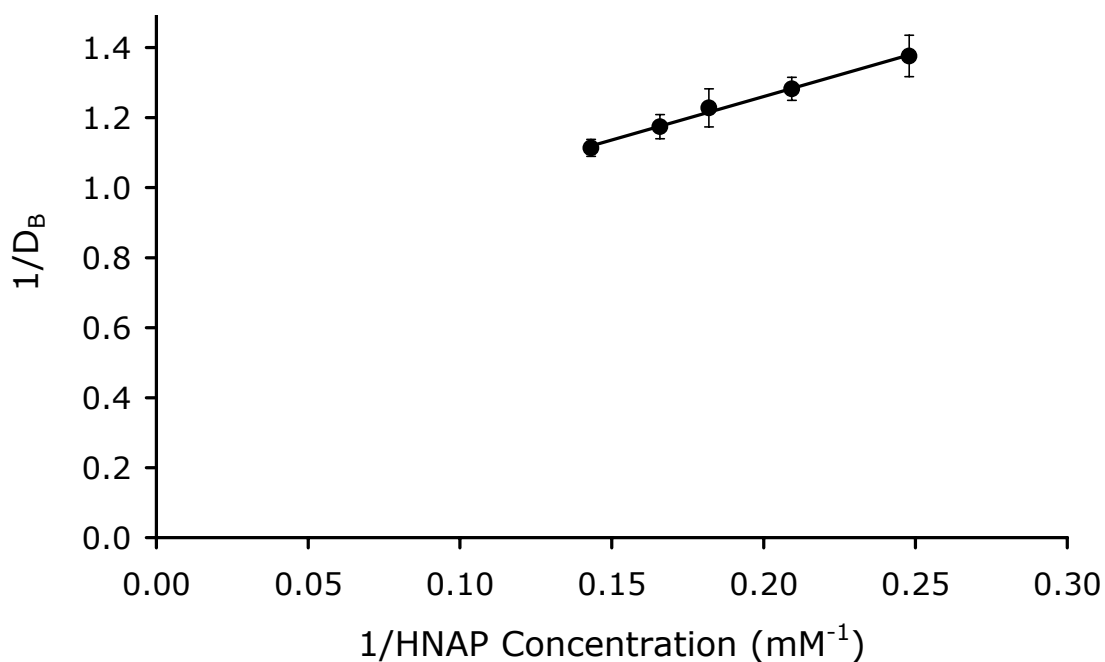
Figure 2.9: Double reciprocal plot of the apparent octanol-buffer (pH 6.5) distribution coefficient of zanamivir methyl ester as a function of 1-hydroxy-2-naphthoic acid concentration.
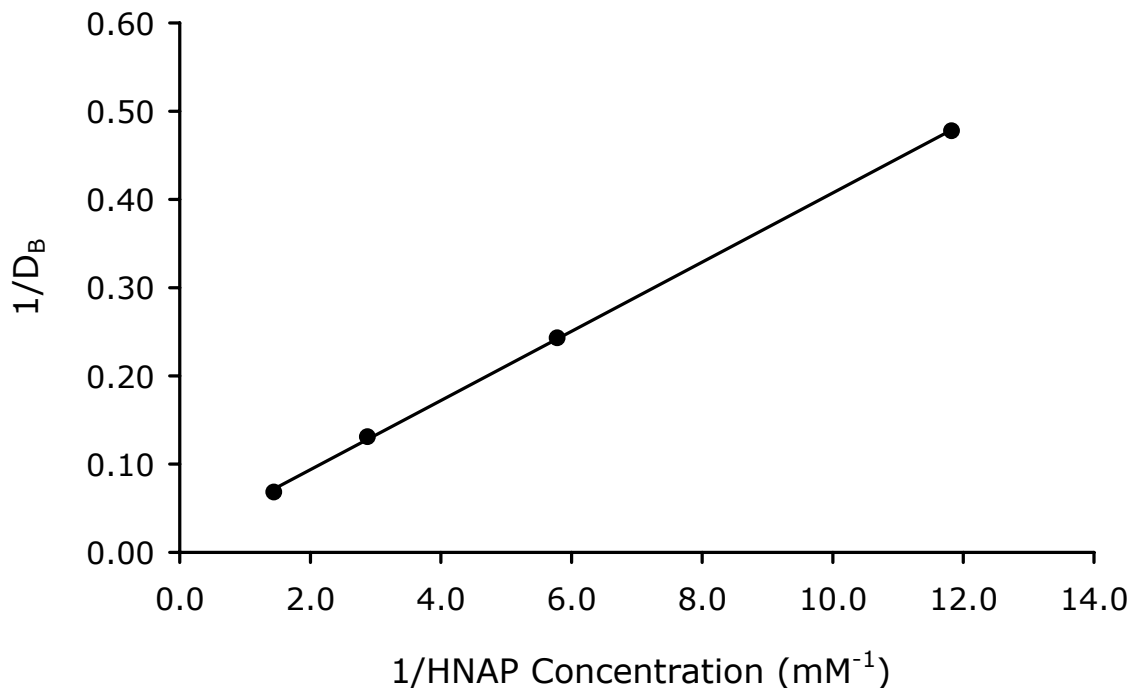
Figure 2.10: Double reciprocal plot of the apparent octanol-buffer (pH 6.5) distribution coefficient of zanamivir heptyl ester as a function of 1-hydroxy-2-naphthoic acid concentration.
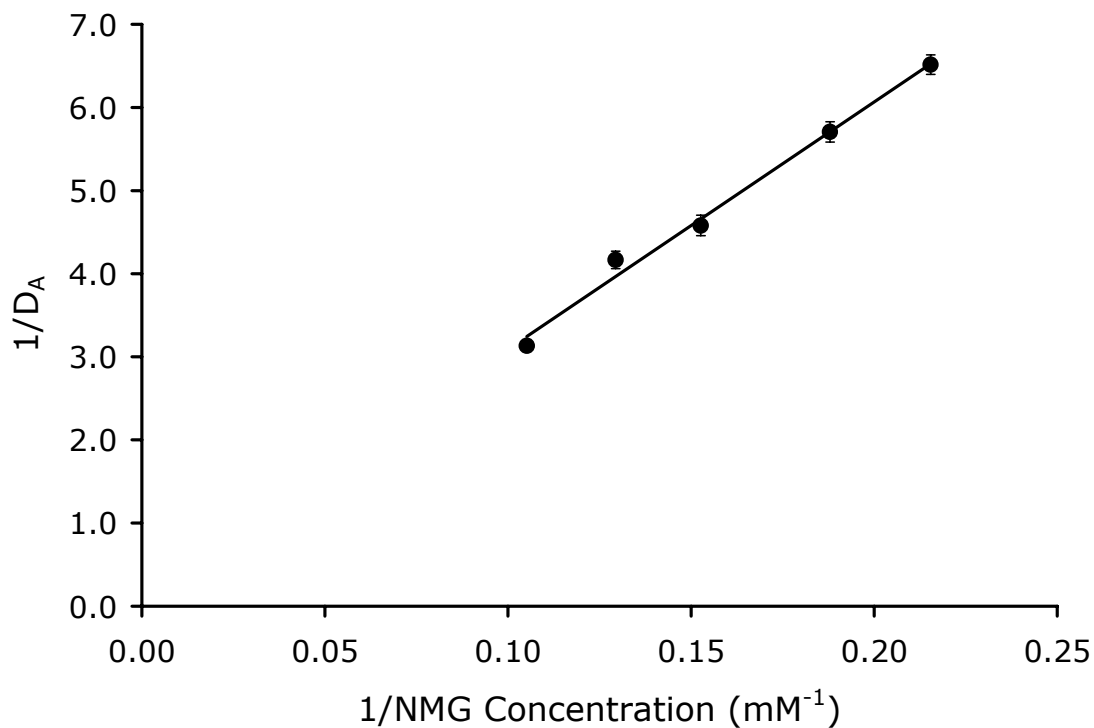
Figure 2.11: Double reciprocal plot of the apparent octanol-buffer (pH 6.5) distribution coefficient of enalaprilat as a function of 1-naphthylmethyl guanidine concentration.
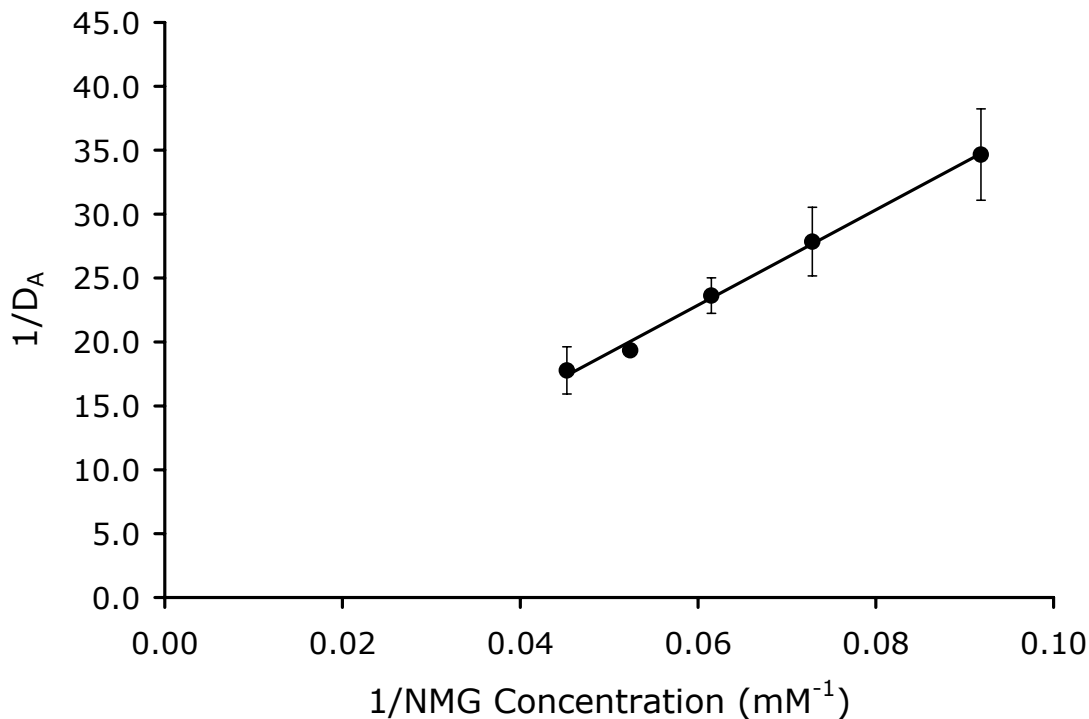
Figure 2.12: Double reciprocal plot of the apparent octanol-buffer (pH 6.5) distribution coefficient of tenofovir as a function of 1-naphthylmethyl guanidine concentration.

Binding Constants (K_{11}) of the Ion-Pairs

Table 2.2 summarizes the values of K_{11aq} for each ion-pair obtained via linear regression of the data using Equation 2.4. The observed values of K_{11aq} varied over a span of nearly 2 orders of magnitude, from a low of 0.86 M^{-1} for the metformin-HNAP ion-pair, to a high of 388 M^{-1} for the zanamivir heptyl ester-HNAP ion-pair.

Knowledge of the K_{11aq} enables calculation of the percentage of ion-pair in the aqueous phase at a given counterion concentration via Equation 2.1 (i.e. %$[AB]_{aq}$ = { $[AB]_{aq}$ / $[AB]_{aq}$ + $[B]_{aq}$ } x 100). A stronger K_{11aq} results in a higher %$[AB]_{aq}$ at a given counterion concentration. For example, Table 2.2 contains the %$[AB]_{aq}$ at counterion concentrations of 1 and 10 mM. The very weak aqueous binding constant for the metformin-HNAP ion-pair results in less than 1% $[AB]_{aq}$ at 1 and 10 mM counterion concentrations. On the other hand, the much stronger aqueous binding constant for the

38

zanamivir heptyl ester with HNAP results in a very high %$[AB]_{aq}$ of about 28% and nearly 80% at HNAP concentrations of 1 mM and 10 mM, respectively. Table 2.2 also contains the values of K_{11oct} for each of the ion-pairs, which were calculated via equation 2.6. Values of K_{11oct} greater than 10^4 M^{-1} were observed for all of the ion-pairs, indicating nearly 100% complexation in the octanol phase.

The magnitude of the binding constant reflects the strength of the interaction between the acid and base components of the ion-pair. The tightness of the ion-pair binding is governed primarily by the strength of the ionic bond. Additionally, other non-ionic interactions, namely hydrogen bonding, may also contribute to the overall strength of the ion-pair interaction. It follows that the magnitude K_{11aq} should be related to the number and strength of ionic and hydrogen bonds in the ion-pair. The difference in pK_a between the acid and base of the ion-pair (ΔcpK_a) should reflect the relative strength of the ionic bond of the ion-pair. Likewise, the number of hydrogen bond donor (HBD) and hydrogen bond acceptor (HBA) moieties in the acidic and basic components should reflect the relative number and strength of hydrogen bonds in the ion-pair. Table 2.3 contains the HBD, HBA, and cpKa values of the drug and counterion components of the ion-pairs. As shown in Figure 2.13, a fairly linear correlation ($R^2 = 0.840$) was found between the Log K_{11aq} values and the sum of HBD + HBA + ΔcpK_a of the ion-pairs. Even better linear correlations between Log K_{11aq} values and the sum of HBD + HBA + ΔcpK_a (Figure 2.13) were obtained when the ion-pairs were separated by drug class, GS 4109, zanamivir-esters ($R^2 = 0.994$) and metformin, phenformin ($R^2 = 0.951$). These simple empirical correlations have practical implications in the design of novel ion-pairs, as the

strength of the binding constant may be easily estimated from calculated properties

(HBD, HBA, cpK_a) of the individual drug and counterion components of the ion-pair.

Table 2.2: Summary of K_{11aq} and K_{11oct} values determined from octanol-buffer (pH 6.5) partitioning studies and calculated values of percent ion-pair in aqueous solution (%[AB]$_{aq}$) at 1 mM and 10 mM counterion concentration

Ion-pair	K_{11aq} (M^{-1})	%[AB]$_{aq}$ 1 mM	%[AB]$_{aq}$ 10 mM	K_{11oct} (M^{-1})
Metformin-HNAP	0.86	0.1%	0.9%	5.2E+05
Phenformin-HNAP	2.88	0.3%	2.8%	1.0E+05
GS 4109-HNAP	2.91	0.3%	2.8%	2.2E+05
Tenofovir-NMG	3.72	0.4%	3.6%	1.7E+07
Enalaprilat-NMG	3.90	0.4%	3.8%	1.1E+06
GS 4109-NAPSA	9.82	1.0%	8.9%	1.1E+06
Metformin-NAPSA	13.6	1.3%	11.9%	4.7E+06
Phenformin-p-TSA	14.9	1.5%	12.9%	6.9E+05
Phenformin-NAPSA	15.4	1.5%	13.3%	7.5E+05
GS 4109-p-TSA	19.0	1.9%	16.0%	9.0E+05
Zanamivir-OMe-HNAP	308	23.5%	75.5%	3.1E+08
Zanamivir-OHept-HNAP	388	28.0%	79.5%	4.8E+04

Table 2.3: Summary of K_{11aq} values determined from octanol-buffer (pH 6.5) partitioning studies and comparison with HBD, HBD, and cpK$_a$ values of drug and counterion

Ion-pair	K_{11aq} (M^{-1})	Drug (HBD+HBA)	Counterion (HBD+HBA)	Drug cpK$_a$	Counterion cpK$_a$
Metformin-HNAP	0.86	10	5	13.9	3.02
Phenformin-HNAP	2.88	11	5	12.7	3.02
GS 4109-HNAP	2.91	13	5	12.8	3.02
Tenofovir-NMG	3.72	9	7	4.11	12.3
Enalaprilat-NMG	3.90	10	7	3.46	12.3
GS 4109-NAPSA	9.82	13	4	12.8	0.27
Metformin-NAPSA	13.6	10	4	13.9	0.27
Phenformin-p-TSA	14.9	11	4	12.7	-0.43
Phenformin-NAPSA	15.4	11	4	12.7	0.27
GS 4109-p-TSA	19.0	13	4	12.8	-0.43
Zanamivir-OMe-HNAP	308	20	5	11.3	3.02
Zanamivir-OHept-HNAP	388	20	5	11.3	3.02
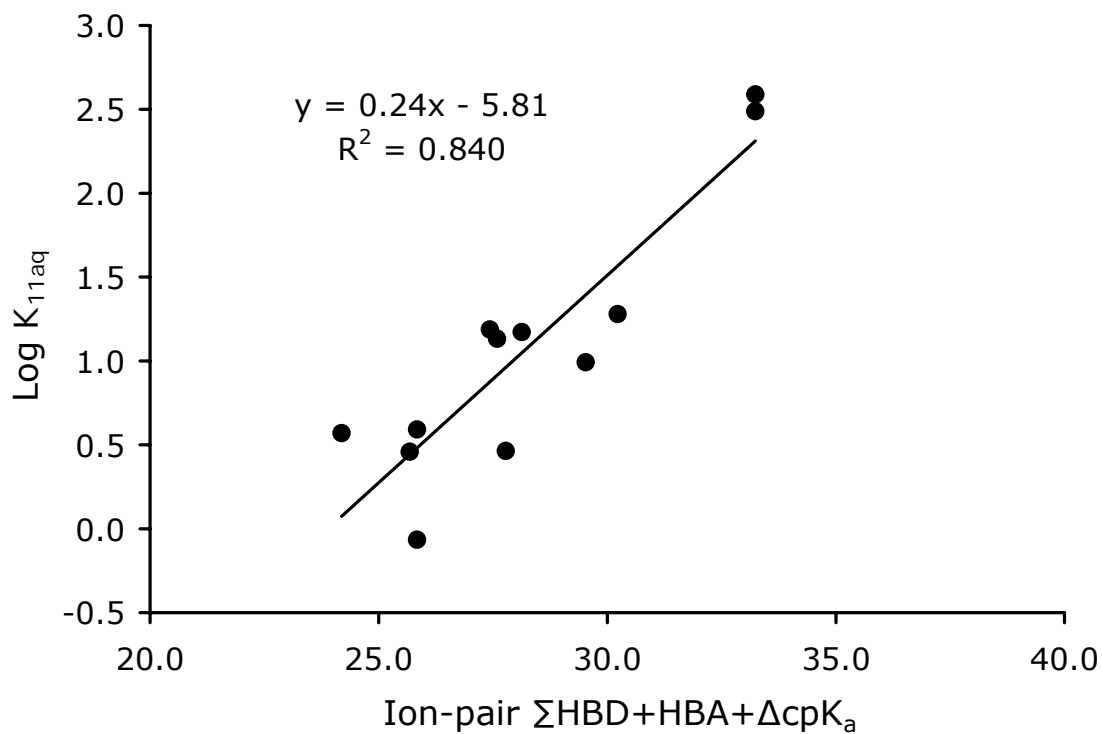
Figure 2.13: Linear correlation between Log K_{11aq} values and sum of ion-pair hydrogen bond donors (HBA) + ion-pair hydrogen bond acceptors (HBA) + difference in cpK_a of drug and counterion (ΔcpK_a). cpK_a was calculated using Advanced Chemistry Development (ACD/Labs) Software V8.14.
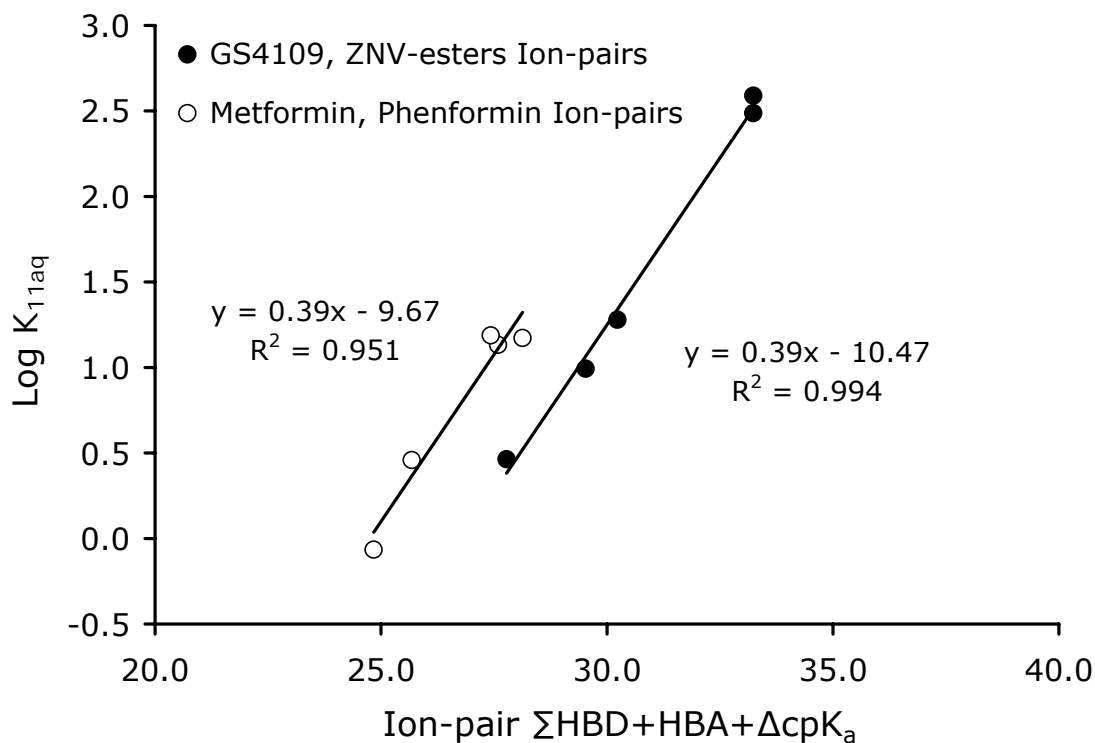
Figure 2.14: Linear correlations between Log K_{11aq} values of ●GS 4109, ZNV-esters ion-pairs and ○Metformin, Phenformin ion-pairs and sum of ion-pair hydrogen bond donors (HBA) + ion-pair hydrogen bond acceptors (HBA) + difference in cpK_a of drug and counterion (ΔcpK_a). cpK_a was calculated using Advanced Chemistry Development (ACD/Labs) Software V8.14.

Intrinsic Octanol-Buffer Partition Coefficients (P_{AB}) of the Ion-Pairs

Values of Log P_{AB} for each of the ion-pairs, obtained from linear regression of the octanol-buffer partitioning data via Equation 2.4, are summarized in Table 2.4. The values of Log P_{AB} varied over a range of 5 log units, with GS 4109-HNAP being the most lipophilic ion-pair with Log P_{AB} of 4.50 and metformin-NAPSA being the least lipophilic ion-pair with Log P_{AB} of -0.52. All of the ion-pairs showed enhanced lipophilicity as compared to the free drug. In general, the most lipophilic counterion HNAP provided the greatest increase in Log P_{AB} values. As shown in Figure 2.15, a simple empirical correlation was found between the experimentally determined Log P_{AB} values and the

sum of drug and counterion cLogP values (Table 2.4) calculated using Advanced

Chemistry Development (ACD/Labs) Software V8.14. As with the empirical correlations

to predict Log K_{11aq} (Figures 2.13-2.14), this correlation has practical implications, as it

shows that an initial estimate of Log P_{AB} may be obtained for any ion-pair combination

by simply summing the cLogP values the of the individual acidic and basic components.

Table 2.4: Summary of Log P_{AB} values determined from octanol-buffer (pH 6.5) partitioning studies and comparison with $\sum$ cLog P values of drug + counterion

Ion-pair	Log P_{AB}	Drug cLog P	Counterion cLog P	$\sum$ cLog P (Drug + Counterion)
Metformin-NAPSA	-0.52	-2.31	1.70	-0.61
Tenofovir-NMG	-0.13	-1.71	1.52	-0.19
Zanamivir-OMe-HNAP	0.12	-3.86	3.29	-0.57
Phenformin-p-TSA	0.49	-0.60	0.93	0.33
Enalaprilat-NMG	0.94	-1.10	1.52	0.42
Phenformin-NAPSA	1.27	-0.60	1.70	1.10
GS 4109-p-TSA	1.55	0.83	0.93	1.76
Metformin-HNAP	1.72	-2.31	3.29	0.98
Zanamivir-OHept-HNAP	1.89	0.69	3.29	3.98
GS 4109-NAPSA	2.69	0.83	1.70	2.53
Phenformin-HNAP	3.13	-0.60	3.29	2.69
GS 4109-HNAP	4.50	0.83	3.29	4.12
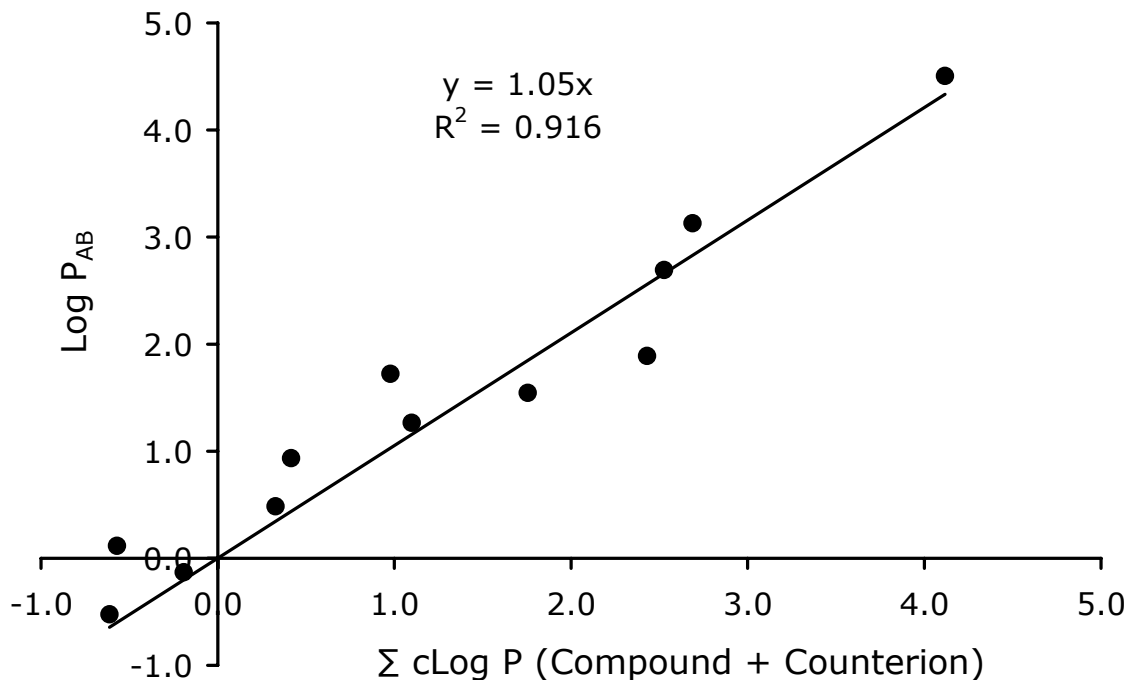
Figure 2.15: Linear correlation between Log P_{AB} and sum of compound and counterion cLogP calculated using Advanced Chemistry Development (ACD/Labs) Software V8.14.

Conclusions

In this work, a quasi-equilibrium transport model has been developed to describe the effect of lipophilic ion-pairing agents on the apparent log D of several highly polar drugs. Values of K_{11aq}, K_{11oct}, and Log P_{AB} for the ion-pairs were obtained by fitting this quasi-equilibrium transport model (Equation 2.4) to double reciprocal plots of D as a function of counterion concentration. Two simple empirical correlations between were found: 1) a linear correlation between Log K_{11aq} and the sum of HBD + HBA + ΔcpK_a of the ion-pairs and 2) a linear correlation between Log P_{AB} and the sum of cLogP of the drug and counterion, revealing that K_{11aq} and Log P_{AB} could easily be estimated from calculated properties of the individual components of the ion-pair.

Based on this work, several key attributes for successful ion-pair mediated membrane transport may be proposed. Lipophilic counterions that provide Log P_{AB}

values in the range of 2-5 may be required to provide sufficient lipophilicity to achieve membrane transport. Initial estimates of Log P_{AB} may be easily obtained by simply summing the cLogP values of the individual acid and base components. Strong K_{11aq} values, perhaps on the order of 100 or 1000 M^{-1} may be necessary for the ion-pair to stay intact during the entire membrane transport process and to prevent ion exchange with competing endogenous ions (e.g. phosphatidylserine, phosphatidylinositol, sialic acid, bile acids) as well as to enable ion-pair mediated transport at relatively low counterion concentrations. Finally, lipophilic counterions that by themselves have significant membrane permeability may be required to provide high counterion concentrations within the membrane and therefore minimize ion-exchange of the ion-pair with competing endogenous ions. The *in-vitro* and *in-vivo* ion-pair mediated membrane transport studies described in Chapter III of this thesis will test these proposed criteria.

CHAPTER THREE

ION-PAIR FACILITATED ORAL ABSORPTION: QUASI-EQUILIBRIUM ANALYSIS OF THE ION-PAIR MEDIATED MEMBRANE TRANSPORT OF LOW-PERMEABILITY DRUGS

Theory

Quasi-Equilibrium Analysis of Ion-pair Mediated Membrane Permeation

Consider the rate of permeation, J_{AB}, of an ion-pair through a membrane separating an aqueous donor solution containing the ion-pair and an aqueous receiver solution containing neat solvent. Assuming quasi-equilibrium conditions, J_{AB} can be described by the following equation (Higuchi, 1960; Higuchi, 1977; Duffey *et. al.*, 1978):

$$ J_{AB} = \frac{P_{AB} \ [AB]_{aq} \mathcal{D}_{AB} \ A}{L} \qquad \text{(Equation 3.1)} $$

Where $[AB]_{aq}$ represents the concentration of the ion-pair in the aqueous donor phase, $\mathcal{D}_{AB}$ is the diffusivity of the ion-pair in the membrane, A is the cross sectional area of the membrane, and L is the thickness of the membrane.

The intrinsic membrane/aqueous partition coefficient of the ion pair, P_{AB}, can be described by the following equation:

$$ P_{AB} = \frac{[AB]_{mem}}{[AB]_{aq}} \qquad \text{(Equation 3.2)} $$

Where $[AB]_{mem}$, represents the concentration of the ion-pair in the membrane.

Likewise, the apparent membrane/aqueous distribution coefficient of the organic acid, D_A and base, D_B can be described by the following equations:

$$D_A = \frac{[A]_{mem}}{[A]_{aq}}$$ (Equation 3.3)

$$D_B = \frac{[B]_{mem}}{[B]_{aq}}$$ (Equation 3.4)

Where $[A]_{mem}$ is the concentration of organic acid in the membrane, $[A]_{aq}$ is the concentration of organic acid in the aqueous donor phase, $[B]_{mem}$ is the concentration of organic base in the membrane, and $[B]_{aq}$ is the concentration of organic base in the aqueous donor phase.

The association constant for ion-pair formation in the membrane, K_{11mem}, can be expressed as:

$$K_{11_{mem}} = \frac{[AB]_{mem}}{[A]_{mem}[B]_{mem}}$$ (Equation 3.5)

Equations 3.1-3.5 can be combined to express the J_{AB} dependence on $[A]_{aq}$ and $[B]_{aq}$:

$$\log J_{AB} = \log[A]_{aq} + \log[B]_{aq} + \log\left(\frac{K_{11mem}D_A D_B \mathcal{D}_{AB} A}{L}\right)$$ (Equation 3.6)

When $[A]_{aq} = [B]_{aq}$, Equation 3.6 becomes:

$$\log J_{AB} = 2\log[A]_{aq} + \log\left(\frac{K_{11mem}D_A D_B \mathcal{D}_{AB} A}{L}\right)$$ (Equation 3.7)

Since the permeability of the ion-pair, $P_{app\,AB} = J_{AB} / [B]_{aq} A$, Equation 3.6 can be re-written to express the $P_{app\,AB}$ dependence on $[A]_{aq}$:

$$\log P_{app\,AB} = \log[A]_{aq} + \log\left(\frac{K_{11mem}D_A D_B \mathcal{D}_{AB}}{L}\right)$$ (Equation 3.8)

Thus, a log-log plot of *J* or P_{app} versus counterion concentration should give a slope of 1 as per Equations 3.6 and 3.8. Likewise, when *[A]$_{aq}$ = [B]$_{aq,}$* a log-log plot of *J* versus counterion concentration should give a slope of 2 as per Equation 3.7. Equations 3.6-3.7 are similar in form to those previously derived by Duffey *et. al.*, (1978) describing the flux of tetrabuytlammonium nitrate through liquid membranes of n-heptyl cyanide.

Materials and Methods

Materials

Phenformin hydrochloride was obtained from Waterstone Technologies (Carmel, IN). Sodium 2-naphthalenesulfonate was obtained from Fluka (Buchs, Switzerland). 1-hydroxy-2-naphthoic acid, *p*-toluenesulfonic acid monohydrate, 1-octanol, dodecane, and 1-dodecanol were obtained from Sigma-Aldrich (St. Louis, MO). All compounds were of the highest available quality and were used as received. GS 4109 and Zanamivir heptyl ester were synthesized as described in the Materials section of Chapter II of this thesis.

High Performance Liquid Chromatography (HPLC)

HPLC experiments were performed on an Agilent Technologies (Palo Alto, CA) HPLC 1100 equipped with photodiode array detector and ChemStation for LC 3D software. Phenformin and counterions were assayed using a 150mm × 4.6mm Waters (Milford, MA) Symmetry C$_{18}$ column with 3.5 μm particle size. The detection wavelength was 235 nm. The mobile phase consisted of 85:15 (v:v) 50 mM ammonium phosphate monobasic in water: acetonitrile and was pumped at a flow rate of 1.0 ml/min. Enalaprilat and metoprolol were assayed using a Zorbax (Aston, PA) XDB-C$_{18}$ column

with 5 μm particle size. The column temperature was held at 60 $^{\circ}$C and the detection wavelength was 215 nm. The mobile phase consisted of 85:15 (v:v) 0.1% phosphoric acid in water: acetonitrile and was pumped at a flow rate of 1.0 ml/min. GS 4109 was assayed using a 150mm × 4.6mm Zorbax (Aston, PA) SB-C$_{18}$ column with 5 μm particle size. The detection wavelength was 210 nm. The mobile phase consisted of 65:35 (v:v) 0.1% heptafluorobutyric acid in water: acetonitrile and was pumped at a flow rate of 1.0 ml/min. Zanamivir heptyl ester was assayed using a 150mm × 4.6mm Agilent (Palo Alto, CA) XDB-C$_{18}$ column with 5 μm particle size. The detection wavelength was 242 nm. The mobile phase consisted of 65:35 (v:v) 0.1% trifluoroacetic acid in water: acetonitrile and was pumped at a flow rate of 1.0 ml/min. Injection volumes for all HPLC analyses ranged from 5 to 100 μL.

Parallel Artificial Membrane Permeation Assay (PAMPA)

PAMPA has been shown to be a valuable tool in the study of the passive membrane permeation of many drugs (Kansy *et. al.*, 1998; Wohnsland and Faller, 2001). PAMPA was employed here to characterize the ion-pair mediated membrane permeation of phenformin. Solutions of phenformin with 1-hydroxy-2-naphthoic acid (1:1 molar ratio) were prepared at concentrations of 0.5, 1.0, 2.5, and 5.0 mM in 50 mM sodium phosphate buffer (pH 6.5). PAMPA experiments were carried out in Millipore (Danvers, MA) 96-well MultiScreen-IP filter plates with 0.3 cm^2 PVDF filter support (0.45 μm). The filter supports in each well were first impregnated with 5 μL of the liquid PAMPA membrane which consisted of 90:10 (w:w) dodecane:dodecanol. The donor wells were then loaded with 0.15 mL of the phenformin-HNAP solution and each receiver well was

loaded with 0.3 mL of 50 mM sodium phosphate buffer pH 6.5. Five wells were loaded at each phenformin-HNAP concentration to enable collection of a well at times points of 30, 60, 90, 120, and 150 minutes and each experiment was repeated 3 times for a total of 15 wells per phenformin-HNAP concentration. The donor plate was then placed upon the 96-well receiver plate and the resulting PAMPA sandwich was incubated at 37 $^{\circ}$C on an orbital shaker rotating at 50 rpm. Receiver plate wells (n=3 for each phenformin-HNAP concentration) were then collected every 30 minutes over 2.5 hours and the phenformin concentration in each well was determined by HPLC. The PAMPA permeability of metoprolol at a concentration of 1 mM was also determined in triplicate as a positive control. In order to assess the effect of HNAP counterion on the integrity of the PAMPA membrane, the membrane flux of the poorly permeable acidic compound enalaprilat was also determined in the presence of 5 mM HNAP as a negative control.

Caco-2 Cell Monolayer Assay

Caco-2 cells (passage 22-25) from American Type Culture Collection (Rockville, MD) were routinely maintained in Dulbecco's modified Eagle's medium (DMEM, Invitrogen Corp., Carlsbad, CA) containing 10% fetal bovine serum, 1% nonessential amino acids, 1 mM sodium pyruvate, and 1% L-glutamine. Cells were grown in an atmosphere of 5% CO_2 and 90% relative humidity at 37°C. The DMEM medium was replaced by fresh medium every three days. Cells were passaged upon reaching approximately 80% confluence using 4 ml trypsin-EDTA (Invitrogen Corp., Carlsbad, CA).

Transepithelial transport studies were performed using a method described previously with minor modifications (Dahan and Amidon, 2009). Briefly, 8×10^4 cells/cm^2 were seeded onto collagen-coated membranes (12-well Transwell plate, 0.4-μm pore size, 12 mm diameter, Corning Costar, Cambridge, MA) and were allowed to grow for 21 days in order to obtain differentiated monolayers. TEER measurements were performed on the monolayers before and after the experiments (Millicell-ERS epithelial Voltohmmeter, Millipore Co., Bedford, MA). Monolayers with TEER values >300 Ωcm^2 were used for the study. On the day of the experiment, the DMEM was removed, and the monolayers were rinsed and incubated for 20 minutes with a blank transport buffer. The apical transport buffer contained 1 mM CaCl$_2$, 0.5 mM MgCl$_2 \cdot$6H$_2$O, 145 mM NaCl, 3 mM KCl, 5 mM D-glucose, and 10 mM sodium phosphate buffer pH 6.5. The basolateral transport buffer was identical to the apical, except the 10 mM sodium phosphate buffer was pH 7.4. Following the 20 minute incubation, blank transport buffer was removed from the apical side and replaced by 0.5 ml of the drug (phenformin, GS 4109, or zanamivir heptyl ester) solution in the uptake buffer (pH 6.5), with HNAP concentrations ranging from 0 to 24 mM. The basolateral side was loaded with 1.5 mL of pH 7.4 transport buffer. Throughout the experiment, the transport plates were kept in a shaking incubator (50 rpm) at 37°C. Samples were taken from the receiver side at various time points up to 120 min (200 μL from basolateral side) and 200 μL of blank transport buffer was added following each sample withdrawal. At the last time point (120 min), sample was taken from the donor side as well, in order to confirm mass balance. Samples were immediately assayed for drug content by HPLC. TEER measurements were carried out after each transport study to assess Caco-2 monolayer confluence. Lucifer yellow

permeability was determined in the presence of 0, 12, and 24 mM HNAP to assess the influence of counterion on Caco-2 monolayer integrity.

Permeability coefficients (P_{app}) across Caco-2 cell monolayers were calculated from the linear plot of drug accumulated in the receiver side versus time, using the following equation:

$$P_{app} = \frac{1}{C_0 A} \times \frac{dQ}{dt} \qquad \text{(Equation 3.9)}$$

where dQ/dt is the steady-state appearance rate of the drug on the receiver side, C_0 is the initial concentration of the drug in the donor side, and A is the monolayer growth surface area (1.12 cm^2). Linear regression was carried out to obtain the steady-state appearance rate of the drug on the receiver side.

Rat Jejunal Perfusion

All animal experiments were conducted using protocols approved by the University Committee of Use and Care of Animals (UCUCA), University of Michigan, and the animals were housed and handled according to the University of Michigan Unit for Laboratory Animal Medicine guidelines. Male albino Wistar rats (Charles River, IN) weighing 250-280 g were used for all perfusion studies. Prior to each experiment, the rats were fasted overnight (12-18 h) with free access to water. Animals were randomly assigned to the different experimental groups.

The procedure for the *in-situ* single-pass intestinal perfusion followed previously published reports (Amidon *et. al.*, 1988, Lipka *et. al.*, 1995, Kim *et. al.*, 2006). Briefly, rats were anesthetized with an intramuscular injection of 1 mL/kg of ketamine-xylazine solution (9%:1%, respectively) and placed on a heated surface maintained at 37 °C

(Harvard Apparatus Inc., Holliston, MA). The abdomen was opened by a midline incision of 3-4 cm. A proximal jejunal segment (3 ± 1 cm average distance of the inlet from the ligament of Treitz) of approximately 10 cm was carefully exposed and cannulated on two ends with flexible PVC tubing (2.29 mm i.d., inlet tube 40 cm, outlet tube 20 cm, Fisher Scientific Inc., Pittsburgh, PA). Care was taken to avoid disturbance of the circulatory system and the exposed segment was kept moist with 37 °C normal saline solution. Solutions of the test drug (phenformin, GS 4109, or zanamivir heptyl ester) were prepared with HNAP at concentrations of 0 and 4-12 mM in the perfusate buffer. The perfusate buffer consisted of 1 mM $CaCl_2$, 0.5 mM $MgCl_2 \cdot 6H_2O$, 145 mM NaCl, 3 mM KCl, 5 mM D-glucose, and 10 mM sodium phosphate buffer pH 6.5 and 0.05 mg/mL phenol red. Phenol red was added to the perfusion buffer as a non-absorbable marker for measuring water flux. All perfusate solutions were incubated in a 37 °C water bath to maintain temperature and were pumped through the intestinal segment (Watson Marlow Pumps 323S, Watson- Marlow Bredel Inc., Wilmington, MA). The isolated segment was first rinsed with blank perfusion buffer, pH 6.5, at a flow rate of 0.5 mL/min in order to clean out any residual debris. At the start of the study, the test solutions were perfused through the intestinal segment at a flow rate of 0.2 mL/min. The perfusion buffer was first perfused for one hour, in order to ensure steady state conditions (as also assessed by the inlet over outlet concentration ratio of phenol red which approaches 1 at steady state). After reaching steady state, samples were taken in 10 min intervals for one hour (10, 20, 30, 40, 50, and 60 min). All samples, including perfusion samples at different time points, original drug solution, and inlet solution taken at the exit of the syringe, were

immediately assayed by HPLC. Following the termination of the experiment, the length of each perfused jejunal segment was accurately measured.

The net water flux in the single-pass rat jejunal perfusion studies, resulting from water absorption in the intestinal segment, was determined by measurement of phenol red, a non-absorbed, non-metabolized marker. The measured C_{out}/C_{in} ratio was corrected for water transport according to the following equation:

$$\frac{C'_{out}}{C'_{in}} = \frac{C_{out}}{C_{in}} \times \frac{C_{in\ phenol.red}}{C_{out\ phenol.red}}$$
(Equation 3.10)

where C_{out} is the concentration of the test drug in the outlet sample, C_{in} is the concentration of the test drug in the inlet sample, $C_{in\ phenol\ red}$ is the concentration of phenol red in the inlet sample, and $C_{out\ phenol\ red}$ is the concentration of phenol red in the outlet sample. The effective permeability (P_{eff}) through the rat gut wall in the single-pass intestinal perfusion studies was determined assuming the "plug flow" model expressed in the following equation (Fagerholm *et. al.,* 1996):

$$P_{eff} = \frac{-Q\ln(C'_{out} / C'_{in})}{2\pi RL}$$
(Equation 3.11)

where Q is the perfusion buffer flow rate, C'_{out}/C'_{in} is the ratio of the outlet concentration and the inlet or starting concentration of the tested drug that has been adjusted for water transport via Equation 3.10, R is the radius of the intestinal segment (set to 0.2 cm), and L is the length of the intestinal segment.

Statistical Analysis

Values are expressed as the mean of at least 3 measurements, +/- the standard deviation (SD). Linear regression of the data using Equation 2.4 was carried out using SigmaPlot 2004 for Windows Version 9.01.

Results and Discussion

Ion-pair Mediated Transport in PAMPA Model

The phenformin ion-pairs were tested in a PAMPA model with 90:10 (w:w) dodecane:dodecanol hydrophobic liquid membrane. No detectable increase in flux was observed for *p*-TSA and NAPSA ion-pairs with phenformin in the PAMPA model. This suggests that the phenformin-*p*-TSA (log P_{AB} 0.49) and phenformin-NAPSA (log P_{AB} 1.27) ion-pairs do not provide sufficient lipophilicity to facilitate flux of phenformin across the PAMPA membrane. However, the phenformin-HNAP (log P_{AB} 3.13) ion-pair showed significant enhancement in flux in the PAMPA model as compared to phenformin alone (Table 3.1). Figure 3.1 shows the dependence of phenformin flux on phenformin-HNAP concentration (0.5, 1.0, 2.5, and 5.0 mM) in the PAMPA model. Mass transport was linear with time at all phenform-HNAP concentrations, indicating that the integrity of the liquid membrane was satisfactory. Phenformin flux increased with phenformin-HNAP concentration, consistent with an ion-pair transport mechanism. Figure 3.2 contains a log-log plot of phenformin flux versus HNAP concentration. A linear relationship with a slope near 2 was obtained, consistent with the quasi-equilibrium transport model expressed in Equation 3.7, thus further supporting an ion-pair mediated transport mechanism.
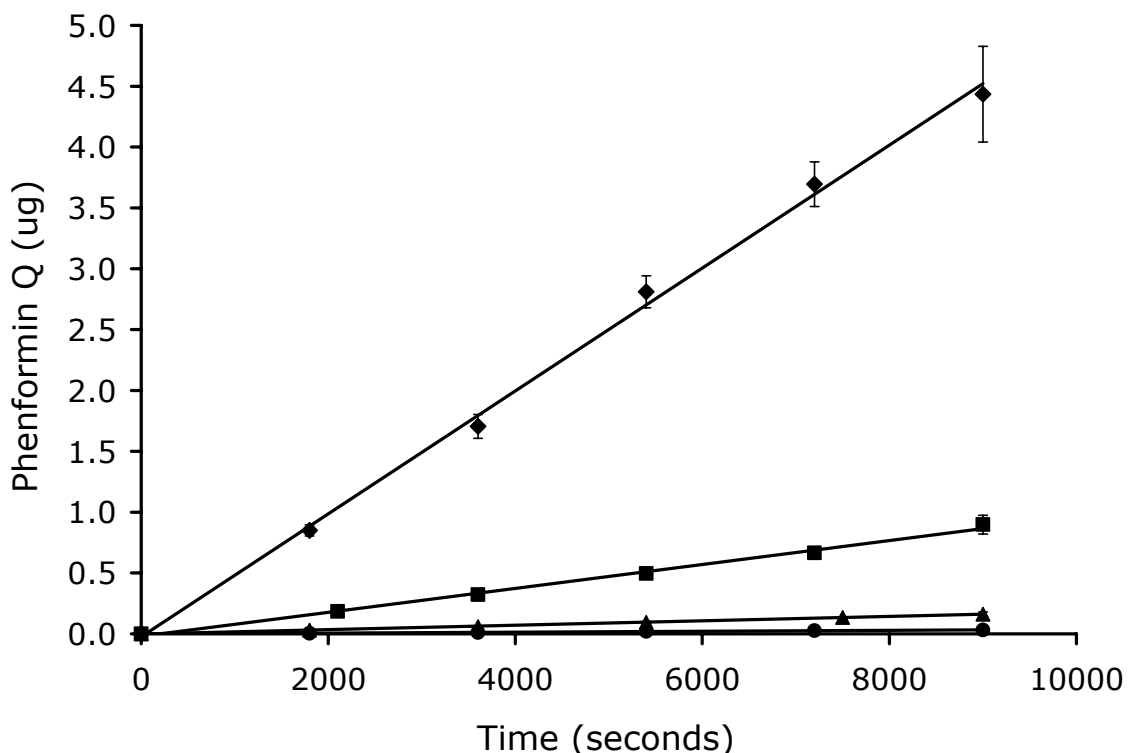
Figure 3.1: Dependence of phenformin flux on phenformin-HNAP concentration in PAMPA experiments; (♦) 5.0 mM phenformin-HNAP, (■) 2.5 mM phenformin-HNAP, (▲) 1.0 mM phenformin-HNAP and (●) 0.5 mM phenformin-HNAP
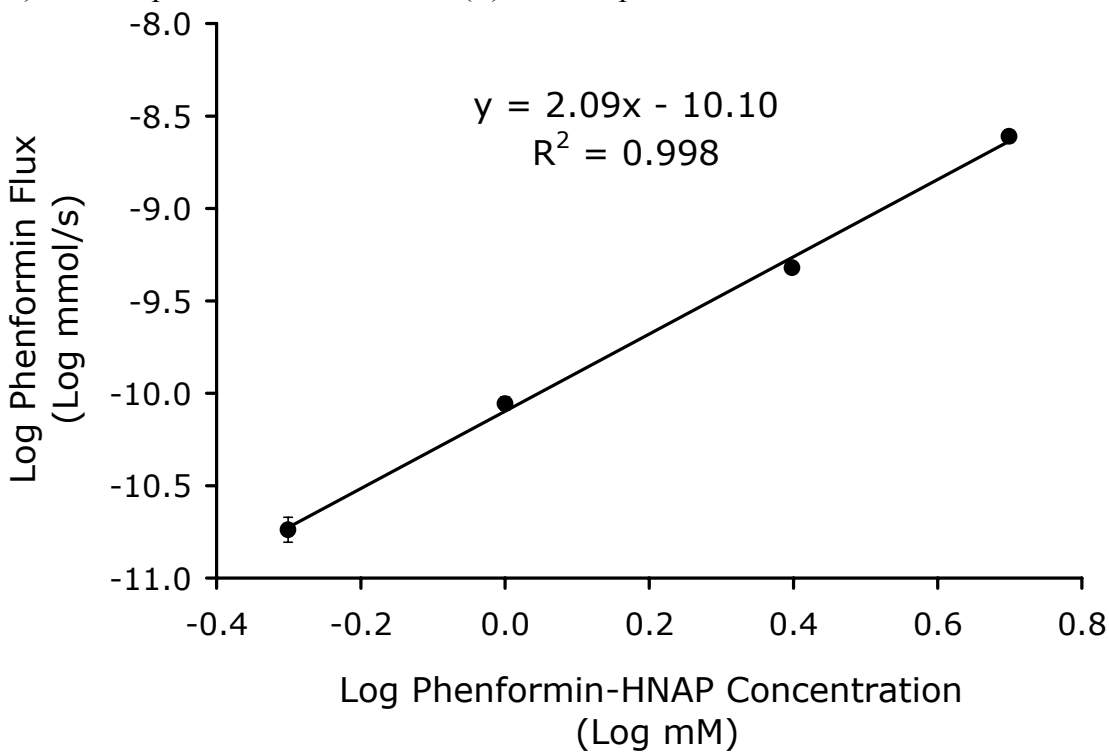
Figure 3.2: Log phenformin flux versus Log phenformin-HNAP concentration in PAMPA experiments. Linear relationship with a slope near 2 is consistent with an ion-pair mediated transport mechanism as per Equation 3.7

Table 3.1 summarizes the permeability values obtained in the PAMPA studies of phenformin-HNAP. HNAP enhanced the apparent PAMPA membrane permeability of phenformin 2.0, 4.8, 10.7, and 27.3 fold at phenformin-HNAP concentrations of 0.5, 1.0, 2.5, and 5.0 mM, respectively. A log unit increase in phenformin P_{app} was observed per log unit increase in HNAP concentration, consistent with the ion-pair mediated transport relationship expressed in Equation 3.8. The PAMPA permeability of metoprolol in the absence of counterion was determined for reference. Phenformin permeability exceeded that of metoprolol at phenformin-HNAP concentrations of 2.5 and 5.0 mM (1.4 and 3.6 fold, respectively). The permeability of enalaprilat acid in the presence of 5.0 mM HNAP was also determined in the PAMPA studies as a negative control. No detectable flux was observed for enalaprilat with 5.0 mM HNAP, indicating the increase in phenformin flux is not due to a reduction in membrane integrity by HNAP, and further supporting an ion-pair transport mechanism for phenformin-HNAP.

Table 3.1: Summary of Phenformin-HNAP PAMPA Studies

Compound	Concentration (mM)	HNAP Concentration (mM)	P_{app} (10^{-6} cm/s)
Phenformin	1.0	0	0.06 ± 0.01
Phenformin	0.5	0.5	0.12 ± 0.02
Phenformin	1.0	1.0	0.29 ± 0.02
Phenformin	2.5	2.5	0.64 ± 0.04
Phenformin	5.0	5.0	1.64 ± 0.13
Metoprolol	1.0	0	0.45 ± 0.06
Enalaprilat	5.0	5.0	<0.01
Enalaprilat	5.0	0	<0.01

Ion-pair Mediated Transport Across Caco-2 Cell Monolayers

The phenformin-HNAP, GS 4109-HNAP, and ZNV heptyl ester-HNAP ion-pairs were evaluated in the Caco-2 cell monolayer assay. In all of the experiments, the drug concentration was held constant and only the HNAP counterion concentration was increased, to clearly discern the effect of HNAP on Caco-2 cell monolayer integrity. The Caco-2 permeability of lucifer yellow in the presence of 0, 12, and 24 mM HNAP was also determined as a negative control. Lucifer yellow permeability was below the limit of quantitation ($<3 \times 10^{-7}$ cm/s) at all HNAP concentrations, indicating that an increase in drug permeability in the presence of HNAP is not due to an effect on membrane integrity. TEER values remained relatively constant before and after experiment at 0, 12, and 24 mM HNAP concentration, indicating that HNAP did not disrupt membrane integrity.

Table 3.2: Summary of Caco-2 cell mono-layer integrity studies with Lucifer Yellow

HNAP Concentration (mM)	Lucifer Yellow P_{app} (10^{-7} cm/s)	% TEER Remaining
0	<3	102.8 ± 4.5
12	<3	94.8 ± 4.0
24	<3	108.8 ± 6.1

Figure 3.3 shows the dependence of phenformin flux on HNAP concentration (0, 12, 18, and 24 mM) in the Caco-2 cell mono-layer assay. Phenformin flux increased with counterion concentration, consistent with an ion-pair transport mechanism. Mass transport was linear with time, suggesting the integrity of the cell monolayer remained intact at all HNAP concentrations. Figure 3.4 shows the dependence of phenformin P_{app} on HNAP concentration. The permeability of phenformin in the absence of counterion

was also determined for reference. Phenformin permeability increased 2.4, 3.6, and 4.9

times at HNAP concentrations of 12, 18, and 24 mM, respectively, as compared to

phenformin alone. A linear relationship with a slope near 1 was obtained from the log-log

plot of phenformin P_{app} versus HNAP concentration (Figure 3.5). This relationship is

consistent with the quasi-equilibrium ion-pair mediated transport model expressed in

Equation 3.8.
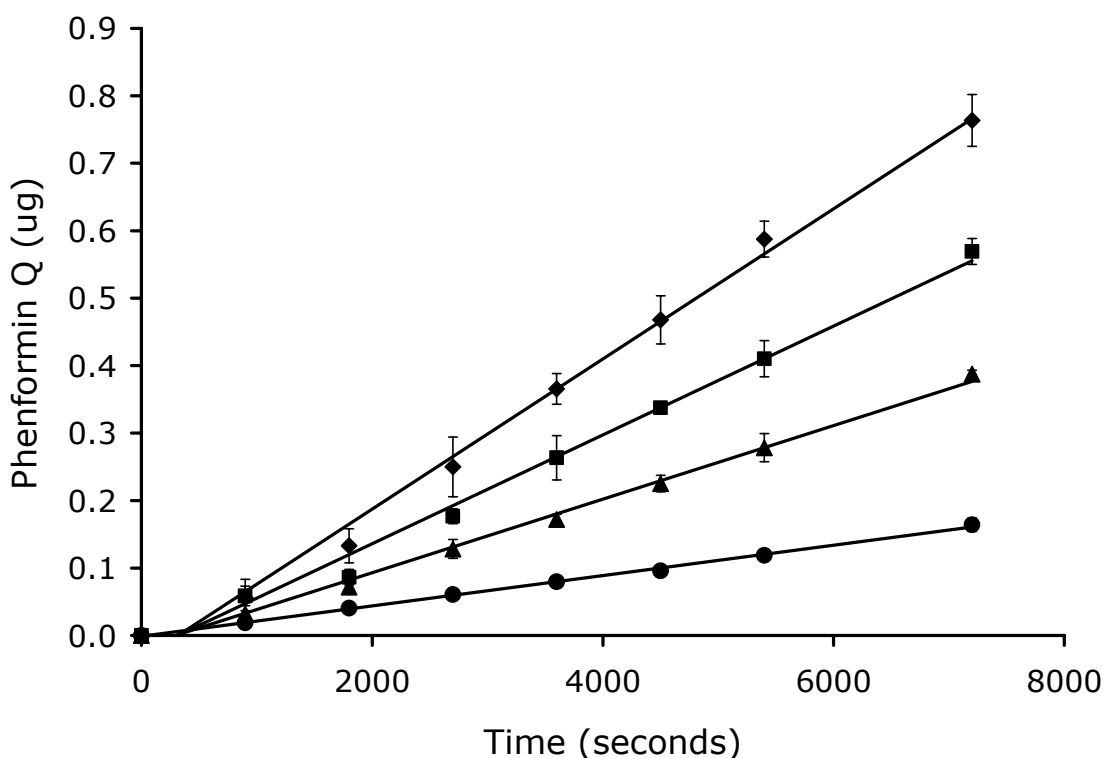
Figure 3.3: Dependence of phenformin flux on counterion concentration in Caco-2 cell
assay; (♦) 24 mM HNAP, (■) 18 mM HNAP, (▲) 12 mM HNAP and (●) 0 mM HNAP
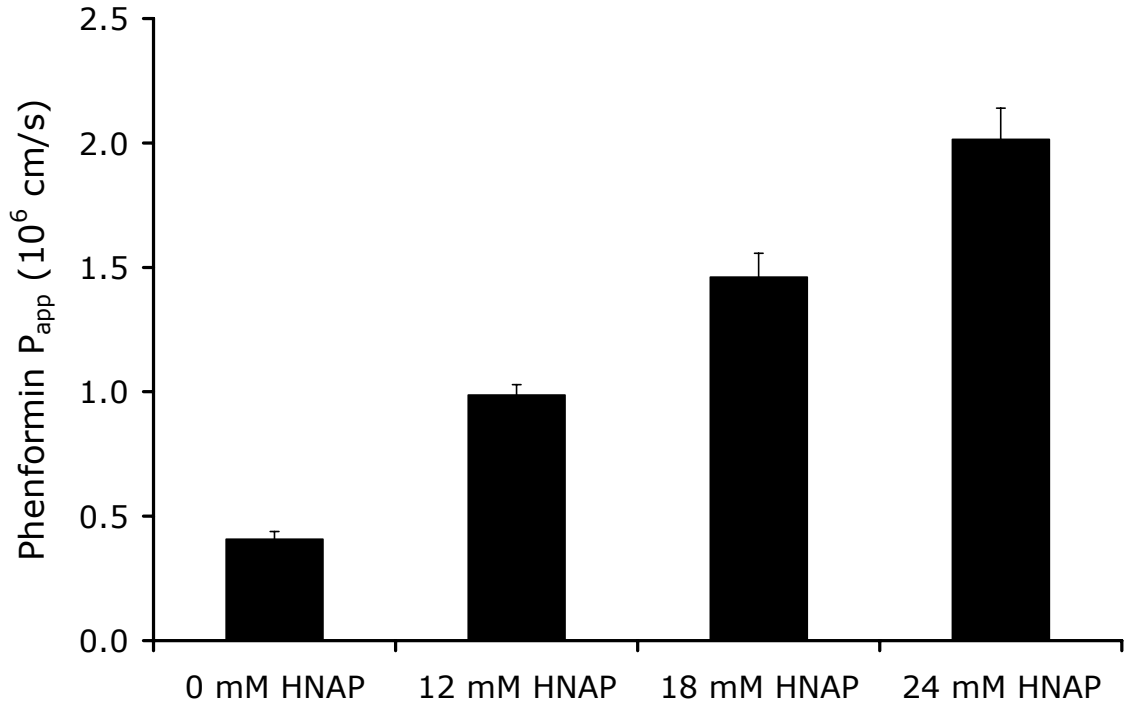
Figure 3.4: Dependence of phenformin P_{app} on counterion concentration in Caco-2 cell assay

Figure 3.5: Log phenformin P_{app} across Caco-2 cell monolayers as a function of Log HNAP concentration. Linear relationship with a slope near 1 is consistent with an ion-pair mediated transport mechanism as per Equation 3.8.

It should be noted that significantly higher concentrations of HNAP (12-18 mM) were required to increase the flux of phenformin in Caco-2 monolayers as compared to PAMPA (0.5-5.0 mM). The aqueous binding constant of the phenformin-HNAP ion-pair is relatively low (2.88 M^{-1}), which makes it more susceptible to ion-exchange with competing anions. In the Caco-2 cell model, there may endogenous anions present (e.g. phosphatidylserine, phosphatidylinositol, sialic acid, bile acids) which may compete with HNAP for binding of phenformin both inside the membrane and at the membrane-aqueous interface. For example, Seo and co-workers (2006) recently showed that the transport of metoprolol in the PAMPA model is significantly altered by the presence of phosphatidylserine. Further competitive binding studies of phenformin-HNAP with endogenous anions would need to be carried out to fully investigate this potential mechanism.

Figure 3.4 shows the dependence of GS 4109 P_{app} on HNAP concentration (0, 12, 18, and 24 mM) in the Caco-2 cell mono-layer assay. GS 4109 P_{app} increased with counterion concentration, consistent with an ion-pair mediated transport mechanism. The permeability of GS 4109 in the absence of counterion was determined for reference. No detectable flux was observed for GS 4109 in the absence of HNAP. This is not surprising as GS 4109 shows very low F < 0.03 in rat (Li *et. al.*, 1998). Substantial permeability was observed for GS 4109 at HNAP concentrations of 12, 18, and 24 mM, respectively. As observed for the phenformin-HNAP system, a linear relationship with a slope near 1 was obtained from a log-log plot of GS 4109 P_{app} versus HNAP concentration (Figure 3.7). This relationship is consistent with the quasi-equilibrium ion-pair mediated transport model expressed in Equation 3.8.
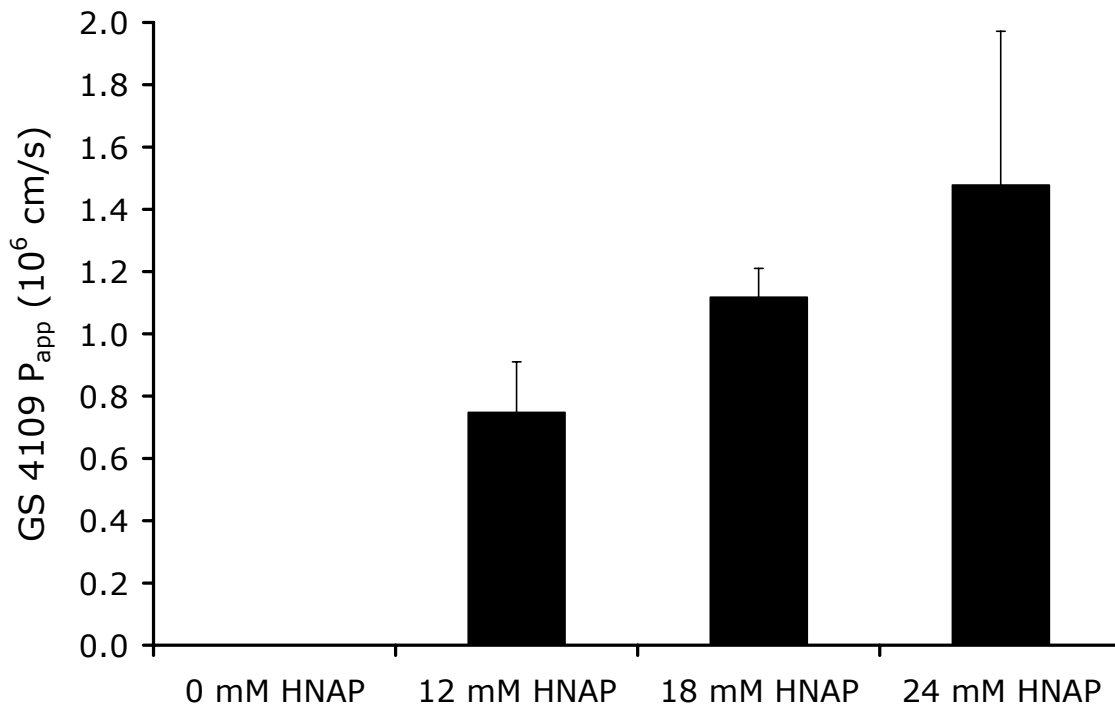
Figure 3.6: Dependence of GS 4109 P_{app} on counterion concentration in Caco-2 cell assay
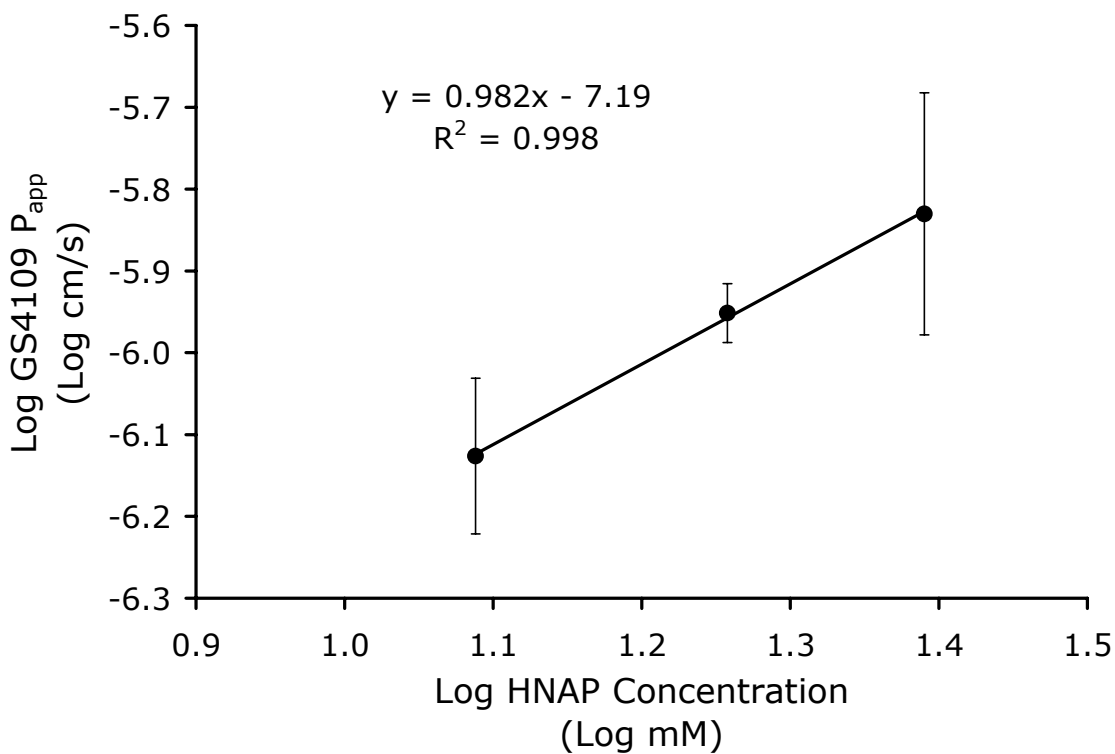
Figure 3.7: Log GS 4109 P_{app} across Caco-2 cell monolayers as a function of Log HNAP concentration. Linear relationship with a slope near 1 is consistent with an ion-pair mediated transport mechanism as per Equation 3.8.

Figure 3.8 shows the dependence of zanamivir (ZNV) heptyl ester P_{app} on HNAP concentration (0, 6, 12, and 24 mM) in the Caco-2 cell assay. ZNV heptyl ester P_{app} increased with HNAP concentration, consistent with an ion-pair transport mechanism. The permeability of ZNV heptyl ester in the absence of counterion was determined for reference. No detectable flux was observed for ZNV heptyl ester in the absence of HNAP. This is not surprising as zanamivir also shows very low F < 0.04 in rat (Li *et. al.*, 1998). Substantial permeability was observed for ZNV heptyl ester at HNAP concentrations of 6, 12, and 24 mM, respectively. As observed for the GS 4109-HNAP and phenformin-HNAP ion-pairs, a linear relationship with a slope near 1 was obtained from a log-log plot of ZNV heptyl ester P_{app} versus HNAP concentration (Figure 3.9). This relationship is consistent with the quasi-equilibrium ion-pair mediated transport model expressed in Equation 3.8.
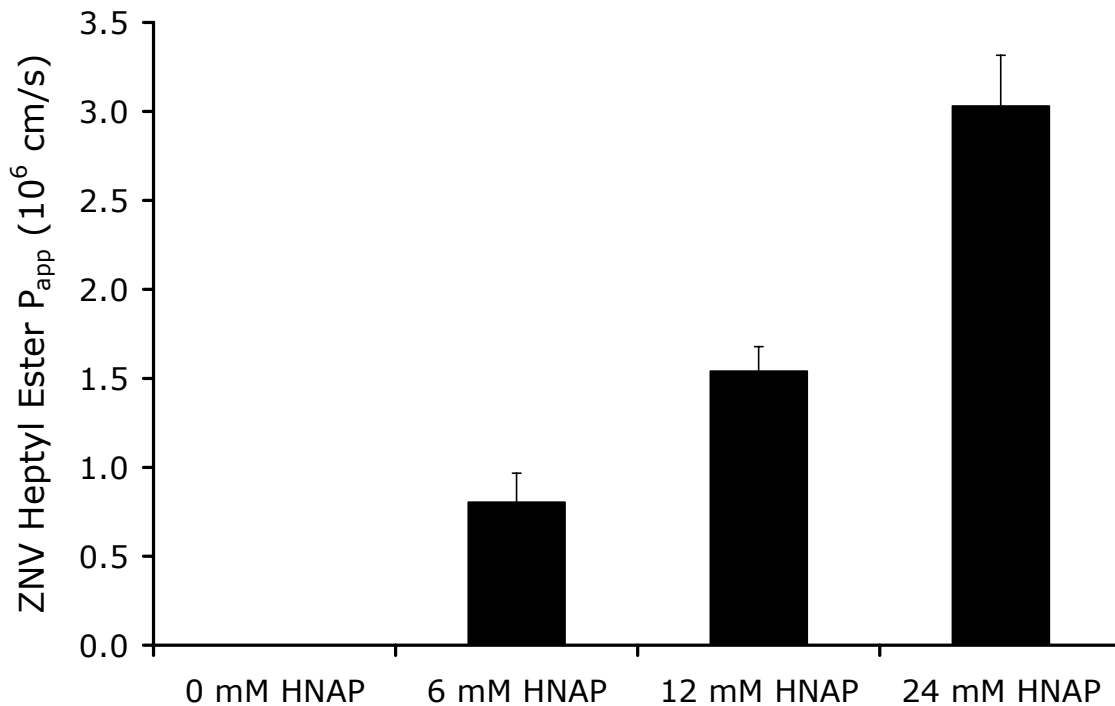
Figure 3.8: Dependence of ZNV heptyl ester P_{app} on counterion concentration in Caco-2 cell assay

$$y = 0.957x - 6.84$$
$$R^2 = 0.999$$
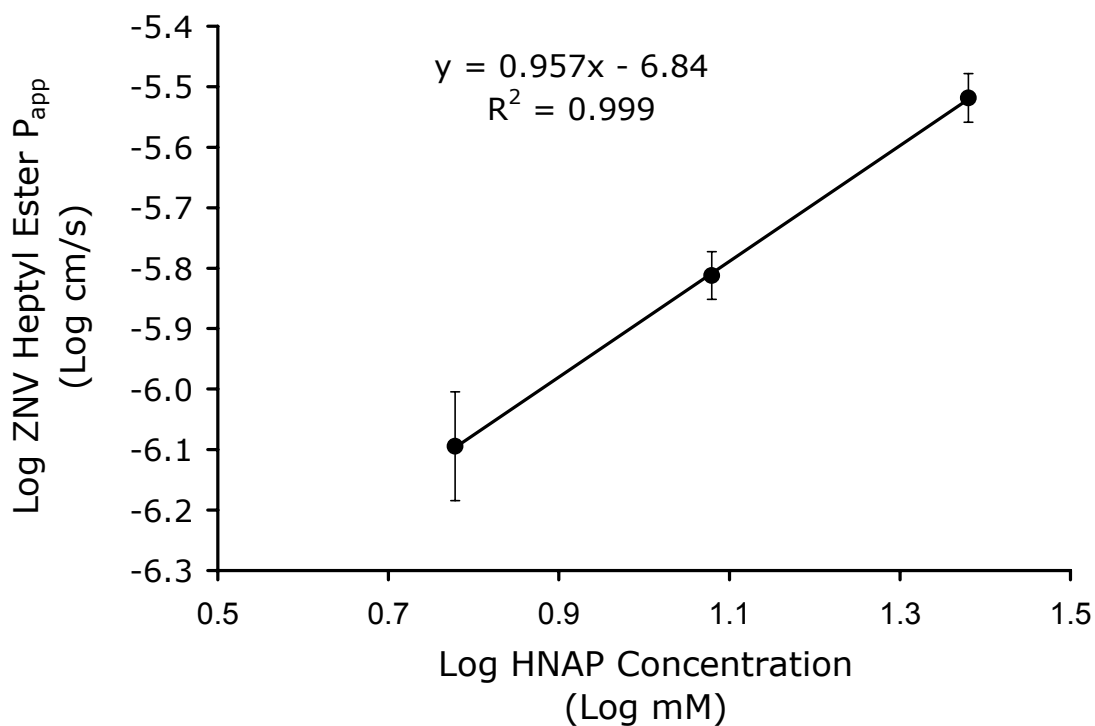
Figure 3.9: Log ZNV heptyl ester P_{app} across Caco-2 cell monolayers as a function of Log HNAP concentration. Linear relationship with a slope near 1 is consistent with an ion-pair mediated transport mechanism as per Equation 3.8.

Table 3.3 compares the K_{11aq}, Log P_{AB}, and Caco-2 P_{app} (0 mM, 12 mM, and 24 mM HNAP) for the ZNV heptyl ester-HNAP, phenformin-HNAP, and GS 4109-HNAP ion-pairs. The ZNV heptyl ester-HNAP ion-pair showed a slightly higher P_{app} (>30% increase) as compared to the phenformin-HNAP and GS 4109-HNAP ion-pairs. This is despite the fact that the ZNV heptyl ester-HNAP ion-pair is significantly less lipophilic than the phenformin-HNAP and GS 4109-HNAP ion pairs (at least 1 log unit lower log P_{AB}). Thus, the higher Caco-2 P_{app} of the ZNV heptyl ester-HNAP may be attributed to the considerably higher value of K_{11aq} (>2 orders of magnitude) as compared to the phenformin-HNAP and GS 4109-HNAP ion-pairs.

Table 3.3: Comparison of K_{11aq}, Log P_{AB}, and Caco-2 P_{app} (0 mM, 12 mM, and 24 mM HNAP) for ZNV heptyl ester-HNAP, phenformin-HNAP, and GS 4109-HNAP ion-pairs

Ion-pair	K_{11aq} (M^{-1})	Log P_{AB}	P_{app} (10^6 cm/s)		
			0 mM HNAP	12 mM HNAP	24 mM HNAP
Zanamivir-OHept-HNAP	388	1.89	BLD	1.54 ± 0.14	3.03 ± 0.29
Phenformin-HNAP	2.88	3.13	0.41 ± 0.04	0.99 ± 0.04	2.01 ± 0.13
GS 4109-HNAP	2.91	4.50	BLD	0.75 ± 0.16	1.48 ± 0.49

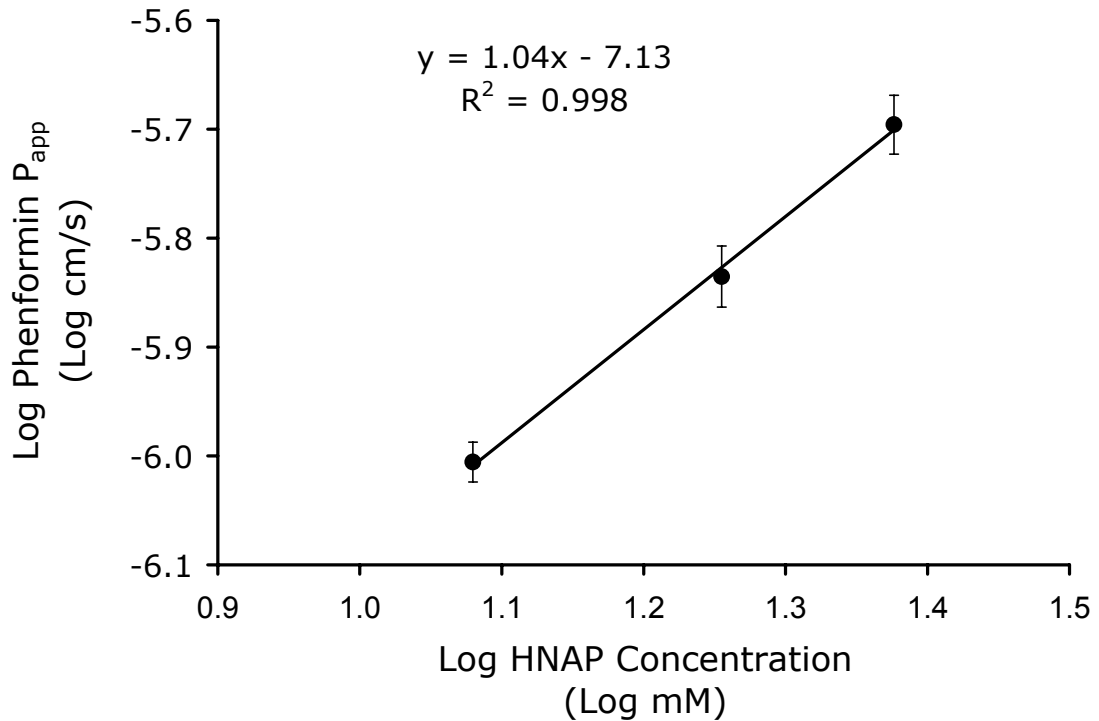***Ion-pair Mediated Transport Across Rat Jejunum***

The ability of HNAP to facilitate the intestinal permeation of phenformin, GS 4109, and ZNV heptyl ester via ion-pair formation was evaluated in the rat jejunal perfusion assay. Figure 3.10 shows the P_{eff} of phenformin across rat jejunal segments during a 60 minute perfusion time. Phenformin was perfused alone and also in the presence of 12.5 mM HNAP. Phenformin showed significant permeability (1.3 x 10^{-5} cm/s) across rat jejunum, even in the absence of HNAP. This is consistent with the

substantial oral absorption (F = 56%) that has been reported for phenformin (Luft *et. al.*, 1978). As shown in Figure 3.10, co-perfusion of phenformin with 12.5 mM HNAP did not result in a significant increase in P_{eff} (1.4 x 10^{-5} cm/s) across the rat jejunal segments.
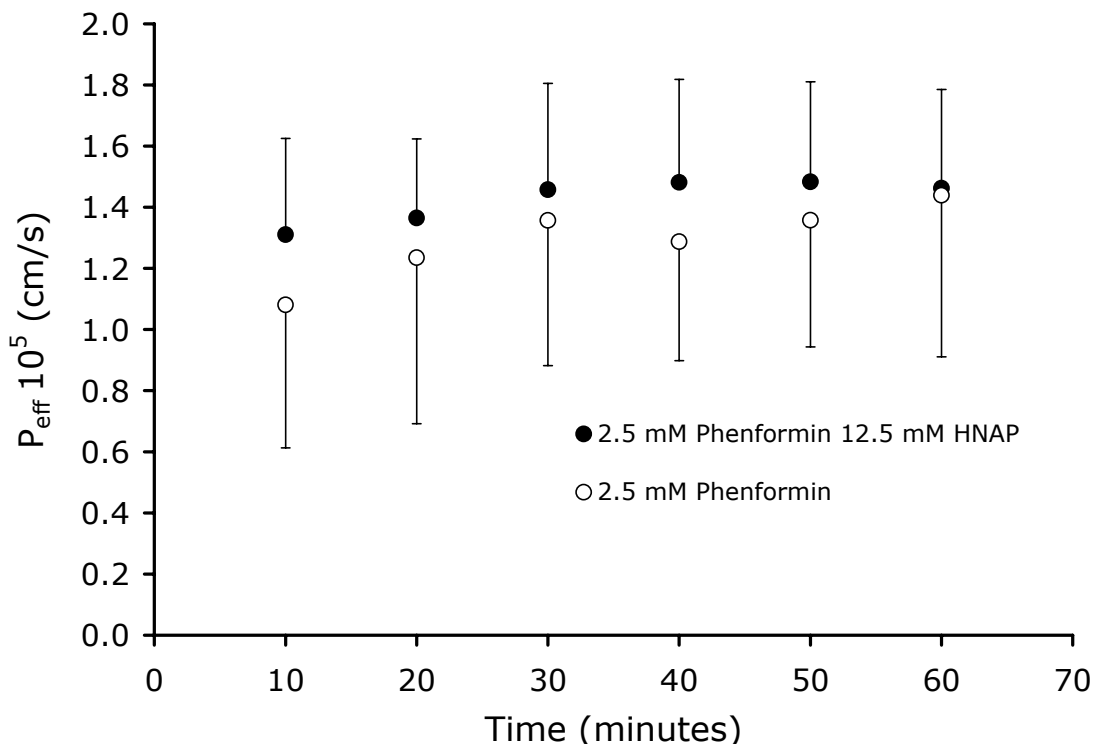
Figure 3.10: Phenformin P_{eff} versus time in rat jejunal perfusion assay at 0 mM and 12.5 mM HNAP concentrations

Figure 3.11 contains the rat jejunal P_{eff} of GS 4109 alone and in the presence of 12 mM HNAP. No effective permeability was observed for GS 4109 in the absence of the HNAP counterion. This is consistent with the very low F < 0.03 that has been reported in rat (Li *et. al.*, 1998), as well as the non-detectable P_{app} observed in the Caco-2 assay (Figure 3.6). As observed for the phenformin-HNAP ion-pair, co-perfusion of GS 4109 with 12 mM HNAP resulted in no significant increase in P_{eff} (Figure 3.11).
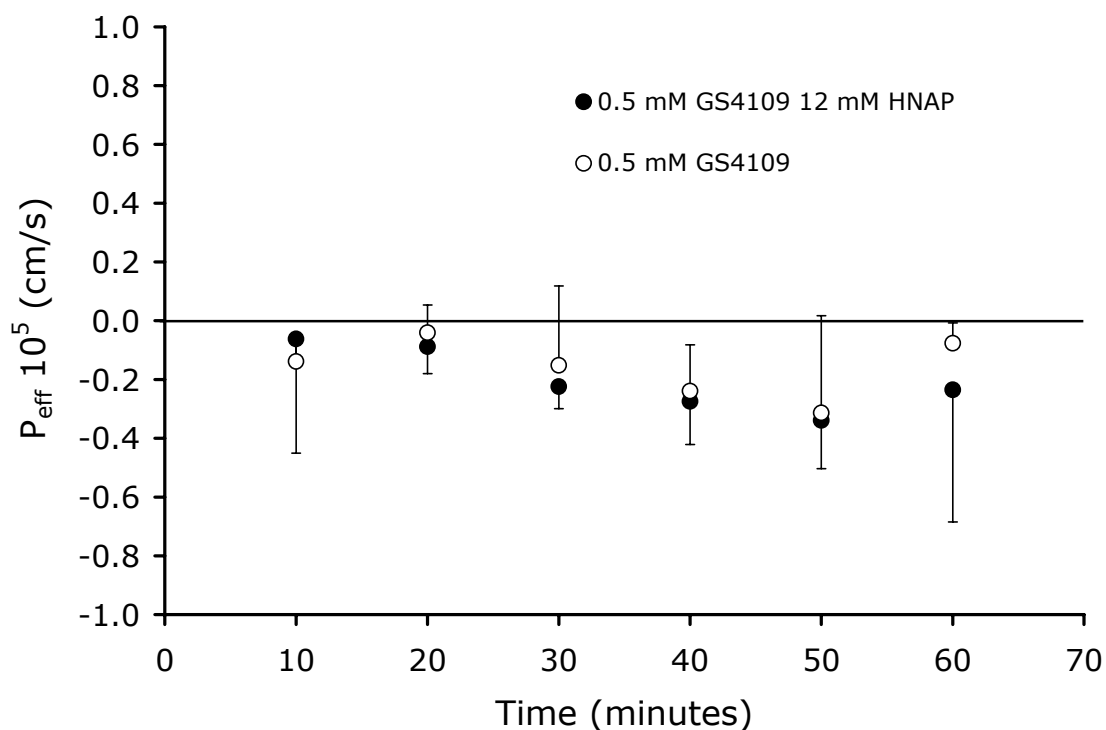
Figure 3.11: GS 4109 P_{eff} versus time in rat jejunal perfusion assay at 0 mM and 12 mM HNAP concentrations

Figure 3.12 shows the dependence of ZNV heptyl ester P_{eff} on HNAP concentration in the rat jejunal perfusion assay. ZNV heptyl ester was perfused alone and also in the presence of 4 and 10 mM HNAP. Essentially zero P_{eff} was observed for ZNV heptyl ester in the absence of HNAP. This is not surprising as zanamivir shows very low $F < 0.04$ in rats (Li *et. al.*, 1998). In contrast to the phenformin-HNAP and GS 4109-HNAP ion-pairs, substantial increases in rat jejunal P_{eff} were observed for ZNV heptyl ester with increasing HNAP concentration. This is a very significant result with practical implications, since no oral delivery route currently exists for zanamivir.
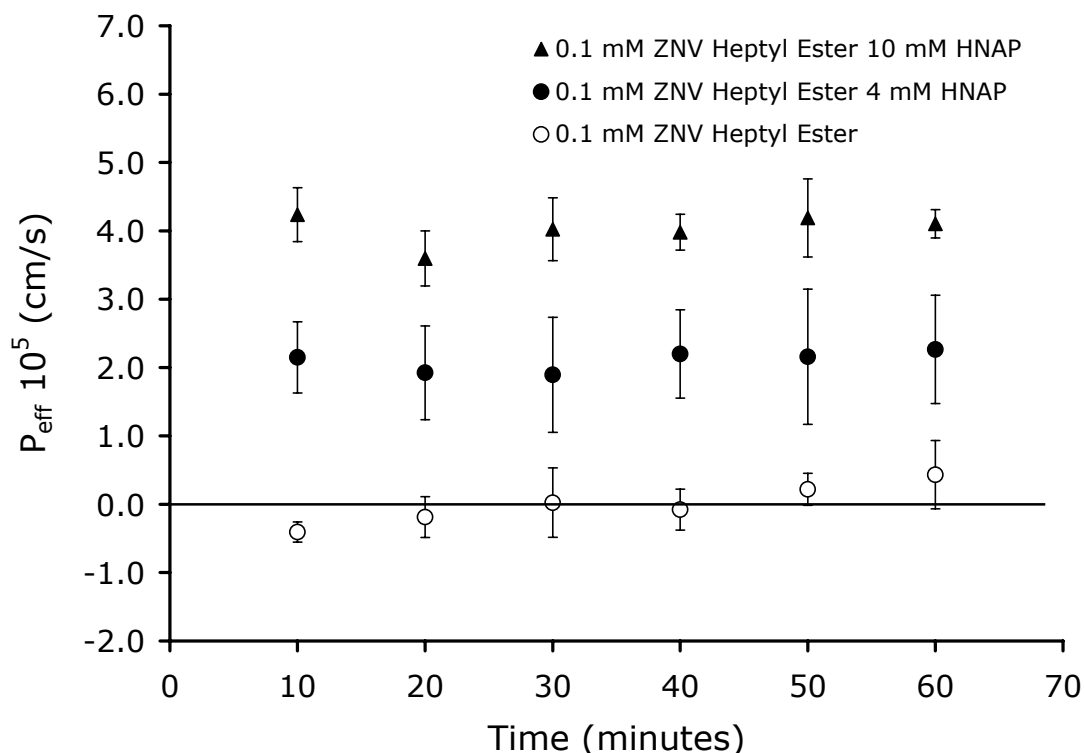
Figure 3.12: ZNV heptyl ester P_{eff} versus time in rat jejunal perfusion assay at 0, 4, and 10 mM HNAP concentrations

Table 3.4 compares the K_{11aq}, Log P_{AB}, and rat jejunal perfusion P_{eff} (0 mM and 10-12 mM HNAP) for the ZNV heptyl ester-HNAP, phenformin-HNAP, and GS 4109-HNAP ion-pairs. For phenformin, the addition of HNAP resulted in no significant increase in rat jejunal P_{eff}. Likewise, GS 4109 showed essentially zero P_{eff} in both the presence and absence of HNAP. On the other hand, the rat jejunal P_{eff} of zanamivir heptyl ester was significantly enhanced by the addition of the HNAP counterion. Zanamivir heptyl ester P_{eff} was essentially zero in the absence of HNAP, but increased in a concentration dependent manner to 2.1 x 10^{-5} cm/s at 4 mM HNAP and 4.0 x 10^{-5} cm/s at 10 mM HNAP. This is despite the fact that the ZNV heptyl ester-HNAP ion-pair is significantly less lipophilic than the phenformin-HNAP and GS 4109-HNAP ion pairs (at least 1 log unit lower log P_{AB}). Therefore, the enhancement of zanamivir heptyl ester rat

jejunal P_{eff} by ion-pairing with HNAP may be attributed to the considerably higher value of K_{11aq} 388 M^{-1} (>2 orders of magnitude) as compared to the phenformin-HNAP and GS 4109-HNAP ion-pairs. The much higher binding constant of the ZNV heptyl ester-HNAP ion-pair makes it much more resistant to ion-exchange with competing endogenous anions. In the rat jejunum there are endogenous anions present such as sialic acid, bile acids, phosphatidylserine, and phosphatidylinositol which may compete with HNAP for binding with the cationic drug. The ion-pairs may be particularly susceptible to dissociation and ion-exchange at the membrane-aqueous interface, where the presence of sialic acid creates a barrier of negative charge at the surface of the membrane. The relatively weak binding constants of the phenformin-HNAP and GS 4109-HNAP ion-pairs make them more likely to dissociate before entering and permeating the membrane, whereas the higher binding constant for the ZNV heptyl ester-HNAP ion-pair makes it more likely to remain intact during the entire membrane permeation process.

Table 3.4: Comparison of K_{11aq}, Log P_{AB}, and rat jejunal P_{eff} (0 mM and 10-12 mM HNAP) for ZNV heptyl ester-HNAP, phenformin-HNAP, and GS 4109-HNAP ion-pairs

Ion-pair	K_{11aq} (M^{-1})	Log P_{AB}	P_{eff} (10^5 cm/s)		
			0 mM HNAP	6 mM HNAP	10-12 mM HNAP
Zanamivir-OHept-HNAP	388	1.89	0.0 ± 0.4	2.1 ± 0.7	4.0 ± 0.4
Phenformin-HNAP	2.88	3.13	1.3 ± 0.4	ND	1.4 ± 0.3
GS 4109-HNAP	2.91	4.50	-0.2 ± 0.2	ND	-0.2 ± 0.2

Conclusions

In this work, quasi-equilibrium transport mass models have been developed to describe the effect of the lipophilic ion-pairing agent HNAP on the apparent membrane transport of the low permeability drugs phenformin, GS 4109, and zanamivir heptyl ester. HNAP enhanced the apparent membrane permeability of phenformin up to 27-fold in the PAMPA model. A linear relationship with a slope near 2 was obtained from a log-log plot of phenformin flux across the PAMPA liquid membrane versus phenformin-HNAP concentration, consistent with the quasi-equilibrium ion-pair mediated membrane transport model, thus supporting an ion-pair mediated transport mechanism. In the Caco-2 cell monolayer assay, HNAP enhanced the apparent permeability of phenformin 4.9 fold at an HNAP concentration of 24 mM. Likewise, significant permeation across Caco-2 cell monolayers was observed for GS 4109 and zanamivir heptyl ester in the presence of 6-24 mM HNAP, whereas no detectable transport was observed in the absence of counterion. As predicted from a quasi-equilibrium analysis of ion-pair mediated membrane transport, an order of magnitude increase in Caco-2 cell monolayer permeability was observed per log increase in counterion concentration for phenformin, GS 4109, and zanamivir heptyl ester. As such, log-log plots of apparent permeability versus HNAP concentration gave linear relationships with slope near 1. In the rat jejunal perfusion assay, the addition of HNAP resulted in no significant increase in P_{eff} for phenformin. Likewise, GS 4109 showed essentially zero P_{eff} across rat jejunum in both the presence and absence of HNAP. However, the rat jejunal P_{eff} of zanamivir heptyl ester was significantly enhanced by the addition of the HNAP counterion as the P_{eff} was essentially zero in the absence of HNAP, but increased to 4.0 x 10^{-5} cm/s at 10 mM

HNAP. The success of the zanamivir heptyl ester-HNAP ion-pair may be explained by the substantially stronger binding constant (388 M^{-1}) as compared to the phenformin-HNAP and GS 4109-HNAP ion-pairs (3 M^{-1}). The stronger binding constant of the ZNV heptyl ester-HNAP makes it less prone to dissociation and ion-exchange with competing endogenous anions and thus able to remain intact during the entire membrane permeation process.

The key attributes for successful ion-pair mediated membrane transport, proposed in Chapter II of this thesis, have been substantiated by this work. Successful ion-pair mediated membrane transport was observed in the Caco-2 monolayer assay when the ion-pair Log P_{AB} values were in the range of approximately 2-5. In addition to sufficient lipophilicity of the ion-pair, a strong K_{11aq} value is required to prevent dissociation and ion-exchange with competing endogenous ions (e.g. phosphatidylserine, phosphatidylinositol, sialic acid, bile acids) such that the ion-pair will remain intact during the entire membrane permeation process. The ZNV heptyl ester-HNAP ion-pair, with binding constant on the order of 100 to 1000 M^{-1}, enabled successful ion-pair mediated membrane transport in the rat jejunal perfusion assay, whereas the phenformin-HNAP and GS 4109-HNAP ion-pairs, with binding constants on the order of 1 to 10 M^{-1}, were not successful. Overall, these results provide increased understanding of the underlying mechanisms of ion-pair mediated membrane transport, emphasizing the potential of this approach to enable the oral delivery of low-permeability drugs.

CHAPTER FOUR

QUASI-EQUILIBRIUM ANALYSIS OF THE EFFECT OF CYCLODEXTRINS ON THE MEMBRANE TRANSPORT OF LOW-SOLUBILITY DRUGS

Theory

Quasi-Equilibrium Analysis of the Effect of Cyclodextrin on Membrane Transport

The intrinsic membrane permeability of the free drug ($P_{m(F)}$) in the absence of cyclodextrin can be written as (Higuchi, 1960):

$$P_{m(F)} = \frac{D_{m(F)} K_{m(F)}}{h_{m(F)}}$$

(Equation 4.1)

Where $D_{m(F)}$ is the intrinsic membrane diffusion coefficient of the free drug in the absence of cyclodextrin, $K_{m(F)}$ is the intrinsic membrane/aqueous partition coefficient of the drug in the absence of cyclodextrin, and $h_{m(F)}$ is the intrinsic membrane thickness experienced by the free drug in the absence of cyclodextrin.

Likewise, the apparent membrane permeability of the drug in the presence of cyclodextrin (P_m) can be written as:

$$P_m = \frac{D_m K_m}{h_m}$$

(Equation 4.2)

Where D_m is the apparent membrane diffusion coefficient of the drug in the presence of cyclodextrin and K_m is the apparent membrane/aqueous partition coefficient of the drug in the presence of cyclodextrin.

Assuming only the free drug permeates the membrane such that $D_{m(F)} = D_m$ and that the presence of cyclodextrin does not effect the membrane thickness such that $h_{m(F)} = h_m$, Equations 4.1 and 4.2 can be combined to give:

$$P_m = \frac{P_{m(F)} K_m}{K_{m(F)}} \qquad \text{(Equation 4.3)}$$

$K_{m(F)}$ and K_m can be expressed as:

$$K_{m(F)} = \frac{S_{m(F)}}{S_{aq(F)}} \qquad \text{(Equation 4.4)}$$

$$K_m = \frac{S_m}{S_{aq}} \qquad \text{(Equation 4.5)}$$

Where $S_{m(F)}$ is the intrinsic membrane solubility of the free drug, $S_{aq(F)}$ is the intrinsic aqueous solubility of the free drug, S_m is the apparent membrane solubility of the drug in the presence of cyclodextrin, and S_{aq} is the apparent aqueous solubility of the drug in the presence of cyclodextrin.

Assuming that the presence of cyclodextrin does not affect the drug solubility in the membrane such that $S_{m(F)} = S_m$, Equations 4.3, 4.4, and 4.5 can be combined to give:

$$P_m = \frac{P_{m(F)} S_{aq(F)}}{S_{aq}} \qquad \text{(Equation 4.6)}$$

Assuming 1:1 complexation between drug and cyclodextrin, the dependence of drug solubility on cyclodextrin concentration (C_{CD}) can be written as:

$$S_{aq} = S_{aq(F)}\left(K_{11aq}C_{CD} + 1\right)$$ (Equation 4.7)

Where K_{11aq} is the aqueous association constant of the 1:1 drug:cyclodextrin complex.

Equations 4.6 and 4.7 can be combined to express the P_m dependence on C_{CD}:

$$P_m = \frac{P_{m(F)}}{\left(K_{11aq}C_{CD} + 1\right)}$$ (Equation 4.8)

Recognizing that the fraction of free drug (F) can be written as:

$$F = \frac{1}{K_{11aq}C_{CD} + 1}$$ (Equation 4.9)

Equations 4.8 and 4.9 can be combined to express the P_m dependence on F:

$$P_m = P_{m(F)}F$$ (Equation 4.10)

The intrinsic permeability of the free drug through the unstirred aqueous boundary layer ($P_{aq(F)}$) in the absence of cyclodextrin can be written as (Amidon *et. al.*, 1982):

$$P_{aq(F)} = \frac{D_{aq(F)}}{h_{aq(F)}}$$ (Equation 4.11)

Where $D_{aq(F)}$ is the intrinsic diffusion coefficient of the free drug through the unstirred aqueous boundary layer in the absence of cyclodextrin and $h_{aq(F)}$ is the intrinsic unstirred aqueous boundary layer thickness experienced by the free drug in the absence of cyclodextrin.

Likewise, the apparent unstirred aqueous boundary layer permeability of the drug in the presence of cyclodextrin (P_{aq}) can be written as:

$$P_{aq} = \frac{D_{aq}}{h_{aq}}$$

(Equation 4.12)

Where D_{aq} is the apparent diffusion coefficient of the drug through the unstirred aqueous boundary layer in the presence of cyclodextrin and h_{aq} is the apparent unstirred aqueous boundary layer thickness in the presence of cyclodextrin.

Equations 4.11 and 4.12 can be combined to give:

$$P_{aq} = \frac{P_{aq(F)}D_{aq}h_{aq(F)}}{D_{aq(F)}h_{aq}}$$

(Equation 4.13)

D_{aq} may be expressed as (Amidon *et. al.*, 1982):

$$D_{aq} = FD_{aq(F)} + BD_{aq(B)}$$

(Equation 4.14)

Where B is the fraction of drug molecules bound to cyclodextrins ($B = 1-F$) and $D_{aq(B)}$ is the aqueous diffusion coefficient of the drug-cyclodextrin complex, which may be approximated by the average of $D_{aq(o)}$ and the aqueous diffusion coefficient of free cyclodextrin, $D_{aq(CD)}$:

$$D_{aq(B)} = \frac{D_{aq(F)} + D_{aq(CD)}}{2}$$

(Equation 4.15)

Likewise, h_{aq} may be expressed as:

$$h_{aq} = Fh_{aq(F)} + Bh_{aq(B)}$$

(Equation 4.16)

Where $h_{aq(B)}$ is the apparent unstirred aqueous boundary layer thickness experienced by the drug-cyclodextrin complex. Assuming that the unstirred aqueous boundary layer is no

longer present for the drug-cyclodextrin complex (i.e. $h_{aq(B)} = 0$), Equation 4.16 reduces to:

$$h_{aq} = Fh_{aq(F)} \qquad \text{(Equation 4.17)}$$

Equations 4.9, 4.13 and 4.17 can be combined to express the P_{aq} dependence on C_{CD}::

$$P_{aq} = \frac{P_{aq(F)}D_{aq}\left(K_{11aq}C_{CD}+1\right)}{D_{aq(F)}} \qquad \text{(Equation 4.18)}$$

Where the dependence of D_{aq} on C_{CD} may be calculated using Equations 4.14 and 4.15. Taking into account the membrane permeability as well as the unstirred aqueous boundary layer permeability on either side of the membrane, $P_{aq(1)}$ and $P_{aq(2)}$, the overall effective permeability (P_{eff}) of the drug and can be written as (Amidon *et. al.*, 1982):

$$P_{eff} = \frac{1}{\dfrac{1}{P_{aq(1)}} + \dfrac{1}{P_m} + \dfrac{1}{P_{aq(2)}}} \qquad \text{(Equation 4.19)}$$

For simplicity, $P_{aq(2)}$ is assumed to have a negligible effect, such that $P_{aq(1)} = P_{aq}$, and Equation 4.19 can be rewritten as:

$$P_{eff} = \frac{1}{\dfrac{1}{P_{aq}} + \dfrac{1}{P_m}} \qquad \text{(Equation 4.20)}$$

Thus, the overall P_{eff} dependence on C_{CD} may be predicted via Equation 4.20 wherein the P_m and P_{aq} dependence on C_{CD} are predicted using Equations 4.8 and 4.18 with knowledge of $P_{m(F)}$, K_{11aq}, $P_{aq(F)}$, $D_{aq(F)}$, and $D_{aq(CD)}$.

The assumptions nested in these analyses include: (1) Quasi-equilibrium conditions (2) 1:1 stoichiometry between drug:cyclodextrin complex; (3) Only the free

drug partitions and diffuses into the membrane, but not the drug:cyclodextrin complex, such that $S_{m(F)} = S_m$ and $D_{m(F)} = D_m$; (4) The presence of cyclodextrin does not effect the membrane thickness such that $h_{m(F)} = h_m$; and (5) Only the free drug encounters a significant unstirred aqueous boundary layer thickness but the unstirred aqueous boundary layer thickness is negligible for the drug-cyclodextrin complex such that . $h_{aq(B)} = 0$.

Materials and Methods

Materials

Progesterone, 2-hydroxypropyl-β-cyclodextrin (HPβCD), phenol red and hexadecane were purchased from Sigma Chemical Co. (St. Louis, MO). Hexane, potassium chloride and NaCl were obtained from Fisher Scientific Inc. (Pittsburgh, PA). Acetonitrile and water (Acros Organics, Geel, Belgium) were HPLC grade. All other chemicals were of analytical reagent grade.

High Performance Liquid Chromatography (HPLC)

HPLC experiments were performed on an Agilent Technologies (Palo Alto, CA) HPLC 1100 equipped with photodiode array detector and ChemStation for LC 3D software. Progesterone was assayed using an Agilent (Palo Alto, CA) 150mm × 4.6mm XDB-C$_{18}$ column with 5 μm particle size. The detection wavelength was 242 nm. The mobile phase consisted of 30:70 (v:v) 0.1% trifluoroacetic acid in water: 0.1% trifluoroacetic acid in acetonitrile and was pumped at a flow rate of 1.0 ml/min. Injection volumes for all HPLC analyses ranged from 5 to 100 μL.

Caco-2 Cell Monolayer Assay

Caco-2 cells (passage 25-32) from American Type Culture Collection (Rockville, MD) were routinely maintained in Dulbecco's modified Eagle's medium (DMEM, Invitrogen Corp., Carlsbad, CA) containing 10% fetal bovine serum, 1% nonessential amino acids, 1 mM sodium pyruvate, and 1% L-glutamine. Cells were grown in an atmosphere of 5% CO_2 and 90% relative humidity at 37°C. The DMEM medium was routinely replaced by fresh medium every three days. Cells were passaged upon reaching approximately 80% confluence using 4 ml trypsin-EDTA (Invitrogen Corp., Carlsbad, CA).

Transepithelial transport studies were performed using a method described previously with minor modifications (Dahan and Amidon, 2009). Briefly, 5×10^4 cells/cm^2 were seeded onto collagen-coated membranes (12-well Transwell plate, 0.4-μm pore size, 12 mm diameter, Corning Costar, Cambridge, MA) and were allowed to grow for 21 days. Mannitol and Lucifer yellow permeabilities were assayed for each batch of Caco-2 monolayers (*n*=3), and TEER measurements were performed on all monolayers (Millicell-ERS epithelial Voltohmmeter, Millipore Co., Bedford, MA). Monolayers with apparent mannitol and Lucifer yellow permeability $<3 \times 10^{-7}$ cm/sec, and TEER values >300 Ωcm^2 were used for the study. On the day of the experiment, the DMEM was removed and the monolayers were rinsed and incubated for 20 min with a blank transport buffer. The apical transport buffer contained 1 mM $CaCl_2$, 0.5 mM $MgCl_2 \cdot 6H_2O$, 145 mM NaCl, 3 mM KCl, 1 mM NaH_2PO_4, 5 mM D-glucose, and 5 mM MES. Following the 20 min incubation, the drug free transport buffer was removed from the apical side and replaced by 0.5 ml of progesterone solution in the uptake buffer, with or

without HPβCD. Throughout the experiment, the transport plates were kept in a shaking incubator (50 rpm) at 37°C. Samples were taken from the receiver (basolateral) side at various time points up to 120 min (50 μl), and similar volumes of blank buffer were added following each sample withdrawal. At the last time point (120 min), sample was taken from the donor (apical) side as well, in order to confirm mass balance. Samples were immediately assayed for drug content. Caco-2 monolayers were checked for confluence by measuring the TEER before and after the transport study.

Permeability coefficient (P_{app}) across Caco-2 cell monolayers was calculated from the linear plot of drug accumulated in the receiver side versus time, using the following equation:

$$P_{app} = \frac{1}{C_0 A} \times \frac{dQ}{dt} \qquad \text{(Equation 4.21)}$$

where dQ/dt is the steady-state appearance rate of the drug on the receiver side, C_0 is the initial concentration of the drug in the donor side, and A is the monolayer growth surface area (1.12 cm^2). Linear regression was carried out to obtain the steady-state appearance rate of the drug on the receiver side.

Parallel Artificial Membrane Permeation Assay (PAMPA)

PAMPA studies were carried out using a method described previously with minor modifications (Wohnsland and Faller, 2007). Solutions of progesterone (25 μM) were prepared with HPβCD at concentrations of 0, 0.1, 0.2, 0.4, 0.8, and 1.6 mM in phosphate buffer saline (PBS) pH 7.4. PAMPA experiments were carried out in Millipore (Danvers, MA) 96-well MultiScreen-Permeability filter plates with 0.3 cm^2 polycarbonate filter support (0.45 μm). The filter supports in each well were first impregnated with 15 μL of

a 5% solution (v/v) of hexadecane in hexanes. The wells were then allowed to dry for 1 hour to ensure complete evaporation of the hexanes resulting in a uniform layer of hexadecane. The donor wells were then loaded with 0.15 mL of the progesterone-HPβCD solution and each receiver well was loaded with 0.3 mL of PBS. Five wells were loaded at each HPβCD concentration to enable collection of a well at times points of 30, 60, 90, 120, and 150 minutes and each experiment was repeated three times for a total of 15 wells per HPβCD concentration. The donor plate was then placed upon the 96-well receiver plate and the resulting PAMPA sandwich was incubated at 25 ^{o}C on an orbital shaker rotating at 50 rpm. Receiver plate wells (n=3 for each HPβCD concentration) were then collected every 30 minutes over 2.5 hours and the progesterone concentration in each well was determined by HPLC. Permeability coefficient (P_{app}) across Caco-2 cell monolayers was calculated from the linear plot of drug accumulated in the receiver side versus time using Equation 4.21.

Solubility Studies

The solubility experiments for progesterone with HPβCD were conducted according to the method described by Higuchi and Connors (1965). To a number of test tubes containing excess amounts of progesterone, 0-0.015 M aqueous HPβCD solutions were added. The intrinsic solubility in water was determined from five individual samples without HPβCD. The test tubes were tightly closed and placed in a shaking water bath at 25°C and 100 rpm. Establishment of equilibrium was assured by comparison of samples after 24 and 48 h. Before sampling, the vials were centrifuged at 10,000 rpm for

10 min. Supernatant was carefully withdrawn from each test tube and immediately assayed for drug content by HPLC.

Rat Jejunal Perfusion

All animal experiments were conducted using protocols approved by the University Committee of Use and Care of Animals (UCUCA), University of Michigan, and the animals were housed and handled according to the University of Michigan Unit for Laboratory Animal Medicine guidelines. Male albino Wistar rats (Charles River, IN) weighing 250-280 g were used for all perfusion studies. Prior to each experiment, the rats were fasted overnight (12-18 h) with free access to water. Animals were randomly assigned to the different experimental groups.

The procedure for the *in-situ* single-pass intestinal perfusion followed previously published reports (Amidon *et. al.*, 1988, Lipka *et. al.*, 1995, Kim *et. al.*, 2006). Briefly, rats were anesthetized with an intramuscular injection of 1 mL/kg of ketamine-xylazine solution (9%:1%, respectively) and placed on a heated surface maintained at 37 °C (Harvard Apparatus Inc., Holliston, MA). The abdomen was opened by a midline incision of 3-4 cm. A proximal jejunal segment (3 ± 1 cm average distance of the inlet from the ligament of Treitz) of approximately 10 cm was carefully exposed and cannulated on two ends with flexible PVC tubing (2.29 mm i.d., inlet tube 40 cm, outlet tube 20 cm, Fisher Scientific Inc., Pittsburgh, PA). Care was taken to avoid disturbance of the circulatory system, and the exposed segment was kept moist with 37 °C normal saline solution. Solutions of progesterone (25 µM) were prepared with HPβCD at concentrations of 0, 0.025, 0.25, and 2.5 mM in the perfusate buffer. The perfusate buffer consisted of 10 mM

MES buffer, pH 6.5, 135 mM NaCl, 5 mM KCl, and 0.1 mg/mL phenol red. Phenol red was added to the perfusion buffer as a non-absorbable marker for measuring water flux. All perfusate solutions were incubated in a 37 °C water bath to maintain temperature and were pumped through the intestinal segment (Watson Marlow Pumps 323S, Watson-Marlow Bredel Inc., Wilmington, MA). The isolated segment was first rinsed with blank perfusion buffer, pH 6.5 at a flow rate of 0.5 mL/min in order to clean out any residual debris. At the start of the study, the test solutions were perfused through the intestinal segment at a flow rate of 0.2 mL/min. The perfusion buffer was first perfused for 1 hour, in order to ensure steady state conditions (as also assessed by the inlet over outlet concentration ratio of phenol red which approaches 1 at steady state). After reaching steady state, samples were taken in 10 min intervals for one hour (10, 20, 30, 40, 50, and 60 min). All samples, including perfusion samples at different time points, original drug solution, and inlet solution taken at the exit of the syringe were immediately assayed by HPLC. Following the termination of the experiment, the length of each perfused jejunal segment was accurately measured.

The net water flux in the single-pass rat jejunal perfusion studies, resulting from water absorption in the intestinal segment, was determined by measurement of phenol red, a non-absorbed, non-metabolized marker. The measured C_{out}/C_{in} ratio was corrected for water transport according to the following equation:

$$\frac{C'_{out}}{C'_{in}} = \frac{C_{out}}{C_{in}} \times \frac{C_{in\ phenol.red}}{C_{out\ phenol.red}} \qquad \text{(Equation 4.22)}$$

where C_{out} is the concentration of progesterone in the outlet sample, C_{in} is the concentration of progesterone in the inlet sample, $C_{in\ phenol\ red}$ is the concentration of phenol red in the inlet sample, and $C_{out\ phenol\ red}$ is the concentration of phenol red in the

outlet sample. The effective permeability (P_{eff}) through the rat gut wall in the single-pass intestinal perfusion studies was determined assuming the "plug flow" model expressed in the following equation (Fagerholm *et. al.,* 1996):

$$P_{eff} = \frac{-Q\ln(C'_{out}/C'_{in})}{2\pi RL}$$
(Equation 4.23)

where Q is the perfusion buffer flow rate, C'_{out}/C'_{in} is the ratio of the outlet concentration and the inlet or starting concentration of the tested drug that has been adjusted for water transport via Equation 4.22, R is the radius of the intestinal segment (set to 0.2 cm), and L is the length of the intestinal segment.

Statistical Analysis

Values are expressed as the mean of at least 3 measurements, +/- the standard deviation (SD). Linear regression of the data using Equation 2.4 was carried out using SigmaPlot 2004 for Windows Version 9.01.

.

Results and Discussion

Effect of HPβCD on Progesterone Solubility

The solubility data for complex formation between progesterone and HPβCD is presented in Figure 4.1. Progesterone solubility increased linearly ($R^2 > 0.99$) with increased HPβCD concentration as per Equation 4.7. The linearity of the phase solubility diagram indicates 1:1 stoichiometric complexation between progesterone and HPβCD. A very strong binding constant of 14,324 M^{-1} was calculated from the phase solubility data via equation 4.7. The high binding constant signifies very tight molecular complexation between progesterone and HPβCD, which results in very little free progesterone even at

relatively low HPβCD concentrations. For example, the free fraction of progesterone is 0.5 at a HPβCD concentration of only 70 μM, and at HPβCD concentrations > 1.4 mM, the free fraction of progesterone is <0.05.
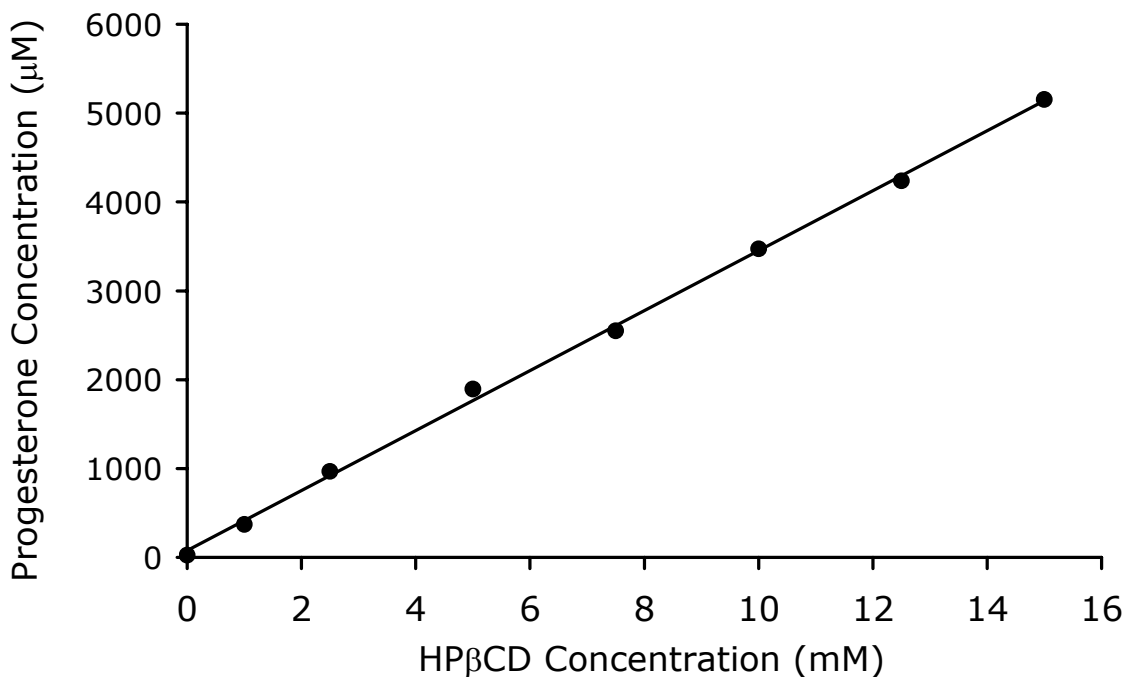
Figure 4.1: Aqueous solubility of progesterone as a function of increasing HPβCD concentration at 25°C.

Effect of HPβCD on Progesterone Transport Across Caco-2 Cell Monolayers

Progesterone membrane permeation was evaluated in the Caco-2 monolayer assay, alone and in the presence of 75 μM HPβCD. Higher concentrations of HPβCD could not be tested due to concerns about the effects on Caco-2 monolayer integrity. Figure 4.2 shows the dependence of progesterone flux on HPβCD concentration (0 and 75 μM) in the Caco-2 cell assay. Mass transport was relatively linear with time, suggesting the integrity of the cell monolayer remained intact. Figure 4.3 shows the

dependence of progesterone P_{app} on HPβCD concentration. Progesterone permeability decreased 2-fold in the presence of 75 μM HPβCD as compared to progesterone alone.
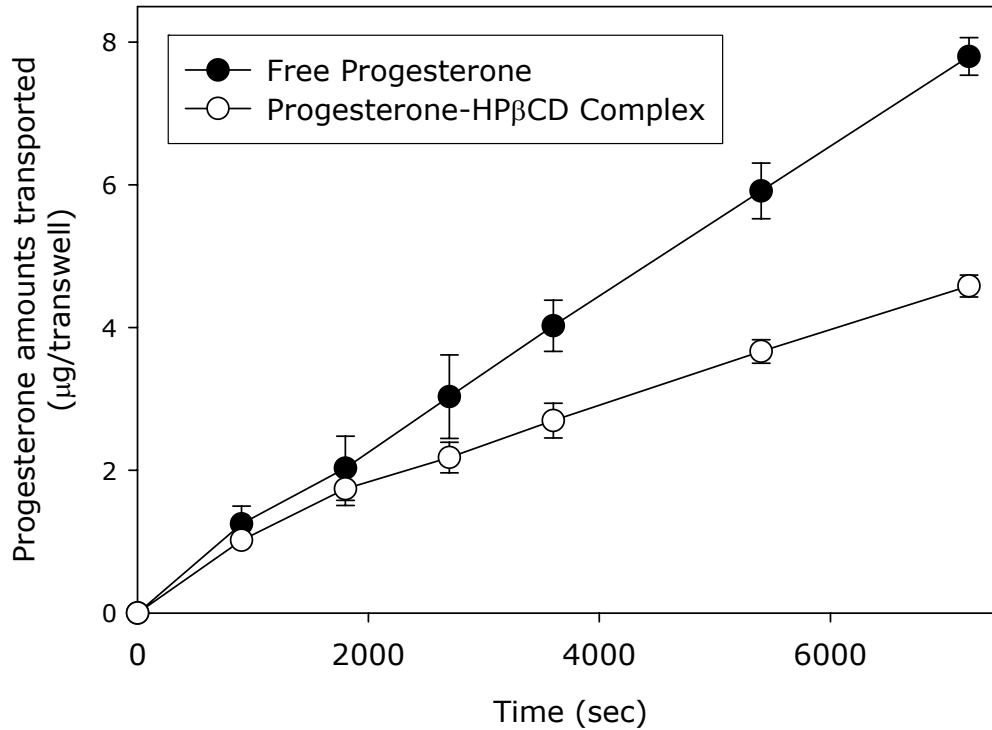
Figure 4.2: Flux of progesterone (25 μM) across Caco-2 monolayers alone (●) and in the presence of 75 μM HPβCD (○).
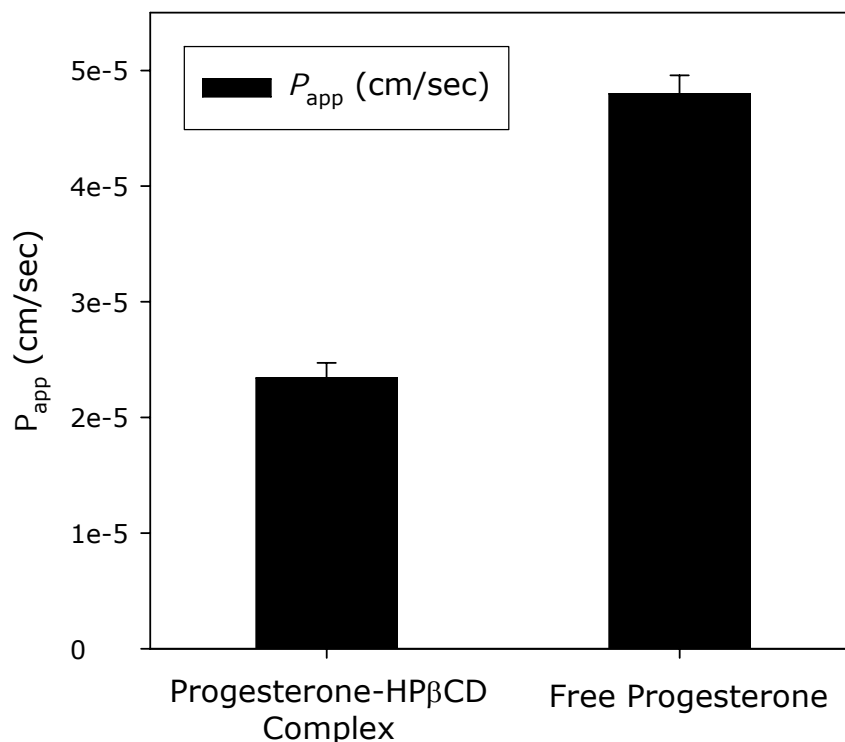
Figure 4.3: P_{app} of progesterone (25 µM) across Caco-2 monolayers alone (right) and in the presence of 75 µM HPβCD (left).

The progesterone Caco-2 membrane permeation data shown in Figures 4.2 and 4.3 were obtained with a constant rotation speed of 50 rpm. In order to determine if the results obtained under this condition represent the true membrane permeability ($P_{m(F)}$) of progesterone, i.e. to assess the effect of the unstirred water layer (UWL), progesterone transport was evaluated across Caco-2 cell monolayers as a function of rotation speed (Figure 4.4). Significantly higher transport was evident with increased rotation speed from 0, to 20, and to 50 rpm, indicating that progesterone P_{app} is limited by the UWL, at low rotation speeds. This observation is in corroboration with previous reports (Komiya *et. al.*, 1980; Amidon *et. al.*, 1982; Johnson and Amidon, 1988). Additional increase in rotation speed to 70 rpm failed to produce increased flux, indicating that the UWL does not limit the overall P_{app} at high rotation speeds. Hence, it is evident that the P_{app} value obtained at 50 rpm (4.8×10^{-5} cm/sec) approximates the true intrinsic membrane

permeability ($P_{m(F)}$) of progesterone across Caco-2 monolayers. The effect of rotation speed on Caco-2 membrane transport was also evaluated for progesterone in the presence of 75 μM HPβCD. As shown in Figure 4.5, similar progesterone permeabilities were obtained at different rotation speeds 0-50 rpm, consistent with the idea that the UWL is no longer rate limiting and progesterone P_{app} is under membrane control at an HPβCD a concentration as low as 75 μM. This is in agreement with previous reports showing that cyclodextrins may reduce the UWL effect on the P_{app} of lipophilic compounds (Loftsson *et. al.*, 1999; Loftsson *et. al.*, 2006; Loftsson *et. al.*, 2007).
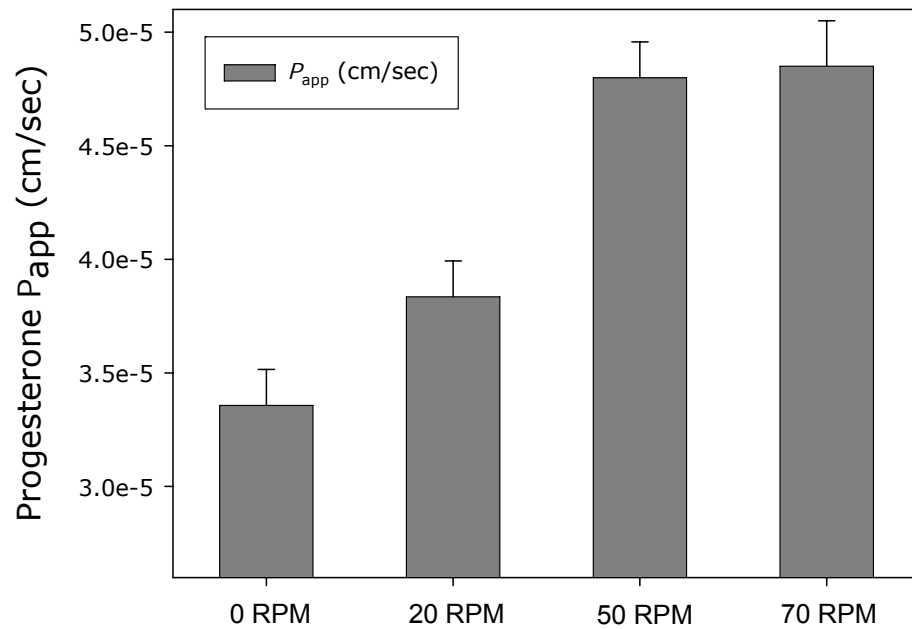
Figure 4.4: P_{app} of progesterone (25 μM) across Caco-2 monolayers at different rotation speeds (0, 20, 50 and 70 rpm).
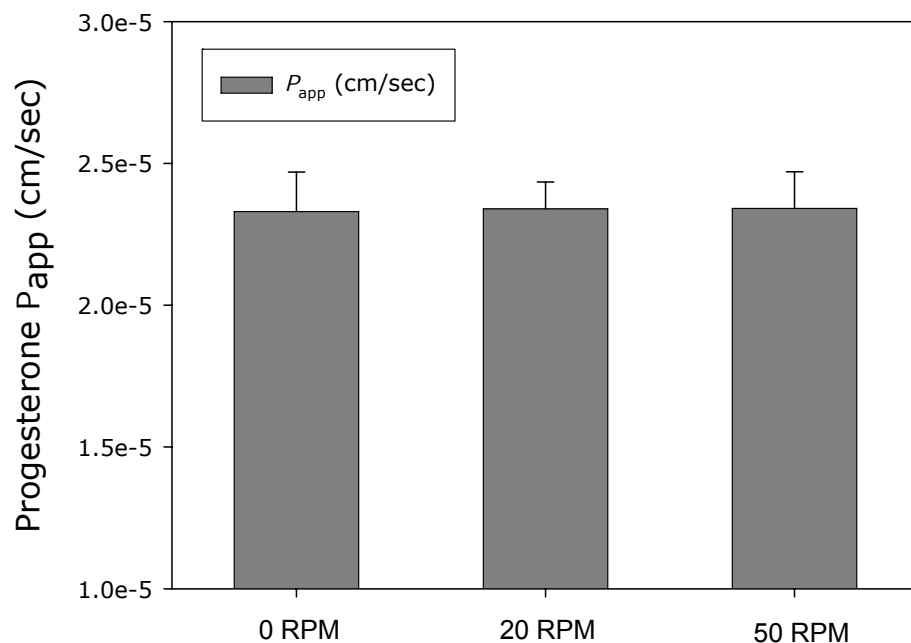
Figure 4.5: P_{app} of progesterone (25 μM) across Caco-2 monolayers in the presence of 75 μM HPβCD at different rotation speeds (0, 20, and 50 rpm).

Figure 4.6 compares the predicted permeability of progesterone across Caco-2 cell monolayers as a function of HPβCD concentration to the experimentally observed P_{app} values. The theoretical lines were calculated via Equation 4.8 (P_m), Equation 4.18 (P_{aq}), and Equation 4.20 (P_{eff}) using the experimental values of $P_{m(F)} = 4.8 \times 10^{-5}$ cm/sec, $K_{11aq} = 14,324$ M^{-1}, $D_{aq(F)} = 8.0 \times 10^{-6}$ cm^2/sec from Amidon *et. al.*, (1982), and $D_{aq(CD)} = 3.2 \times 10^{-6}$ cm^2/sec from Ribeiro *et. al.*, (2007). The value of $P_{aq(F)}$ was calculated to be 10.6 x 10^{-5} cm/s via Equation 4.20 using the experimentally observed P_{app} value of 3.3×10^{-5} cm/sec at 0 rpm rotation speed in the absence of cyclodextrin for P_{eff} and the experimental value of 4.8×10^{-5} cm/sec for $P_{m(F)}$.

The predicted values for both P_{eff} and P_m agreed quite well with the experimentally observed P_{app} value of 2.3×10^{-5} cm/sec at a cyclodextrin concentration of 75 μM (Figure 4.6). In fact, the theoretical value of P_m calculated via Equation 4.8

exactly matched the experimentally observed P_{app} value. This is because the unstirred aqueous boundary layer is no longer rate-limiting the progesterone permeation at the 50 rpm stir speed used (Figure 4.4) and HPβCD concentration of 75 µM (Figure 4.5), such that the overall observed P_{app} is membrane controlled and $P_{eff} \approx P_m$ under these experimental conditions.
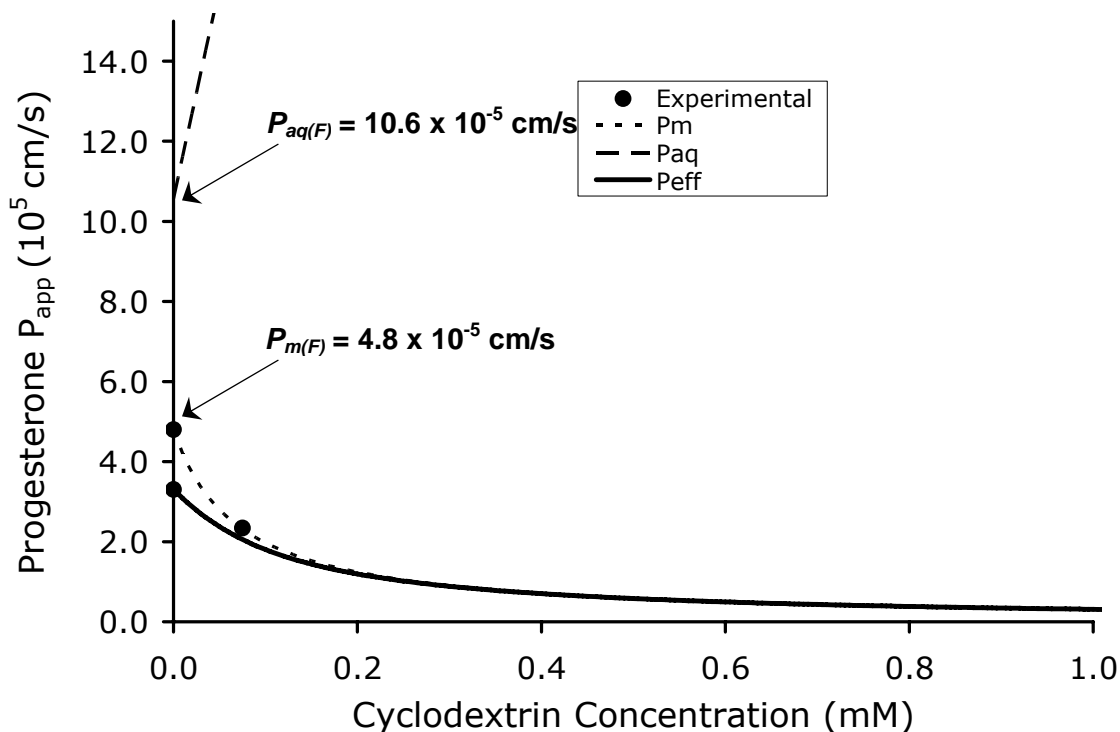
Figure 4.6: P_{app} of progesterone across Caco-2 cell monolayers as a function of HPβCD concentration. The theoretical lines were calculated via Equation 4.8 (P_m), Equation 4.18 (P_{aq}), and Equation 4.20 (P_{eff}).

Effect of HPβCD on Progesterone Transport in PAMPA Model

Progesterone permeability in the presence of increasing HPβCD concentrations was evaluated in the PAMPA model with hexadecane as the liquid membrane. Figure 4.7 shows the dependence of progesterone P_{app} on HPβCD concentration. The permeability of progesterone in the absence of cyclodextrin was also determined for reference.

Progesterone permeability decreased 2.1, 3.5, 6.4, 15.4, and 33.1 times at HPβCD concentrations of 0.1, 0.2, 0.4, 0.8, and 1.6 mM, respectively, as compared to progesterone alone. The progesterone PAMPA permeability was assessed at increasing rotation speeds in the absence of HPβCD, in order to assess the effect of the unstirred aqueous boundary layer. As shown in Figure 4.8, progesterone permeability in PAMPA model with hexadecane membrane remained constant with increasing rotation speed up to 100 rpm. This indicates the progesterone permeability is under membrane control in the PAMPA model with hexadecane membrane. Thus, the P_{app} in the absence of HPβCD can be assumed to be approximately equal to $P_{m(F)}$. Moreover, since the progesterone membrane permeability is not affected by the unstirred aqueous boundary layer, the overall P_{eff} is under membrane control and only the affect of cyclodextrin on P_m needs to be considered (i.e. $P_{eff} \approx P_m$). Thus, Equation 4.8 may be applied to predict the dependence of progesterone apparent membrane permeability on HPβCD concentration. Figure 4.9 compares the theoretical PAMPA P_{app} of progesterone as a function of HPβCD concentration to the experimentally observed values. The theoretical line was calculated via Equation 4.8 using the experimental values of $P_{m(F)} = 11 \times 10^{-6}$ cm/sec and $K_{11aq} = 14,324$ M^{-1}. Excellent agreement between the experimental data and predicted values was obtained at all of the HPβCD concentrations tested (Figure 4.9).
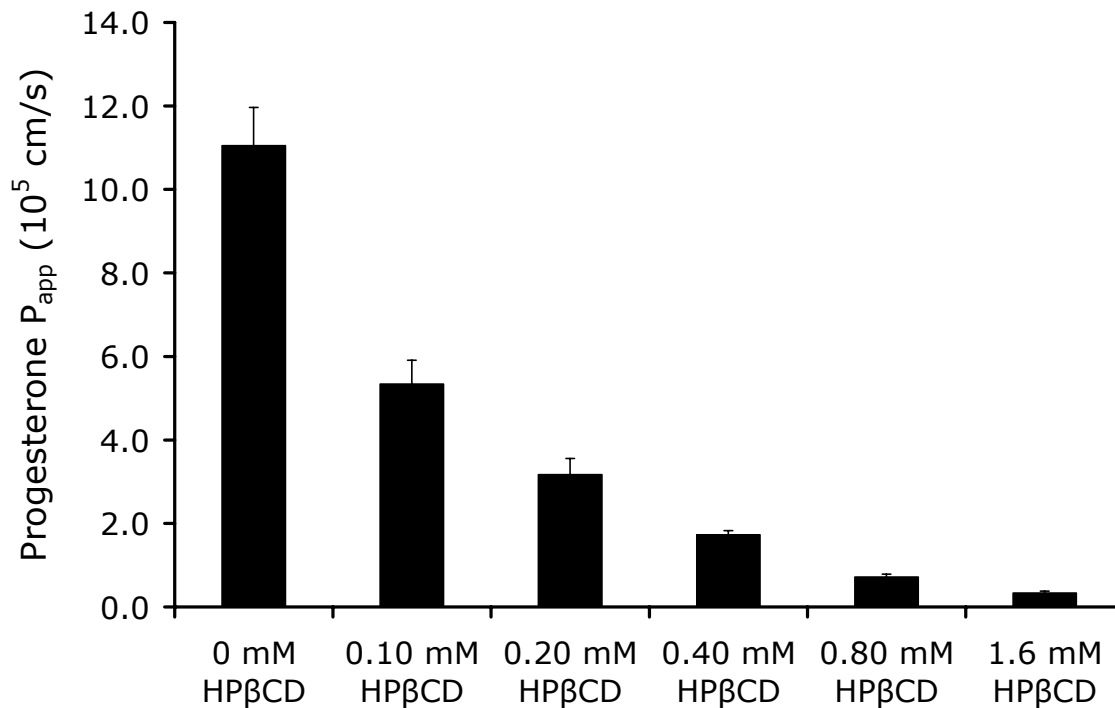
Figure 4.7: Dependence of progesterone P_{app} on HPβCD concentration in the PAMPA model.
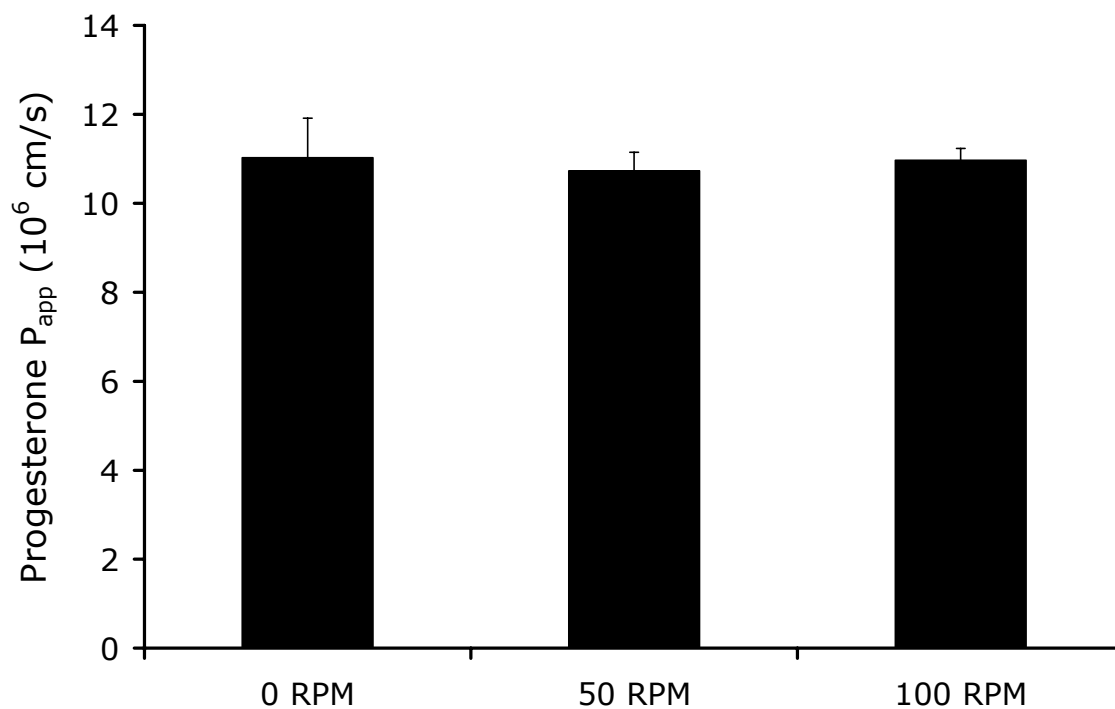
Figure 4.8: P_{app} of progesterone (25 μM) in the PAMPA model at different rotation speeds (0, 50, and 100 rpm).

Figure 4.9: P_{app} of progesterone as a function of HPβCD concentration in PAMPA experiments. The theoretical line was calculated via Equation 4.8 using the experimental values of $P_m = 11.0 \times 10^{-6}$ cm/sec and $K_{11aq} = 14{,}324$ M^{-1}.

The quasi-equilibrium membrane transport analysis developed here was also applied to some experimental permeability as a function of HPβCD concentration data from the literature. Brewster *et. al.* (2007) determined the P_{app} of carbamazepine and hydrocortizone as a function of HPβCD concentration in the PAMPA model, with a 2% (w/v) dioleylphosphadityl choline in dodecane solution as the liquid membrane. The authors determined the P_{app} of the compounds at varying stir speeds in the absence of HPβCD to create approximate unstirred water layer (UWL) thicknesses of 25, 40, and >100 μm. The P_{app} was essentially the same at UWL thicknesses of 25 and 40 μm, indicating that the overall transport was under membrane control at these UWL thicknesses. Therefore, the P_{app} at UWL thickness of 25 μm was assumed to be approximately equal to $P_{m(F)}$ for both compounds ($P_{m(F)} = 81.5 \times 10^{-6}$ cm/s for

carbamazepine and $P_{m(F)}$ = 32.5 x 10^{-6} cm/s for hydrocortizone). Likewise, the P_{app} at UWL length of >100 μm in the absence of cyclodextrin was used to calculate $P_{aq(F)}$ for both compounds via Equation 4.20 ($P_{aq(F)}$ = 33.4 x 10^{-6} cm/s for carbamazepine and $P_{aq(F)}$ = 26.4 x 10^{-6} cm/s for hydrocortizone).

Figures 4.10 and 4.11 compare the theoretical P_{app} as a function of HPβCD concentration to the experimentally observed values for carbamazepine and hydrocortisone, respectively. The theoretical curves for P_{aq}, P_m, and P_{eff} were calculated via Equations 4.8, 4.14, and 4.20 using the experimentally observed values of K_{11aq} = 461.1 M^{-1} for carbamazepine and K_{11aq} = 606.2 M^{-1} for hydrocortisone. It should be noted that these K_{11aq} values were re-calculated from the solubility data reported by Brewster *et. al*. (2007) via Equation 4.7 using the single experimental data point for $S_{aq(F)}$ rather than the y-intercept of the S_{aq} versus HPβCD concentration curve, which is thought to be a more appropriate treatment of the data.

Excellent agreement was achieved between the experimental and predicted P_{eff} values for both compounds at all of the HPβCD concentrations tested (Figures 4.10-4.11). The predicted values for P_m also agreed quite well with the experimentally observed P_{app} values at the high HPβCD concentrations. This is because the unstirred aqueous boundary layer is no longer rate-limiting the the permeability of the compounds in the presence of significant amounts of cyclodextrins, such that the overall observed P_{app} is membrane controlled and $P_{eff} \approx P_m$ under these experimental conditions.
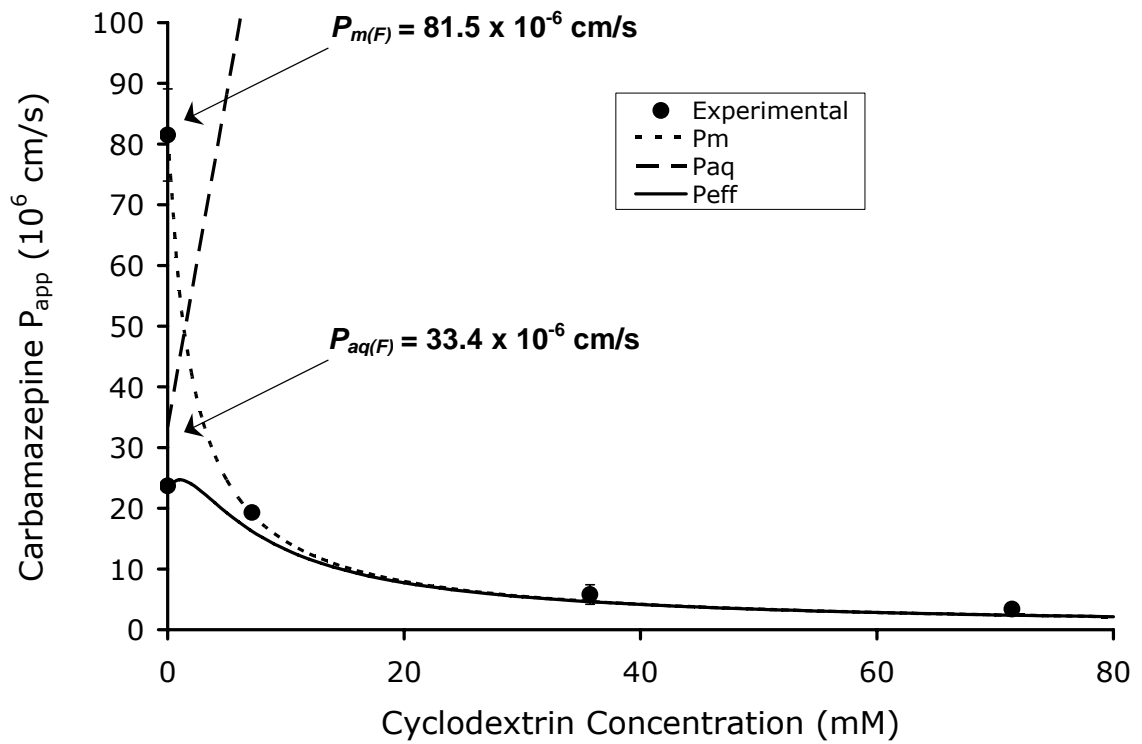
Figure 4.10: P_{app} of carbamazepine as a function of HPβCD concentration in PAMPA experiments. The theoretical lines were calculated via Equation 4.8 (P_m), Equation 4.18 (P_{aq}), and Equation 4.20 (P_{eff}).
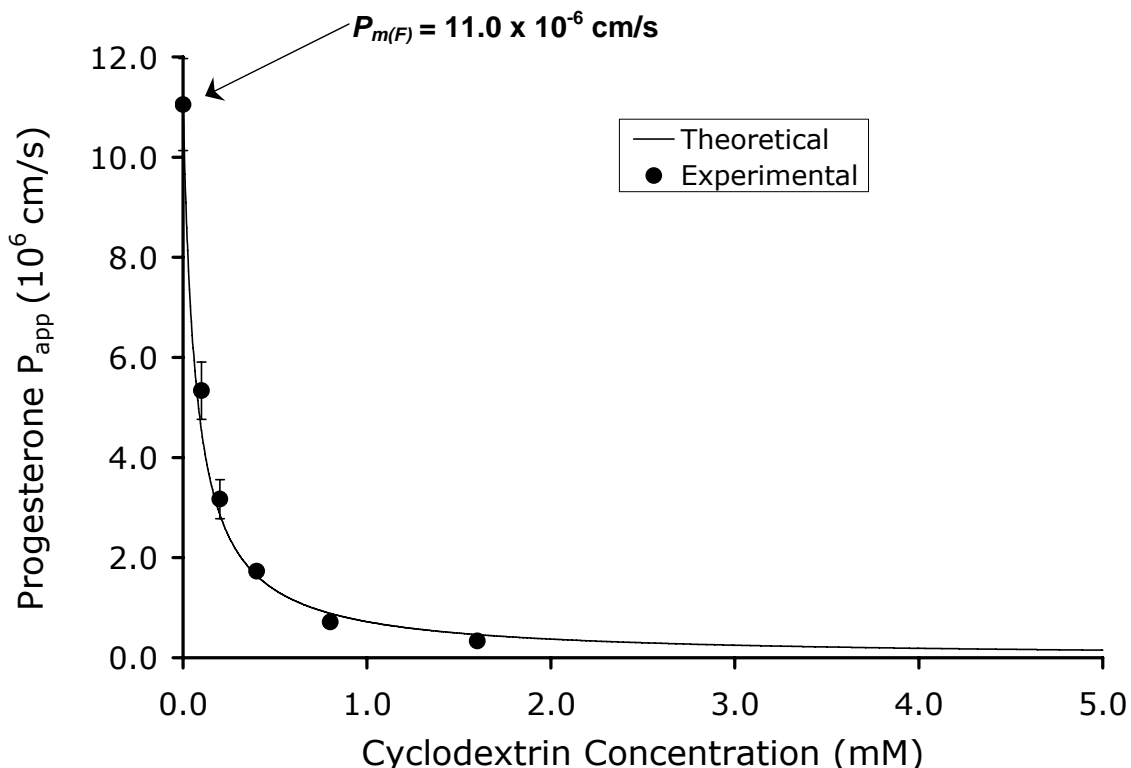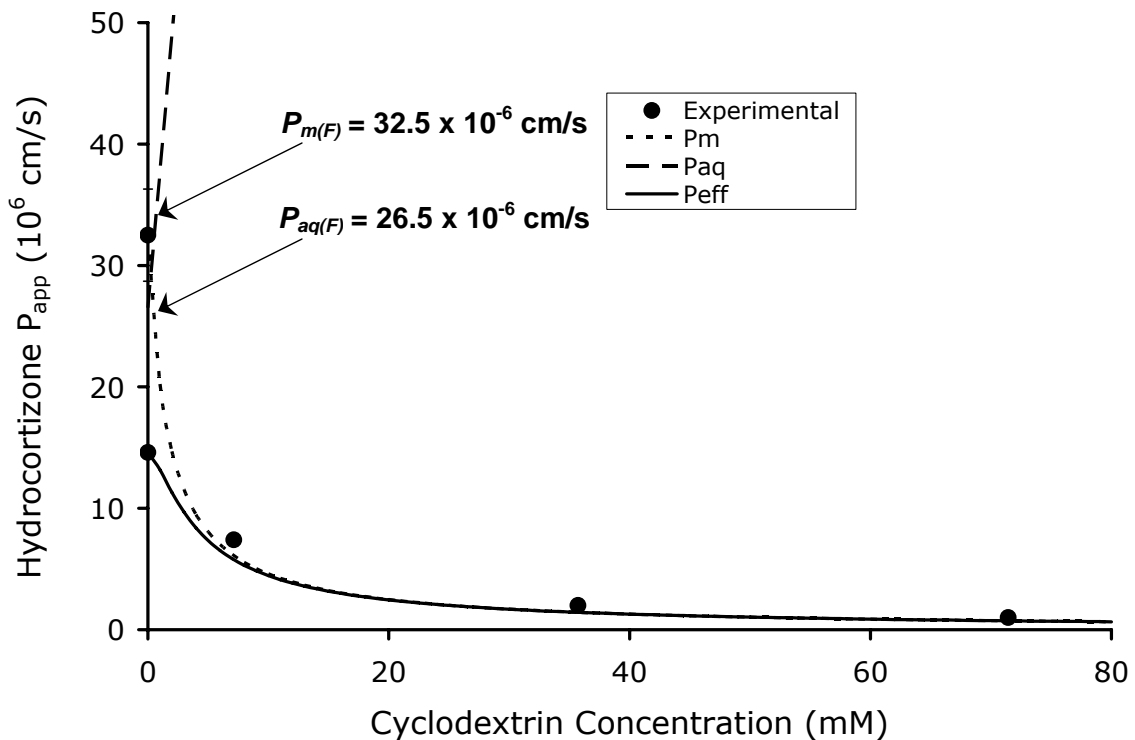
Figure 4.11: P_{app} of hydrocortizone as a function of HPβCD concentration in PAMPA experiments. The theoretical lines were calculated via Equation 4.8 (P_m), Equation 4.18 (P_{aq}), and Equation 4.20 (P_{eff}).

Effect of HPβCD on Progesterone Transport in Rat Jejunal Perfusion Assay

Progesterone permeability in the presence of increasing HPβCD concentrations was evaluated in the rat jejunal perfusion assay. Progesterone was perfused alone and also in the presence of 0.025, 0.25, and 2.5 mM HPβCD. Figure 4.12 shows the average P_{eff} of progesterone across rat jejunal segments with increasing HPβCD concentrations during the 60 minute perfusion time. In the absence of HPβCD, progesterone showed high permeability (82.4×10^{-5} cm/s) across rat jejunum. The addition of an equi-molar amount of 25 μM HPβCD resulted in no significant increase in P_{eff} (84.8×10^{-5} cm/s). However, the P_{eff} of progesterone decreased 1.8 fold in the presence of 0.25 mM HPβCD and 7.8 fold in the presence of 2.5 mM HPβCD.
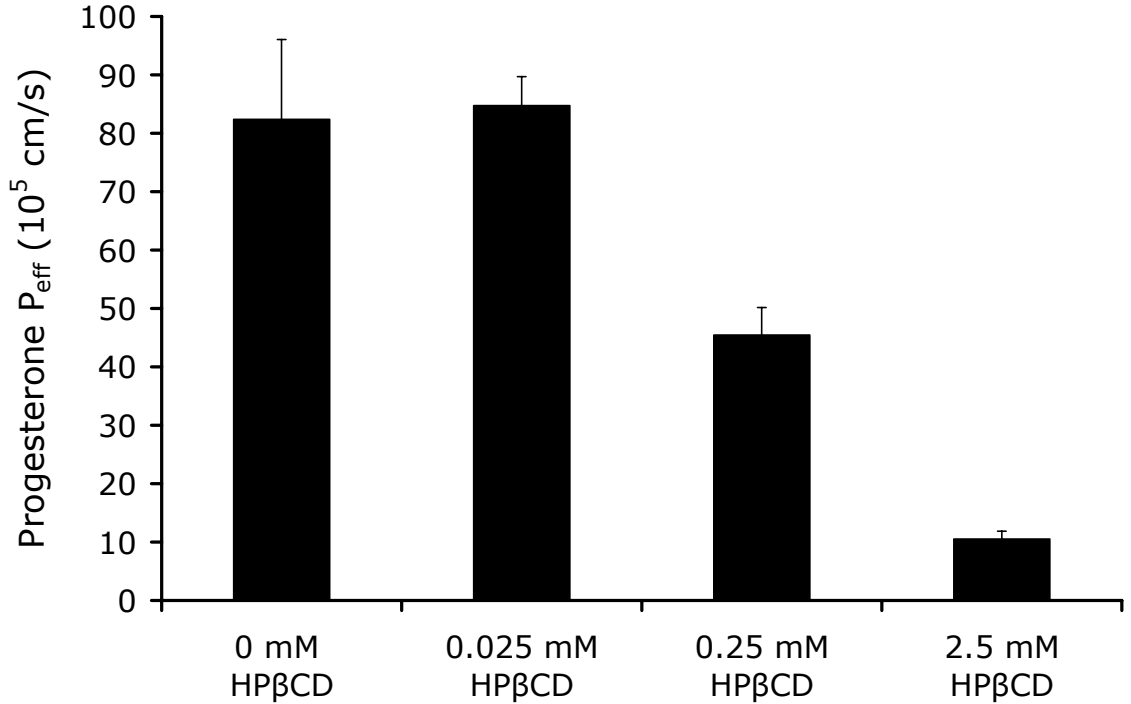
Figure 4.12: Dependence of progesterone P_{eff} on HPβCD concentration in the rat jejunal perfusion model.

Figure 4.13 compares the predicted permeability of progesterone as a function of HPβCD concentration to the experimentally observed P_{eff} values at 0, 0.025, 0.25, and 2.5 mM HPβCD. The predicted lines for P_m, P_{aq}, and P_{eff} were calculated via Equations 4.8 4.18, and 4.20, respectively. The experimental parameters used in the calculations were $K_{11aq} = 14,324$ M^{-1} (from this work), $D_{aq(F)} = 8.0 \times 10^{-6}$ cm^2/sec (Amidon *et. al.*, 1982), and $D_{aq(CD)} = 3.2 \times 10^{-6}$ cm^2/sec (Ribeiro *et. al.*, 2007). The experimental value for $P_{m(F)}$ of 250 x 10^{-5} cm/s used in the calculations was previously estimated by Komiya *et. al.*, (1980) in the rat jejunal perfusion model by determining the P_{eff} of progesterone at increasing perfusate flow rates. The value of $P_{aq(F)}$ used in the predictions was calculated according to Equation 4.20 from the experimental values of $P_{m(F)}$ and the P_{eff} of progesterone determined in the absence of cyclodextrins (82.4 x 10^{-5} cm/s).

As shown in Figure 4.13, the predicted P_{aq} increases markedly with increasing cyclodextrin concentration. This may be explained by the high value of K_{11aq}, as the unstirred aqueous boundary layer is effectively eliminated for the progesterone-HPβCD complex (i.e. $h_{aq(B)} = 0$), such that the effective thickness of the boundary layer decreases with decreasing free fraction as per Equation 4.17. The value of progesterone D_{aq} decreases with increasing cyclodextrin concentration (Equation 4.14), which does contribute to a decrease in the overall value of P_{aq} as expressed in Equation 4.12. However, this effect is essentially negligible in comparison to the effect of the shrinking value of h_{aq}, which leads to a marked increase in P_{aq} with increasing HPβCD concentration. On the other hand, P_m decreases rapidly with increasing cyclodextrin concentration. This may also be attributed to the high binding constant between progesterone and HPβCD, which causes the amount of free drug available for membrane permeation to decrease rapidly with increasing cyclodextrin concentration, as described in Equations 4.8 and 4.10. Figure 4.13 also contains the overall predicted P_{eff} as a function of cyclodextrin concentration which was calculated via Equation 4.20. Excellent agreement was obtained between the experimental and predicted progesterone P_{eff} values at all of the HPβCD concentrations tested. The overall P_{eff} stays relatively consistent at very low HPβCD concentrations, but then decreases rapidly with increasing cyclodextrin concentration. This results because at very low cyclodextrin concentrations, the overall P_{eff} is limited by the unstirred aqueous boundary layer. This is in corroboration with previous reports that have shown progesterone permeability to be limited by the aqueous boundary layer in the rat intestinal perfusion model (Komiya *et. al.*, 1980). However, the rapidly decreasing effective h_{aq} with increasing HPβCD concentration causes P_{aq} to

markedly increase, such the unstirred aqueous boundary layer is quickly eliminated and the overall P_{eff} is under membrane control at higher HPβCD concentrations. This is evidenced by the fact that the experimental and predicted values of P_{eff} are essentially equal to the predicted values of P_m at the higher HPβCD concentrations of 0.25 and 2.5 mM (Figure 4.13).
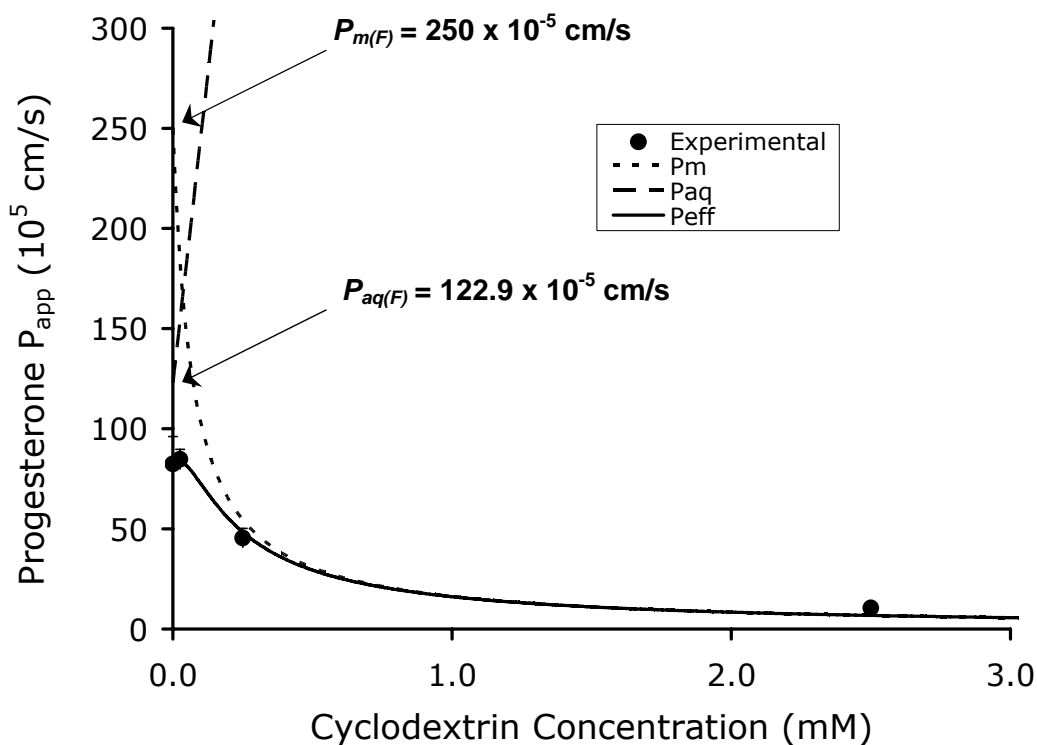
Figure 4.13: P_{eff} of progesterone as a function of HPβCD concentration in the rat jejunal perfusion model. The theoretical lines were calculated via Equation 4.8 (P_m), Equation 4.18 (P_{aq}), and Equation 4.20 (P_{eff}).

Figure 4.14 illustrates the interplay between opposing effects of cyclodextrins on the apparent solubility and permeability of progesterone. S_{aq} as a function of cyclodextrin concentration was calculated via equation 4.7 using the experimentally determined values of K_{11aq} and $S_{aq(F)}$ (Figure 4.1). The P_{eff} as a function of cyclodextrin concentration was calculated via Equation 4.20. From this curve, it is evident that a trade-off exists between

the apparent solubility increase and permeability decrease when using cyclodextrins as pharmaceutical solubilizers. Thus, the effects of this solubility-permeability interplay on the overall fraction of drug absorbed must be considered when using cyclodextrins to increase the apparent solubility of a poorly soluble drug.
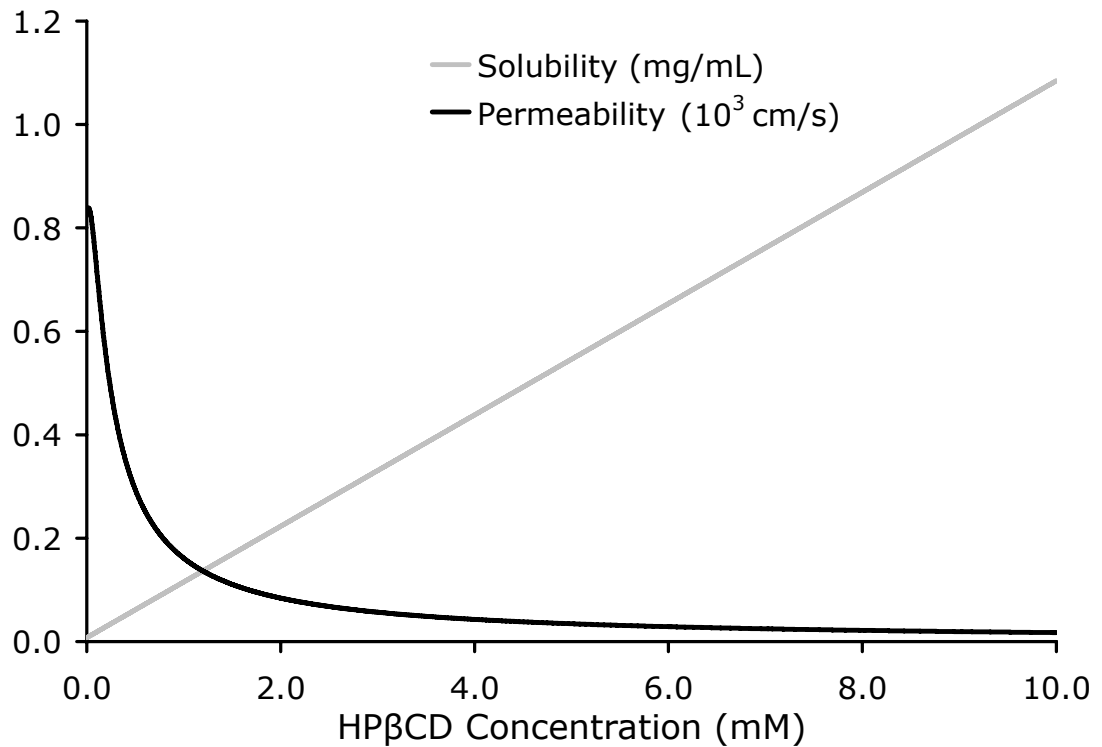
Figure 4.14: The effect of HPβCD on progesterone solubility (○) and permeability (●) based on the theoretical quasi-equilibrium transport analysis. Solubility and permeability were calculated using equations 4.7 and 4.20, respectively.

Conclusions

In this work, a quasi-equilibrium mass transport analysis has been carried out to describe the effect of cyclodextrins on the membrane transport of the poorly soluble drug progesterone. The solubility analysis showed that progesterone aqueous solubility was linearly dependent on HPβCD concentration, indicating 1:1 stoichiometric complexation between progesterone-HPβCD with a very high binding constant of 14,324 M^{-1}. The apparent permeability of progesterone decreased with increasing cyclodextrin concentration in multiple *in-vitro* and *in-situ* intestinal membrane transport models (PAMPA, Caco-2 monolayer, and rat jejunal perfusion). The transport model predicts the effect of cyclodextrin concentration on overall P_{eff} by considering the individual effects on both the apparent membrane permeability (P_m) and aqueous boundary layer permeability (P_{aq}). The model revealed that: 1) P_{aq} increases with increasing cyclodextrin concentration due to the fact that the aqueous boundary layer thickness quickly decreases as the fraction of cyclodextrin bound to progesterone increases, 2) P_m decreases with increasing cyclodextrin concentration, due to the decrease in the free fraction of progesterone available for membrane permeation, and 3) Since P_{aq} increases and P_m decreases with increasing cyclodextrin concentration, the overall permeability becomes membrane controlled with increasing cyclodextrin concentration such that the overall P_{eff} decreases with increasing cyclodextrin concentration and P_{eff} is essentially equal P_m at high cyclodextrin concentrations.

It was demonstrated that the membrane transport model developed here could successfully predict the P_{eff} dependence on HPβCD concentration with knowledge of K_{11aq}, $P_{m(F)}$, $P_{aq(F)}$ and the aqueous diffusion coefficients of the free drug and

cyclodextrin, $D_{aq(F)}$, and $D_{aq(CD)}$. Excellent quantitative prediction of progesterone P_{app} as a function of HPβCD concentration was achieved in the PAMPA, Caco-2 monolayer, and rat jejunal perfusion assays through application of the membrane transport model developed here. Moreover, the membrane transport analysis developed here was applied to some experimental P_{app} as a function of HPβCD concentration data from the literature for carbamazepine and hydrocortisone (Brewster *et. al.* 2007). Excellent agreement was achieved between the predicted and experimental P_{app} values for both compounds as a function of HPβCD concentration.

In conclusion, this work demonstrates that when using cyclodextrins as pharmaceutical solubilizers, a trade-off exists between solubility increase and permeability decrease that will govern the overall fraction of drug absorbed. Given these opposing effects, both apparent solubility and permeability considerations must be taken into account, to strike the appropriate balance to achieve optimal absorption from a cyclodextrin based formulation. Knowledge of the solubility-permeability interplay and the dependence of these parameters on cyclodextrin concentration enables the more efficient and intelligent use of cyclodextrins in oral drug product formulation.

CHAPTER FIVE

SUMMARY AND CONCLUSIONS

This thesis considers two cases in which solution phase molecular complexation may impact intestinal membrane transport. The first case considers the enhancement of intestinal membrane permeation of low-permeability drugs through the formation of ion-pairs in solution with lipophilic counterions. The second case considers the reduction of the apparent intestinal membrane permeation of low-solubility drugs as a consequence of complexation with cyclodextrins. Quasi-equilibrium mass transport analyses were developed to describe the ion-pair mediated octanol-buffer partitioning and membrane permeation of the BCS class III drugs phenformin, GS 4109, and zanamivir heptyl ester. Likewise, a quasi-equilibrium mass transport analysis was carried to describe the impact of cyclodextrins on the membrane transport of the BCS class II drug progesterone. The theoretical quasi-equilibrium mass transport analyses were compared to experimental data from multiple *in-vitro* and *in-situ* intestinal membrane transport models including: parallel artificial membrane permeation assay (PAMPA), Caco-2 cell monolayer assay, and rat jejunal perfusion assay.

In Chapter II of this thesis, a quasi-equilibrium transport model was developed to describe the effect of the lipophilic counterions 1-hydroxy-2-naphthoic acid (HNAP), 2-naphthalenesulfonic acid (NAPSA), and *p*-toluenesulfonic acid (*p*-TSA) on the apparent

octanol-buffer (pH 6.5) partition coefficient (D) of several highly polar drugs. Aqueous phase association constants (K_{11aq}), octanol phase association constants (K_{11oct}), and intrinsic octanol-water partition coefficients (P_{AB}) for the ion-pairs were obtained by fitting a quasi-equilibrium transport model to double reciprocal plots of D as a function of lipophilic counterion concentration. A linear correlation was found between the experimentally determined values of Log P_{AB} and the sum of cLogP of the individual drug and counterion components. This result demonstrated that the Log P_{AB} of any potential ion-pair could be easily estimated from calculated properties by simply summing the cLogP values of the individual acidic and basic components. Likewise, a linear correlation was found between Log K_{11aq} and the sum of HBD + HBA + ΔcpK_a of the ion-pairs, revealing that the aqueous binding constant could also be estimated from calculated properties of the individual components of the ion-pair.

Chapter III of this thesis reports the membrane permeation enhancement of the BCS class III drugs phenformin, GS 4109, and zanamivir heptyl ester through ion-pairing with the lipophilic counterion HNAP. The ability of HNAP to enhance the membrane permeation of the poorly permeable drugs through ion-pair formation was assessed in the PAMPA, Caco-2 cell monolayer, and rat jejunal perfusion assays. HNAP enhanced the apparent membrane permeability of phenformin up to 27-fold in the PAMPA model. A linear relationship with a slope near 2 was obtained from a log-log plot of phenformin flux across the PAMPA liquid membrane versus phenformin-HNAP concentration, consistent with the quasi-equilibrium ion-pair mediated membrane transport model, thus supporting an ion-pair mediated transport mechanism. In the Caco-2 cell monolayer assay, HNAP enhanced the apparent permeability of phenformin 4.9 fold at an HNAP

concentration of 24 mM. Ion-pair formation with HNAP also significantly enhanced the permeation of GS 4109 and zanamavir heptyl ester across Caco-2 cell monolayers, as significant permeability was observed for these compounds in the presence of 6-24 mM HNAP, whereas no detectable transport was observed in the absence of counterion. As predicted from the quasi-equilibrium mass transport analysis of ion-pair mediated membrane transport, an order of magnitude increase in Caco-2 cell monolayer permeability was observed per log increase in counterion concentration for phenformin, GS 4109, and zanamivir heptyl ester. As a result, log-log plots of apparent permeability versus HNAP concentration gave linear relationships with slope near 1. In the rat jejunal perfusion assay, the addition of HNAP failed to significantly increase the effective permeability of phenformin. Similarly, GS 4109 showed essentially zero effective permeability across rat jejunum in both the presence and absence of HNAP. On the other hand, HNAP significantly enhanced the effective permeability of zanamivir heptyl ester in the rat jejunal perfusion assay, as the permeability was essentially zero in the absence of HNAP, but increased to 4.0×10^{-5} cm/s in the presence of 10 mM HNAP. The success of the zanamivir heptyl ester-HNAP ion-pair in the rat jejunal perfusion assay was explained by the substantially stronger binding constant ($388\ M^{-1}$) as compared to the phenformin-HNAP and GS 4109-HNAP ion-pairs ($3\ M^{-1}$). The stronger binding constant of the zanamivir heptyl ester-HNAP ion-pair enables it to remain intact throughout the entire membrane transport process and renders it more resistant to dissociation and ion-exchange with competing endogenous anions.

Several key attributes for successful ion-pair mediated membrane transport were apparent from this work. Successful ion-pair mediated membrane transport was observed

in the Caco-2 monolayer assay when the ion-pair Log P_{AB} values were the range of approximately 2-5. In addition to sufficient lipophilicity of the ion-pair, a strong K_{11aq} value was required to prevent dissociation and ion-exchange with competing endogenous ions (e.g. phosphatidylserine, phosphatidylinositol, sialic acid, bile acids) such that the ion-pair will remain intact during the entire membrane permeation process. The zanamivir heptyl ester-HNAP ion-pair, with binding constant on the order of 100 to 1000 M^{-1}, enabled successful ion-pair mediated membrane transport in the rat jejunal perfusion assay. On the other hand, the phenformin-HNAP and GS 4109-HNAP ion-pairs, with binding constants on the order of 1 to 10 M^{-1}, failed to increase the effective permeability across rat jejunum.

Chapter IV of this thesis focused on the impact of cyclodextrins on the membrane permeation of the BCS class II drug progesterone. A quasi-equilibrium mass transport analysis was developed to quantitatively describe the effect of hydroxypropylbeta cyclodextrins (HPβCD) on the apparent membrane permeability of progesterone. The transport model predicted the effect of cyclodextrin concentration on overall P_{eff} by considering the individual effects on both the apparent membrane permeability (P_m) and aqueous boundary layer permeability (P_{aq}). The model revealed that: 1) P_{aq} increases with increasing cyclodextrin concentration due to the fact that the aqueous boundary layer thickness quickly decreases as the fraction of cyclodextrin bound to progesterone increases, 2) P_m decreases with increasing cyclodextrin concentration, due to the decrease in the free fraction of progesterone available for membrane permeation, and 3) Since P_{aq} increases and P_m decreases with increasing cyclodextrin concentration, the overall permeability becomes membrane controlled with increasing cyclodextrin concentration

such that the overall P_{eff} decreases with increasing cyclodextrin concentration and P_{eff} is essentially equal P_m at high cyclodextrin concentrations.

A phase solubility analysis showed that progesterone aqueous solubility was linearly dependent on HPβCD concentration, indicating 1:1 stoichiometric complexation between progesterone and HPβCD with a very high binding constant of 14,324 M^{-1}. The membrane transport model developed here successfully predicted the progesterone apparent permeability dependence on HPβCD concentration in multiple *in-vitro* and *in-situ* intestinal membrane transport models including: PAMPA, Caco-2 cell monolayer, and rat jejunal perfusion. In addition, the transport analysis was applied to some experimental apparent permeability as a function of HPβCD concentration data from the literature for carbamazepine and hydrocortisone (Brewster *et. al*. 2007). Excellent agreement was achieved between the predicted and experimental apparent permeability values for both compounds as a function of HPβCD concentration.

In summary, this dissertation provides a more in-depth and quantitative understanding of the underlying mechanisms that govern the impact of molecular complexation on intestinal membrane transport. This increased understanding enables the more efficient and intelligent design of drug delivery systems which utilize molecular complexation to improve oral absorption.

BIBLIOGRAPHY

Amidon GE, Higuchi WI, and Ho NFH. Theoretical and Experimental Studies of Transport of Micelle-Solubilized Solutes. *J Pharm Sci* 1982, 71, 77-84

Amidon GL, and Johnson KC. Intestinal Aminopeptidase Distribution and Specificity: Basis for a Prodrug Strategy. *Biorev Carr Drug Des* 1987, 243-261

Amidon GL, Sinko PJ, and Fleisher D. Estimating Human Oral Fraction Dose Absorbed: A Correlation Using Rat Intestinal Membrane Permeability for Passive and Carrier-Mediated Compounds. *Pharm Res* 1988, 5, 651-654

Amidon GL, and Lee HJ. Absorption of Peptide and Peptidomimetic Drugs. *Ann Rev Pharm Tox* 1994, 34, 321-341

Amidon GL, Lennernaes H, Shah VP, and Crison JR. A Theoretical Basis for a Biopharmaceutic Drug Classification: The Correlation of In-Vitro Drug Product Dissolution and In-Vivo Bioavailability. *Pharm Res* 1995, 12, 413-420

Amidon GL, Han H, Oh DM, Walter E, and Hilfinger JM. Oral Administration of Peptide and Protein Drugs. *Alfred Benzon Symposium* 1998, 43, 146-156

Amidon GL. Molecular Pharmaceutics Strategies for Targeting Transporters and Enzymes in the GI Tract. *Abstract of Papers, 231st ACS National Meeting* 2006

Brewster ME, and Loftsson T. Cyclodextrins as Pharmaceutical Solubilizers. *Adv Drug Del Rev* 2007, 59, 645-666

Brewster ME, Noppea M, Peeters J, and Loftsson T. Effect of the Unstirred Water Layer on Permeability Enhancement by Hydrophilic Cyclodextrins. *Int J Pharm*, 2007, 342, 250-253

Buxton RC, Edwards B, Juo RR, Voyta JC, Tisdale M, Bethell RC. Development of a Sensitive Chemiluminescent Neuraminidase Assay for the Determination of Influenza Virus Susceptibility to Zanamivir. *Anal Biochem* 2000, 280, 291-300

Carrier RL, Miller LA, and Ahmed I. The Utility of Cyclodextrins for Enhancing Oral Bioavailability. *J of Con Rel* 2007, 123, 78-99

Chandler M, Bamford MJ, Conroy R, Lamont B, Patel B, Patel VK, Steeples IP, Storer R, Weir NG, Wright M, and Williamson C. Synthesis of the Potent Influenza Neuraminidase Inhibitor 4-Guanidino Neu5Ac2en. X-Ray Molecular Structure of 5-Acetamido-4-Amino-2,6-Anhydro-3,4,5-Trideoxy-D-Erythro-L-Gluco-Nonionic Acid. *J Chemical Soc Perk Trans 1* 1995, 9, 1173-80

Chiou WL, Jeong HY, Chung SM, Wu TC. Evaluation of Using Dog as an Animal Model to Study The Fraction of Oral Dose Absorbed of 43 Drugs in Humans. *Pharm Res* 2000, 17, 135-140

Connors KA. *Binding Constants. The Measurement of Molecular Complex Stability.* New York, NY: John Wiley & Sons, 1987

Dahan A, and Hoffman A. Enhanced Gastrointestinal Absorption of Lipophilic Drugs. In: Touitou E, and Barry BW (eds). *Enhancement in Drug Delivery.* Boca Raton: CRC Press LLC, 2007, 111-131

Dahan A. and Amidon GL. Segmental Dependent Transport of Low Permeability Compounds Along the Small Intestine Due to P-Glycoprotein: The Role of Efflux Transport in the Oral Absorption of BCS Class III Drugs. *Mol Pharm* 2009, 6 , 19-28

Dahan AS, and Amidon GL. Gastrointestinal Dissolution and Absorption of Class II Drugs. In: *Methods and Principles in Medicinal Chemistry.* Wiley-VCH Verlag GmbH & Co. KGaA, 2009, 40, 33-51

Dal Pozzo A, Acquasaliente M, and Geron MR. New Heparin Complexes Active By Intestinal Absorption: I-Multiple Ion Pairs With Basic Organic Compounds. *Thromb Res* 1989, 56, 119-124

Davis ME, and Brewster ME. Cyclodextrin-Based Pharmaceutics: Past, Present and Future. *Nature Rev Drug Disc* 2004, 3, 1023-1035

Duffey ME., Evans DF, and Cussler EL. Simultaneous Diffusion of Ions and Ion Pairs Across Liquid Membranes. *J Mem Sci* 1978, 3, 1-14

Ettmayer P, Amidon GL, Clement B, and Testa B. Lessons Learned from Marketed and Investigational Prodrugs. *J Med Chem* 2004, 47, 2393-2404

Fagerholm U, Johansson M, and Lennernas H. Comparison Between Permeability Coefficients in Rat and Human Jejunum. *Pharm Res* 1996, 13, 1336–1342

Fleisher D, Stewart B, and Amidon GL. Design of Prodrugs for Improved Gastrointestinal Absorption by Intestinal Enzyme Targeting. *Meth Enzym* 1985, 112, 360-381

Gaginella TS, Bass P, Perrin JH, and Vallner JJ. Effect of Bile Salts on Partitioning Behavior and GI Absorption of a Quaternary Ammonium Compound, Isopropamide Iodide. *J Pharm Sci* 1973, 62, 1121-1125

Gasco MR, Trotta M, and Eandi M. The Influence of Bile Salts on the Absorption *in Vitro* and *in Vivo* of Propranolol. *J Pharm Biomed Anal* 1984, 2, 425-439

Gibaldi M, and Grundhofer B. Enhancement of Intestinal Absorption of a Quaternary Ammonium Compound by Salicylate and Trichloroacetate. *J Pharm Sci*, 1973, 62, 343-344

Goizman MS, Sarkisyan SO, Sarkisyan AA, Persianova IV Differential Spectro-Photometric Determination of Biguanide Derivatives. *Pharm Chem J* 1985, 19, 503-507

Grant DJW, and Higuchi T. Ion Pairs and Solubility Behavior. In: Weissberger A (ed.). *Solubility Behavior of Organic Compounds*. New York: John Wiley & Sons, 1990, 399-43

Hallén B, Sundwall A, and Sandquist S. Ion Pair Formation and Gastrointestinal Absorption of Emepronium. *Acta Pharm et Tox* 1985, 57, 271-278

Han HK, and Amidon GL. Targeted Prodrug Design to Optimize Drug Delivery. *AAPS PharmSci* 2000, 2, E6

Higuchi T. Physical Chemical Analysis of Percutaneous Absorption Process from Creams and Ointments. *J Soc Cosmet Chem* 1960, 11, 85-97

Higuchi T, and Connors KA. Phase-Solubility Techniques. *Advan Anal Chem Instr* 1965, 4, 117-212

Higuchi T. Prodrug, Molecular Structure and Percutaneous Delivery. In: Roche EB (ed.). *Design of Biopharm Properties Through Prodrugs and Analogs*. Washington D.C.: American Pharmaceutical Association Academy of Pharmaceutical Sciences, 1977, 409-421

Irwin GM, Kostenbauder HB, Dittert LW, Staples R, Misher A, and Swintosky JV. Enhancement of Gastrointestinal Absorption of a Quaternary Ammonium Compound by Trichloroacetate. *J Pharm Sci* 1969, 58, 313-315

Johnson DA, and Amidon GL. Determination of Intrinsic Membrane Transport Parameters from Perfused Intestine Experiments: A Boundary Layer Approach to Estimating the Aqueous and Unbiased Membrane Permeabilities. *J Theor Biol* 1988, 131, 93-106

Jonkman JHG, Van Bork LE, Wijsbeek J, Bolhuis-De Vries AS, De Zeeuw RA, Greving JE, and Orie NGM. *Pharm Weekblad, Sci Ed* 1979, 1, 937-940

Jonkman JHG, and Hunt CA. Ion Pair Absorption of Ionized Drugs- Fact or Fiction? *Pharm Weekblad Sci Ed,* 1983, 5, 41-48

Kansy M, Senner F, and Gubernator K. Physicochemical High-Throughput Screening: Parallel Artificial Membrane Permeation Assay in The Description of Passive Absorption Processes. *J Med Chem* 1998, 41, 1007-1010

Kasim NA, Whitehouse M, Ramachandran C, Bermejo M, Lennernäs H, Hussain AS, Junginger HE, Stavchansky SA, Midha KK, Shah VP, and Amidon GL. Molecular Properties of WHO Essential Drugs and Provisional Biopharmaceutical Classification. *Mol Pharm* 2004, 1, 85-96

Kim JS, Mitchell S, Kijek P, Tsume Y, Hilfinger J, and Amidon GL. The Suitability of an In-Situ Perfusion Model for Permeability Determinations: Utility for BCS Class I Biowaiver Requests. *Mol Pharm* 2006, 3, 686–694

Komiya I, Park JY, Kamani A, Ho NFH, and Higuchi WI. Quantitative Mechanistic Studies in Simultaneous Fluid Flow and Intestinal Absorption Using Steroids as Model Solutes. *Int Journal Pharm* 1980, 4, 249-262

Kubo SH, and Cody RJ. Clinical Pharmacokinetics of the Angiotensin Converting Enzyme Inhibitors. *Clin Pharmaco* 1985, 10, 377–391

Lengsfeld CS, Pitera D, Manning M, and Randolph TW. Dissolution and Partitioning Behavior of Hydrophobic Ion-Paired Compounds. *Pharm Res*, 2002, 19, 1572-1576

Lennernäs H, Ahrenstedt Ö, and Ungell A. Intestinal Drug Absorption During Induced Net Water Absorption in Man, a Mechanistic Study Using Antipyrine, and Atenolol and Enalaprilat. *Brit J Clin Pharm* 1994, 37, 589-596

Li W, Escarpe PA, Eisenberg EJ, Cundy KC, Sweet C, Jakeman KJ, Merson J, Lew W, Williams M, Zhang L, Kim CU, Bischofberger N, Chen MS, and Mendel DB. Identification of GS 4104 as an Orally Bioavailable Prodrug of the Influenza Virus Neuraminidase Inhibitor GS 4071. *Antimicrob Agents Chemo* 1998), 42, 647-653

Lignieres, B. Oral Micronized Progesterone. *Clin Ther* 1999, 21, 41-60

Lipinski CA. Drug-Like Properties and the Causes of Poor Solubility and Poor Permeability. *J Pharmacol and Toxicol Meth* 2001, 44, 235-249

Lipka E, Lennernas H, and Amidon GL. Interspecies Correlation of Permeability Estimates: The Feasibility of Animal Data for Predicting Oral Absorption in Humans. *Pharm Res* 1995, 12, S311

Lipka E, Crison J, and Amidon GL. Transmembrane Transport of Peptide Type Compounds: Prospects for Oral Delivery. *J Con Rel* 1996, 39, 121-129

Lobenberg R, and Amidon GL. Modern Bioavailability, Bioequivalence and Biopharmaceutics Classification System. New Scientific Approaches to International Regulatory Standards. *Eur J Pharm and Biopharm* 2000, 50, 3-12

Loftsson T, and Brewster ME. Pharmaceutical Applications of Cyclodextrins 1. Drug Solubilization and Stabilization. *J Pharm Sci* 1996, 85, 1017-1025

Loftsson T, Brewster ME, and Masson M. Role of Cyclodextrins in Improving Oral Drug Delivery. *Amer J of Drug Del* 2004, 2, 261-275

Loftsson T, Konradsdottir F, and Masson M. Influence of Aqueous Diffusion Layer on Passive Drug Diffusion from Aqueous Cyclodextrin Solutions Through Biological Membranes. *Pharmazie* 2006, 61, 83-89

Loftsson T, Vogensen SB, Brewster ME, and Konraosdottir F. Effects of Cyclodextrins on Drug Delivery Through Biological Membranes. *J of Pharm Sci* 2007, 96, 2532-2546

Luft D, Schmulling RM, and Eggstein M. Lactic Acidosis in Biguanide Treated Diabetics. *Diabetologia* 1978, 14, 75-87

Martin R, Witte KL, and Wong CH. The Synthesis and Enzymatic Incorporation of Sialic Acid Derivatives for Use as Tools to Study the Structure, Activity, and Inhibition of Glycoproteins and Other Glycoconjugates. *Bioorg Med Chem* 1998, 6, 1283-1292

Martinez MN, and Amidon GL. A Mechanistic Approach to Understanding the Factors Affecting Drug Absorption: A Review of Fundamentals. *Pharmacokinetics and Pharmacodynamics* 2002, 42, 620-643

Masson M, Loftsson T, Masson G, and Stefansson E. Cyclodextrins as Permeation Enhancers: Some Theoretical Evaluations and In-Vitro Testing. *J Con Rel* 1999, 59, 107-118

Masuda T, Yoshida S, Arai M, Kaneko S, Yamashita M, and Honda T. Synthesis and Anti-Influenza Evaluation of Polyvalent Sialidase Inhibitors Bearing 4-Guanidino-Neu5Ac2en Derivatives. *Chem Pharm Bull Tokyo* 2003, 51, 1386-98

Meyer JD, and Manning MC. Hydrophobic Ion Pairing: Altering the Solubility Properties of Biomolecules. *Pharm Res*, 1998, 15, 188-193

Miller LA, Carrier RL, and Ahmed I. Practical Considerations in Development of Solid Dosage Forms That Contain Cyclodextrin. *J Pharm Sci* 2007, 96, 1691-707

Mrestani Y, Härtl A, and Neubert RHH. Influence of Absorption Enhancers on the Pharmacokinetic Properties of Non-Oral β-Lactam-Cefpirom Using the Rabbit (Chinchilla) *in Vivo* Model. *Int J Pharm* 2006, 309, 67-70

Naesens L, Bischofberger N, Augustijns P, Annaert P, Van Den Mooter G, Arimilli MN, Kim, CU, De Clercq E. Antiretroviral Efficacy and Pharmacokinetics of Oral Bis(Isopropyloxycarbonyloxymethyl)-9-(2-Phosphonylmethoxypropyl)Adenine in Mice. *Antimicrob Agents Chemo* 1998, 42, 1568-1673

Neubert R, Albrecht G, Taube C, Weiss M, and Fürst W. Influence of Ion-Pair Formation on the Pharmacokinetic Properties of Drugs Part 3: Influence of Hexylsalicylic Acid on the Pharmacokinetics of Pholedrine. *Pharmazie* 1988, 43, 632-633

Neubert R. Ion Pair Transport Across Membranes. *Pharm Res*, 1989, 6, 743-747

Ogura H, Furuhata K, Sato S, Anazawa K, Itoh M, and Shitori Y. Synthesis of 9-O-Acyl-And 4-O-Acetyl-Sialic Acids. *Carbohydr Res* 1987, 167, 77-86

Quintanar-Guerrero D, Allémann E, Fessi F, and Doelker E. Applications of the Ion-Pair Concept to Hydrophilic Substances with Special Emphasis on Peptides. *Pharm Res*, 1997, 14, 119-127

Rajewski RA, and Stella VJ. Pharmaceutical Applications of Cyclodextrins 2. In-Vivo Drug Delivery. *J of Pharm Sci* 1996, 85, 1142-1169

Ranadive SA, Chen AX, and Serajuddin ATM. Relative Lipophilicities and Structural-Pharmacological Considerations of Various Angiotensin-Converting Enzyme (ACE) Inhibitors. *Pharm Res* 1992, 9, 1480-1486

Rao VM, and Stella VJ. When Can Cyclodextrins be Considered for Solubilization Purposes? *J Pharm Sci* 2003, 92, 927-932

Ribeiro ACF, Valente AJM, Santos CIAV, Prazeres MRA, Lobo VMM, Burrows HD, Esteso MA, Cabral AMTDPV, and Veiga FJB. Binary Mutual Diffusion Coefficients of Aqueous Solutions of α-Cyclodextrin, 2-Hydroxypropyl-α -cyclodextrin, and 2-Hydroxypropyl-β-cyclodextrin at Temperatures from (298.15 to 312.15) K. *J Chem & Eng Data* 2007, 52, 586-590.

Ross BP, DeCruz SE, Lynch TB, Davis-Goff K, and Toth I. Design, Synthesis, and Evaluation of a Liposaccharide Drug Delivery Agent: Application to the Gastrointestinal Absorption of Gentamicin. *J Med Chem* 2004, 47, 1251-1258

Schanker LS. On the Mechanism of Absorption of Drugs from the Gastrointestinal Tract. *J Med Pharm Chem*, 1960, 2, 343-359

Seo PR, Teksina ZS, Kao JPY, and Polli, JE. Lipid composition effect on permeability across PAMPA *Eur J Pharm Sci* 2006, 29, 259-268

Shin H. Landowski CP, Sun D, and Amidon GL. Transporters in the GI Tract. *Meth Prin Med Chem* 2003, 18, 245-287

Shitara E, Nishimura Y, Nerome K, Hiramoto Y, and Takeuchi T. Synthesis of 6-Acetamido-5-Amino- and -5-Guanidino-3, 4-Dehydro-N-(2-Ethylbutyryl)- 3-Piperidinecarboxylic Acids Related to Zanamivir and Oseltamivir, Inhibitors of Influenza Virus Neuraminidases. *Org Lett* 2000, 2, 3837-40

Stahl PH, and Wermuth CG. Monographs on Acids and Bases. In: Stahl PH, and Wermuth CG (eds). *Handbook of Pharmaceutical Salts Properties, Selection, and Use.* Zürich: Verlag Helvetica Chimica Acta, 2002, 265-327

Takagi T, Ramachandran C, Bermejo M, Yamashita S, Yu LX, and Amidon GL. A Provisional Biopharmaceutical Classification of the Top 200 Oral Drug Products in the United States, Great Britain, Spain, and Japan. *Mol Pharm* 2006, 3, 631-643

Tomlinson E. Never Mix a Cation with an Anion? *Pharm Int*, 1980, 8, 156-158

Todd PA, and Goa KL. Enalapril: A Re-appraisal of its Pharmacology and Therapeutic Use in Hypertension. *Drugs* 1992, 43, 346-381.

Van de Waterbeemd H, Smith DA, Beaumont K, and Walker DK. Property-Based Design: Optimization of Drug Absorption and Pharmacokinetics. *J Med Chem* 2001, 44, 1313-1333

Walkling WD, Holmes DG, Cressman WA, Dix RK, Piperno E, and Mosher AH. Possible Ion-Pair Mediated Absorption of Mixidine II: Plasma Levels and Histology. *J Pharm Sci*, 1978, 67, 948-950

Walter E, Kissel T and Amidon GL. The Intestinal Peptide Carrier: A Potential System for Small Peptide Derived Drugs. *Adv Drug Del Rev* 1996, 20, 33-58

Wohnsland F and Faller B. High-Throughput Permeability pH Profile and High Throughput Alkane/Water Log P with Artificial Membranes. *J Med Chem* 2001, 44, 923-930

Van Gelder J, Witvrouw M, Pannecouque C, Henson G, Bridger G, Naesens L, De Clercq E, Annaert P, Shafiee M, Van den Mooter G, Kinget R, and Augustijns P. Evaluation of the Potential of Ion Pair Formation to Improve the Oral Absorption of Two Potent Antiviral Compounds, AMD3100 and PMPA. *Int J Pharm*, 1999, 186, 127-136

Yee S, and Amidon G. Oral Absorption of Angiotensin Converting Enzyme Inhibitors and Peptide Prodrugs. In: Taylor MD, and Amidon GL (eds.). *Peptide Based Drug Design*. Washington D.C.: American Chemical Society, 1995, 135-147

Yu LX, Amidon GL, Polli JE, Zhao H, Mehta MU, Conner DP, Shah VP, Lesko LJ, Chen M, Lee VHL, and Hussain AS. Biopharmaceutics Classification System: The Scientific Basis for Biowaiver Extensions. *Pharm Res* 2002, 19, 921-925